# Ankle and Foot Biomechanics during Human Walking:
# Powerful Insights on Multiarticular Muscles, Soft Tissues, and Toe Joint Dynamics

By

Eric Honert

Dissertation

Submitted to the Faculty of the

Graduate School of Vanderbilt University

in partial fulfillment of the requirements

for the degree of

DOCTOR OF PHILOSOPHY

in

Mechanical Engineering

May 10, 2019

Nashville, Tennessee

Approved:

Karl E. Zelik

Michael Goldfarb

Gerasimos Bastas

Thomas Withrow

Kota Takahashi

ACKNOWLEGEMENTS

I would like to thank my advisor, Dr. Karl Zelik. He has been the best advisor and mentor that I would have hoped for. He has fostered my growth, ensured that my research was innovative and that I could communicate it to the wider research community as well.

I want to thank my committee for the valuable feedback about this research and for their many discussions about research and life.

None of this work would have been possible without my CREATe family:

Matt Yandell, Harrison Bartlett, Erik Lamers, Emily Matijevich, Andres Martinez, Maura Eveld, Ben Gasser, Dave Comber, Shane King, Rachel Teater, David Ziemnicki, Leila Capozzi, Kirsty McDonald and all of the BAT lab undergrads.

Special thanks to:

My parents, Kim and Jeff, for being there every step of the way along this process

Ben Gasser for always being there to help with machining, climbing, and hiking

Erik Lamers for the hours doing research, ping pong, mountain biking and laughing

Brannon Cox for being there every step of the way at 5 am and for the great climbing trips

Craig Goehler for starting me on this research journey at Valparaiso University

Kristina Barber and Nick Goodman for being there for the twists and turns in life

Meredith Jackson for bringing more positivity into my life as well as being my trail running and climbing buddy

TABLE OF CONTENTS

Page

LIST OF TABLES

Table Page

LIST OF FIGURES

# Chapter 1

# Introduction

## 1.1 Background

The biomechanical contributions of the ankle, knee, and hip have received the majority of attention biomechanical studies which has left the biomechanical contributions of the foot largely overlooked. Ankle, knee and hip biomechanics have been the primary focus of the human motion studies as they are considered the main mechanical power producers during gait. How each of these three joints contributes functionally to movement have led to advancements of assistive technology like prostheses and orthoses that aid the locomotion for persons with disability (Bartlett, Lawson, and Goldfarb 2017; Martínez, Lawson, and Goldfarb 2018; Herr and Grabowski 2012). Distal to the ankle, the foot biomechanical contributions to locomotion have been largely overlooked as the foot has been traditionally treated as a rigid body that can neither store nor return mechanical power (Ranchos Los Amigos National Rehabilitation Center 2001; Baker 2013; Whittle 2014; D. Winter 2009; Inman, Ralston, and Todd 1981; D. G. E. Robertson et al. 2013). However, studies have revealed that the foot has a significant biomechanical contribution to walking (Takahashi and Stanhope 2013; Takahashi, Kepple, and Stanhope 2012; Siegel, Kepple, and Caldwell 1996; Zelik, Takahashi, and Sawicki 2015; Bruening, Cooney, and Buczek 2012b; MacWilliams, Cowley, and Nicholson 2003). These biomechanical contributions stem from a variety of sources including intrinsic foot musculatures that act about foot joints, such as the toe joint. Yet, there is still a gap in knowledge with respect to how

different multi-articular (multi-joint) foot musculatures contribute to walking and different toe joint properties (e.g., toe length, toe joint stiffness) can affect walking performance. Bridging this gap in foot biomechanics knowledge could enhance assistive technology advancements in order to aid locomotion for persons with disability.

Though a variety of studies have examined the biomechanical contributions of the foot, these different estimates appear to be inconsistent. Examination of the overall foot contributions, during walking have shown that the foot is a dissipative structure (Takahashi, Kepple, and Stanhope 2012; Zelik, Takahashi, and Sawicki 2015). Interestingly, multi-segment foot models have shown storage and return by the different joints of the foot (MacWilliams, Cowley, and Nicholson 2003; Bruening, Cooney, and Buczek 2012b), which is in line with however cadaver studies have shown that the foot have energy storage and return properties via the plantar facia (Ker et al. 1987; Stearne et al. 2016). It is currently not known why there is this discrepancy between the overall characterization of the foot contributions and the individual foot joint contributions.

The biomechanical contributions of the toe joints of the forefoot have been previously studied as they have been shown to impact walking performance. During typical walking, the human toe joints undergo substantial flexion (sometimes termed the toe rocker phase of gait, Perry and Burnfield 2010), followed by extension. This toe joint articulation has been shown to impact locomotor economy and other performance metrics is found in the fields of prosthetics (Grabowski, Rifkin, and Kram 2010; Zhu, Wang, and Wang 2014b), footwear (Takahashi et al. 2016; Oh and Park 2017), sport biomechanics (Oh and Park 2017; Nigg et al. 1998; Willwacher et al. 2013; Roy and Stefanyshyn 2006) and humanoid robotics (Ahn, Lee, and Go 2003; Buschmann, Lohmeier, and Ulbrich 2009). However, the effects of specific toe properties (e.g., joint stiffness, shape, length) have not

been fully or systematically studied, and it remains unclear if or how we should be mimicking or augmenting biological toe joint behaviors in devices such as prostheses, exoskeletons and robot feet, or in the design of shoes.

The goal of my research here is to investigate the biomechanical contributions of the human foot to walking. My research examines both the human foot and a custom-designed prosthetic foot during walking. Human studies enable the characterization of the physiological response. Examining different features of a prostheses allows us to systematically examine foot properties that are similar to and different from the typical human foot. This biological and non-biological understanding of the foot can inform design parameters for assistive devices, such as prostheses, to enhance walking for persons with amputation.

## 1.2 Dissertation Overview

This dissertation is divided into five separate research chapters. Chapter 2 examines the role of mono- and multi- articular (multi-jointed) musculatures across the ankle and foot during walking through an electromyography-driven musculoskeletal model. Chapter 3 examines an assumption made in many gait analyses: the entire foot is a single rigid-body segment. This assumption neglects power generated/absorbed within the foot which can lead to misunderstandings related to (biological and prosthetic) foot function and thus distort our understanding of ankle and underlying muscle-tendon dynamics. Chapter 4 examines the contributions of the foot and the shoe versus the rest-of-the-body to the soft tissue energy absorption during early stance of walking. Chapter 5 examines the role of ankle stiffness, toe joint stiffness and toe shape through a custom-designed adjustable ankle-toe prosthesis during walking. Chapter 6 examines the role of foot arch length (from heel to toe joint) and toe length as well as toe joint axis angle to walking biomechanics. Both Chapters 5 and 6 demonstrate that toe joint stiffness and foot arch length can be leveraged in future studies to enhance walking for persons with amputation.

## 1.3 Dissertation Contributions

The contribution of Chapter 2 is the development of a new musculoskeletal model that examines both mono- and multi- articular muscle contributions. This differs from conventional inverse dynamics approaches which assume kinetic contributions only from mono-articular sources. We showed that multi-articular musculature about the ankle and foot affect do not have a large effect ankle kinetic estimates (~2 – 7%) during walking. This modeling approach can be applied to understand kinetic contributions of larger multi-articular musculatures such as the biceps femoris or rectus femoris that may confound inverse dynamics estimates of knee and hip kinetics.

The contribution of Chapter 3 is a new framework for quantifying ankle, foot, and combined anklefoot power during walking. Typically, the foot is modeled as a single rigid body which neither stores or returns energy. We showed that this assumption can lead to overestimates in ankle power (here up to 77%) in comparison to an anatomically relevant model. When we applied same model for foot power estimates, we found results were consistent with *in vivo* and *in vitro* studies on the storage and return properties of the plantar fascia. In prosthetic foot analyses, we found that estimating power with a rigid foot approach can skew comparisons between the biological limb and prosthetic limb as compared to a more complete anklefoot approach (which accounts for storage and return along the entire prosthesis). In conjunction with these findings, we provide guidelines for implementing ankle, foot, and anklefoot kinetic estimates for gait analysis studies. To enhance these guidelines, we demonstrated the analytical equivalence of two different anklefoot kinetic estimates that have been used to estimate storage and return from foot prostheses. Additionally, we derived the foot power estimate and demonstrated that this is an inverse dynamics style estimate similar to those commonly used in the gait analysis

community such as ankle, knee and hip power.

The contribution of chapter 4 was the first study to evaluate the soft tissue absorption performed by the foot and the shoe versus the rest of the body during sloped and level ground walking. Previous works have quantified the soft tissue absorption by the foot and shoe only during level ground locomotion. Additionally, previous studies have examined the net soft tissue absorptions throughout the entire body. Here, we expanded upon prior literature by combining a foot and shoe soft tissue absorption estimate with a whole-body soft tissue absorption estimate during early stance over a wide range of walking speeds and slopes. We found that the foot and the shoe contributed ~60-70% of the soft tissue work during level and uphill walking and rose to ~80-90% during downhill walking. These results provide new insight into how mechanical work is distributed amongst various tissues in the human body.

The contribution of chapter 5 is the first study to systematically evaluate the effects of toe joint stiffness and toe shape to human walking. We examined these toe properties using a custom-designed ankle-toe prosthesis that provides an emulation platform for systematically testing different foot properties with both a passive ankle (Chapters 5 and 6) and active ankle (future studies). We found that changing toe joint stiffness, not toe shape, altered human walking – particularly during the step-to-step transition. These results indicate that altering toe joint stiffness in foot prosthesis for persons with amputation may provide a complementary means of enhancing locomotor performance, in conjunction with the more conventional approach of augmenting ankle dynamics.

The contribution of chapter 6 is the first study to evaluate the biomechanical role of toe length, foot arch length (measured from heel to toe joint) and toe joint axis to human walking. We examined these different foot properties through the custom-designed ankle-

to prosthesis presented in the previous chapter. We found that foot arch length had greater effect on walking kinetics than toe length and toe joint axis. These results indicate that augmenting the foot arch length of a prosthesis for a person with amputation provides another means to enhance locomotor performance in addition to toe and ankle joint stiffness.

# Chapter 2

# Inferring Muscle-Tendon Unit Kinetics from Ankle Power Estimates during Human Walking: Insights from a Multiarticular EMG-Driven Model

## 2.1 Introduction

Inverse dynamics estimates of joint kinetics are often used to infer underlying contributions from muscle-tendon units (MTUs), allowing the use of external force and motion recordings to gain insight into musculoskeletal biomechanics and neuromuscular coordination (Zajac, Neptune, and Kautz 2002). For instance, net joint moments are often estimated as a surrogate for net torques created by MTUs about individual joints. These torques created by MTUs, often called net muscle moments (Biewener et al. 2004; Ren, Jones, and Howard 2008), assume negligible torque contributions from non-MTU sources (e.g. ligaments). Similarly, joint power (computed by multiplying net joint moment by joint angular velocity) is often interpreted as a reflection of net power generated by MTUs crossing the joint (D. G. E. Robertson et al. 2013; David A. Winter et al. 1990). However, this interpretation is technically only correct if joint power originates entirely from monoarticular MTUs, which cross only a single joint (Fig. 2.1A). When multiarticular (multi-joint) MTUs generate force or power during movement, then inverse dynamics joint power may over- or under-estimate the actual net MTU power (Fig. 2.1), due to inadvertently subdividing power from a single multiarticular MTU into positive power at one joint and offsetting negative power at another. This methodological issue confounds our ability to infer MTU dynamics from traditional motion analysis. In practice, over- or under-

estimating MTU power could lead to incorrect scientific conclusions, or to empirical estimates that misguide musculoskeletal simulations, assistive device designs, or clinical interventions. It is therefore critical to evaluate and understand the degree to which inverse dynamics joint power estimates reflect underlying MTU power.

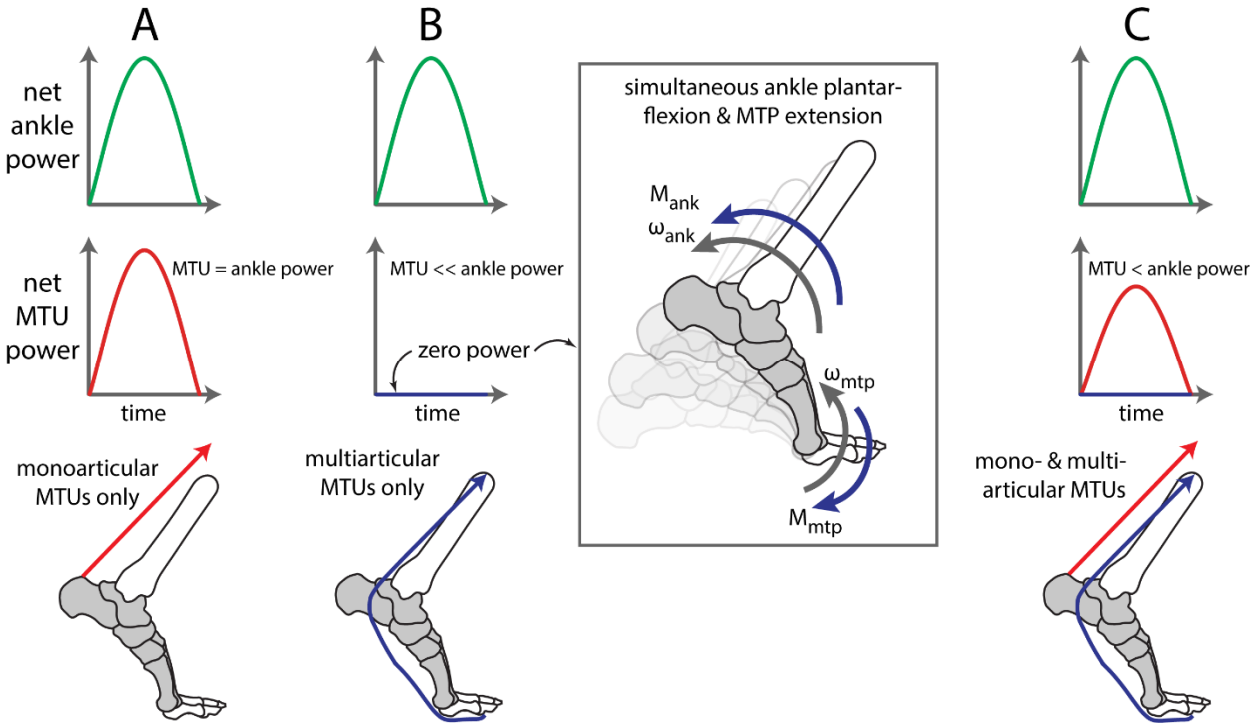


**Figure 2.1 Conceptual summary of ankle joint vs. muscle-tendon-unit (MTU) power**
Net ankle joint power (green, top row) can be computed from inverse dynamics by multiplying ankle joint moment, $M_{ank}$, by ankle angular velocity, $\omega_{ank}$ (sagittal plane depicted). Due to assumptions in inverse dynamics, this ankle power may or may not correspond with net MTU power (second row), depending on the underlying MTU contributions (cartoon depicted in bottom row). (A) Ankle power is expected to reflect MTU power when MTUs are monoarticular (red, acting solely about the ankle). (B) Ankle power may not reflect power contributions from multiarticular MTUs (blue). In the extreme example depicted, the multiarticular MTU provides torque about both the ankle and MTP (toe) joints, but due to the simultaneous plantarflexion of the ankle and extension of the toes, the MTU does not change length. Thus the MTU behaves like a rigid cable and performs zero net power. However, inverse dynamics (joint-by-joint) analysis would indicate positive power about the ankle ($M_{ank} \cdot \omega_{ank}$), and equal offsetting negative power about the toe joints ($M_{MTP} \cdot \omega_{mtp}$, inset). In this case, net ankle power would greatly overestimate net MTU power. (C) In actuality, both mono- and multi-articular MTUs contribute to human movement. However, it remains unclear if and by how much ankle power overestimates net MTU power. If multiarticular MTUs act isometrically (i.e., perform zero net power, as depicted here) or close to isometrically, then it is expected that ankle power magnitude will be larger than net MTU power.

The aim of this study was to evaluate the degree to which net ankle power overestimates net MTU power due to multiarticular MTU dynamics, which are neglected by standard inverse

dynamics. Specifically, we sought to test the hypothesis that net ankle power overestimates net plantarflexor MTU power during the end of stance phase in human walking, termed Push-off. This objective was intentionally specific to a single joint, a subset of MTUs (the ankle plantarflexors), and a single phase of gait (Push-off). This is because interpreting net MTU power from joint power is highly task- and joint-specific. For instance, if for one locomotor task the multiarticular MTUs that cross the ankle and metatarsophalangeal (MTP, i.e. toe) joints are largely unloaded (i.e., contribute little force), then inverse dynamics joint power estimates may provide a reasonable approximation of the net MTU power. However, for a different locomotor task the multiarticular MTUs may generate substantial force and power, and confound our ability to infer net MTU power directly from joint-level estimates (Fig. 2.1 B & C). At the same time, other multiarticular MTUs that cross the knee and hip (e.g., hamstrings) may be behaving completely differently. These joints/muscles would require their own separate task-specific assessment of whether joint powers are reflective of net MTU power (for the subset of muscles crossing the joints). In light of this task- and joint-specificity we focused this study solely on MTUs that directly contribute to ankle joint plantarflexion.

Ankle plantarflexion was studied because these MTUs are major power producers during walking (David A. Winter 1983a; David A. Winter and Robertson 1978). The majority of this power is produced in a burst-like fashion during the Push-off phase of walking. Push-off helps accelerate the leg into swing (Lipfert et al. 2014; Meinders, Gitter, and Czerniecki 1998; David A. Winter and Robertson 1978) and redirect the body's center-of-mass, reducing collisional energy losses after heelstrike and facilitating economical gait (Donelan, Kram, and Kuo 2002; A. D Kuo, Donelan, and Ruina 2005). Inverse dynamics calculations are commonly used to estimate power about a single joint, but do not account for the behavior of multiarticular musculature,

such as the flexor digitorum and hallucis longus (FDHL) MTUs, which cross the ankle and MTP joints. Based on published ankle and toe kinematics (MacWilliams, Cowley, and Nicholson 2003b) and the multiarticular FDHL functions (McCullough et al. 2011; Bogey, Perry, and Gitter 2005), we expect that inverse dynamics ankle power overestimates net positive MTU power generation during Push-off. Conceptually, this scenario is depicted in Fig. 2.1C. As a consequence, the amount of negative power absorbed by the foot may also be overestimated, which could explain why the foot appears to undermine ankle Push-off (Zelik, Takahashi, and Sawicki 2015). Misestimating ankle or foot kinetics would have important implications on our fundamental scientific understanding of human gait, on musculoskeletal simulations that rely (directly or indirectly) on empirical kinetics estimates, and on assistive devices (e.g., foot prostheses) that are often designed to mimic biological function. However, the magnitude of the power overestimate is currently unknown, as it requires us to account for multiarticular MTU contributions.

Accounting for multiarticular power contributions requires the ability to parse out individual MTU kinetics. Biomechanical estimates such as inverse dynamics are derived directly from empirical recordings; however, these can only approximate net joint kinetics, and cannot resolve individual MTU contributions (Zajac, Neptune, and Kautz 2002; Buchanan et al. 2004). More direct measurements would require a comprehensive set of implantable force and strain sensors, which is impractical for in vivo human experiments. In lieu of direct measures, one common alternative is to develop a complex musculoskeletal simulation to approximate individual MTU contributions (Bogey, Perry, and Gitter 2005; Buchanan et al. 2004; Hamner, Seth, and Delp 2010; Thelen and Anderson 2006; Sartori et al. 2012). These simulations can be powerful tools, enabling direct access to individual MTU behaviors in the model. However, these

simulations typically require many muscle-specific input parameters (e.g., Hill-type muscle models), which are generally not known empirically and which exhibit inter-subject variability. This complexity makes the simulation approach computationally intensive and difficult to validate empirically. Another alternative is to distribute joint-level kinetics (e.g., from inverse dynamics) amongst individual MTUs using simplifying assumptions; for instance, assuming forces are distributed proportionally based on relative muscle size (Farris and Sawicki 2012b), or using a biosignal-to-force mapping algorithm (Sartori et al. 2012; Killian Bouillard, Nordez, and Hug 2011; Bogey, Perry, and Gitter 2005). In this study we employed the latter approach based on electromyography (EMG) recordings. We implemented a data-driven musculoskeletal analysis using a simple EMG-to-force mapping algorithm, which allowed us to approximate individual MTU contributions to gait. We then used this approach to investigate ankle-foot interplay during human walking, and specifically to evaluate the hypothesis that ankle joint Push-off power overestimates net plantarflexor MTU power due to neglected multiarticular dynamics.

## 2.2 Methods

We employed a data-driven musculoskeletal model to determine if inverse dynamics joint power overestimates the net MTU power during the Push-off phase of walking, due to inadvertently subdividing multiarticular MTU power into positive power at one joint (ankle) and offsetting negative power at another (MTP). We conducted a human gait analysis experiment to collect kinematics, kinetics, and surface EMG data. First we computed joint power using a standard inverse dynamics approach. Then, anthropometric and empirical data were combined via a musculoskeletal model to estimate the power contributions from mono- and multi-articular MTUs that cross the ankle. Net MTU power (and work) was then compared to inverse dynamics estimated joint power (and work).

### 2.2.1 Experimental Data Collection

Six healthy subjects (3 males and 3 females, mean±standard deviation, 24±5 years, 88±14 kg, 1.8±0.1 m height) completed a gait analysis study. All subjects gave informed consent to the protocol, which was approved by the Institutional Review Board at Vanderbilt University. The study was performed over two days. The first day was a subject screening session that involved training and verification of EMG signals. Data were collected the second day, to avoid confounds due to muscle fatigue.

The purpose of the screening session (day 1) was to determine if we could independently record surface EMG from the ankle plantarflexor muscles, without excessive signal cross-talk (Zelik, Scaleia, et al. 2014b). Delsys Trigno surface EMG sensors (Delsys, Natick, MA, USA) were placed unilaterally on the participant's major ankle plantarflexor muscles, specifically the triceps surae (soleus, medial gastrocnemius, and lateral gastrocnemius) and peroneus longus,

according to the recommendations of Surface Electromyography for the Non-Invasive Assessment of Muscles (seniam.org), the European project on surface EMG (Hermens et al. 1999). An additional surface EMG sensor, a Delsys Trigno Mini, was placed above the ipsilateral flexor digitorum and hallucis longus (FDHL) muscles. The FDHL muscles are multiarticular in nature and contribute to ankle plantarflexion, longitudinal arch support, and MTP flexion. Due to the proximity of the flexor digitorum longus and flexor hallucis longus muscles at the surface EMG sensing site, the EMG signals were measured together, similar to prior literature (Zelik, Scaleia, et al. 2014b, 2014a; La Scaleia et al. 2014). These plantarflexing muscles were chosen based on their accessibility via surface EMG. Based on our prior experience recording ankle-foot muscles, the primary concern was with soleus muscle cross-talk affecting the FDHL recording (Zelik, Scaleia, et al. 2014b). Subjects were given visual biofeedback of the muscle EMG signals, and asked to activate soleus vs. FDHL separately. If the subject could independently activate their soleus muscle without exhibiting FDHL EMG activation, then they were invited to participate in the day 2 data collection. Six of the seven subjects initially recruited were able to demonstrate separate soleus vs. FDHL signals, and thus these six individuals completed the second day experimental protocol.

The gait analysis session (day 2) involved participants walking on an instrumented treadmill in a motion capture space while collecting EMG signals. We placed surface EMG sensors in the same locations detailed for day 1 and again verified the sensor placement through the day 1 protocol. In addition, 19 retro-reflective motion capture makers were affixed to the subject's ipsilateral shank and foot, similar to marker sets used in prior foot studies (Kelly, Lichtwark, and Cresswell 2015; Leardini et al. 2007), so that ankle and MTP joints, and longitudinal arch motion could be estimated. Prior to walking trials, subjects performed a set of

quasi-static maximum voluntary contraction trials against manual resistance which targeted each of the muscles recorded via EMG. Next, subjects performed walking trials at three speeds (0.75, 1.00 and 1.25 m/s) on a force instrumented split-belt treadmill (Bertec, Columbus, OH, USA), while we recorded ground reaction forces under each foot at 2000 Hz, EMG at 2000 Hz, and kinematics at 100 Hz (Vicon T40, Oxford, UK).

### 2.2.2 Experimental Data Processing

Post-processing was performed using Visual3D software (C-Motion, Germantown, MD, USA) and custom MATLAB (MathWorks, Natick, MA, USA) code. Marker and force data were low-pass filtered at 6 Hz and 15 Hz, respectively. EMG signals were demeaned, high-pass filtered at 150 Hz, rectified, low-pass filtered at 10 Hz (Potvin and Brown 2004; Zelik, Scaleia, et al. 2014b), and then normalized based on the maximum muscle activation magnitude that occurred throughout all of the recorded trials. All filters used were $3^{rd}$ order, zero-lag Butterworth filters. Foot and ankle kinematics were estimated from the motion capture data. Inverse dynamics was used to compute sagittal ankle power. We divided and averaged across strides (from footstrike to ipsilateral footstrike), to obtain subject-specific kinematics, kinetics, and EMG waveforms. We used these averaged measurements as inputs to a musculoskeletal model we developed, implemented in MATLAB, to estimate sagittal plane power contributions from individual ankle-foot MTUs. For reporting and comparison purposes, we computed the peak Push-off power and Push-off work, the latter by integrating underneath the power curve.

### 2.2.3 Musculoskeletal Model

We developed an EMG-driven musculoskeletal model to estimate power contributions

from individual MTUs. The model used was an extension of methods published by Farris and Sawicki (2012). We began by computing inverse dynamics ankle power, $P_{ank}$, from experimental motion and force data. We then combined surface EMG recordings with published anthropomorphic data – physiological cross sectional area (Ward et al. 2008), pennation angle (Ward et al. 2008), and moment arms for each muscle (McCullough et al. 2011), $m$ – to estimate the relative moment (torque) contributions from individual MTUs about the ankle joint, $M'_{m,ank}$. Next we used these EMG-driven model estimates to approximate ankle joint power ($P'_{ank}$), by multiplying the summed MTU moment waveform ($\sum M'_{m,ank}$) by the sagittal plane ankle angular velocity, $\omega_{ank}$ – computed from motion capture data (Eqn. 2.1). Note that "prime" variables (e.g., $P'_{ank}$) are all obtained from the EMG-driven model. The $P'_{ank}$ estimate was then scaled to the peak inverse dynamics ankle power, $P_{ank}$, through the use of a speed- and subject- specific scaling factor $C$, so that $P'_{ank}$ was reported in the units of W/kg. $P'_{ank}$ was then decomposed into individual MTU power contributions. We performed additional computations to account for multiarticular MTU behaviors (as detailed below) and to thereby test our hypothesis that inverse dynamics ankle joint Push-off power overestimates the net power provided by MTUs crossing the ankle. Since the model we used was reasonably similar to previously published approaches we elected to only briefly summarize here; however, for completeness and reproducibility full model details are presented in 2.6 Appendix.

$$P'_{ank}(t) = \sum_{m} P'_{m,ank}(t) = \sum_{m} M'_{m,ank}(t) \cdot \omega_{ank}(t) \qquad \text{[Eqn. 2.1]}$$

### 2.2.4 Model Validation

We performed a model validation test prior to investigating our hypothesis. We

calculated the correlation (coefficient of determination, $R^2$) between model-estimated ankle power, $P'_{ank}$, and inverse dynamics estimated ankle power, $P_{ank}$, at each walking speed. We would lack confidence in our musculoskeletal model if it was unable to reasonably reproduce ankle kinetics.

### 2.2.5 Estimating MTU Power

We estimated net plantarflexing MTU power by examining the contributions of the multiarticular FDHL in two different ways: first for a simplified case by assuming the multiarticular FDHL MTUs act isometrically (i.e., MTUs performed zero net power), and second by estimating FDHL power from ankle and foot kinematics (similar to (Kelly, Lichtwark, and Cresswell 2015). The first case was useful to assess the worst case scenario, i.e., when the net MTU power from the ankle plantarflexors would be smallest in magnitude and, therefore, inverse dynamics would be expected to maximally overestimate net MTU power. This would occur if the multiarticular FDHL MTUs performed no mechanical work (i.e., MTUs acted like a rigid cable). In our model, we computed this minimum MTU power ($P'_{MTU,min}$) by subtracting the FDHL power due to ankle rotation ($M'_{fdhl,ank} \cdot \omega_{ank}$) from the model-estimated net ankle power $P'_{ank}$ (Eqn. 2.2).

$$P'_{MTU,min}(t) = P'_{ank}(t) - P'_{fdhl,ank}(t) \qquad \text{[Eqn. 2.2]}$$

Next, we estimated net MTU power from the ankle plantarflexors without the simplifying (isometric MTU) assumption. Instead we took into account the entire MTU excursion by combining kinematic estimates of angular velocities ($\omega_{ank}$ and $\omega_{mtp}$), moment arms ($r_{fdhl,ank}$ and $r_{fdhl,mtp}$ reported in (McCullough et al. 2011; Stokes, Hutton, and Stott 1979; Aper, Saltzman, and Brown 1996), and longitudinal arch length, $l_{arch}$ (Kelly, Lichtwark, and Cresswell

2015; Leardini et al. 2007), see Fig. 2.2) to estimate power from the multiarticular FDHL MTUs. We first estimated FDHL power contributions about the ankle only (Eqn. 2.3), then FDHL power contributions due to motion within the foot (Eqn. 2.4), and finally summed these to obtain a complete estimate of the net FDHL MTU power (Eqn. 2.5). As an intermediate computation, the rate of FDHL length change due to ankle rotation was attributed to ankle power ($P'_{fdhl,ank}$, Eqn. 2.3), and the rate of change due to longitudinal arch lengthening/shortening and to MTP joint rotation were attributed to foot power ($P'_{fdhl,foot}$, Eqn. 2.4). We then defined the summation of these quantities as the net FDHL MTU power ($P'_{fdhl}$, Eqn. 2.5). This estimate reflects power generated or absorbed by the multiarticular FDHL MTUs themselves rather than estimated contributions about a single joint. This formulation avoids the problem in which a multiarticular MTU's power may be inadvertently subdivided into positive power at one joint and offsetting negative power at another.

$$P'_{fdhl,ank}(t) = \omega_{ank}(t) \cdot r_{fdhl,ank} \cdot F'_{fdhl}(t) \quad \text{[Eqn. 2.3]}$$

$$P'_{fdhl,foot}(t) = \omega_{mtp}(t) \cdot r_{fdhl,mtp} \cdot F'_{fdhl}(t) + \frac{d}{dt}(l_{arch}(t)) \cdot F'_{fdhl}(t) \quad \text{[Eqn. 2.4]}$$

$$P'_{fdhl}(t) = P'_{fdhl,ank}(t) + P'_{fdhl,foot}(t) \quad \text{[Eqn. 2.5]}$$

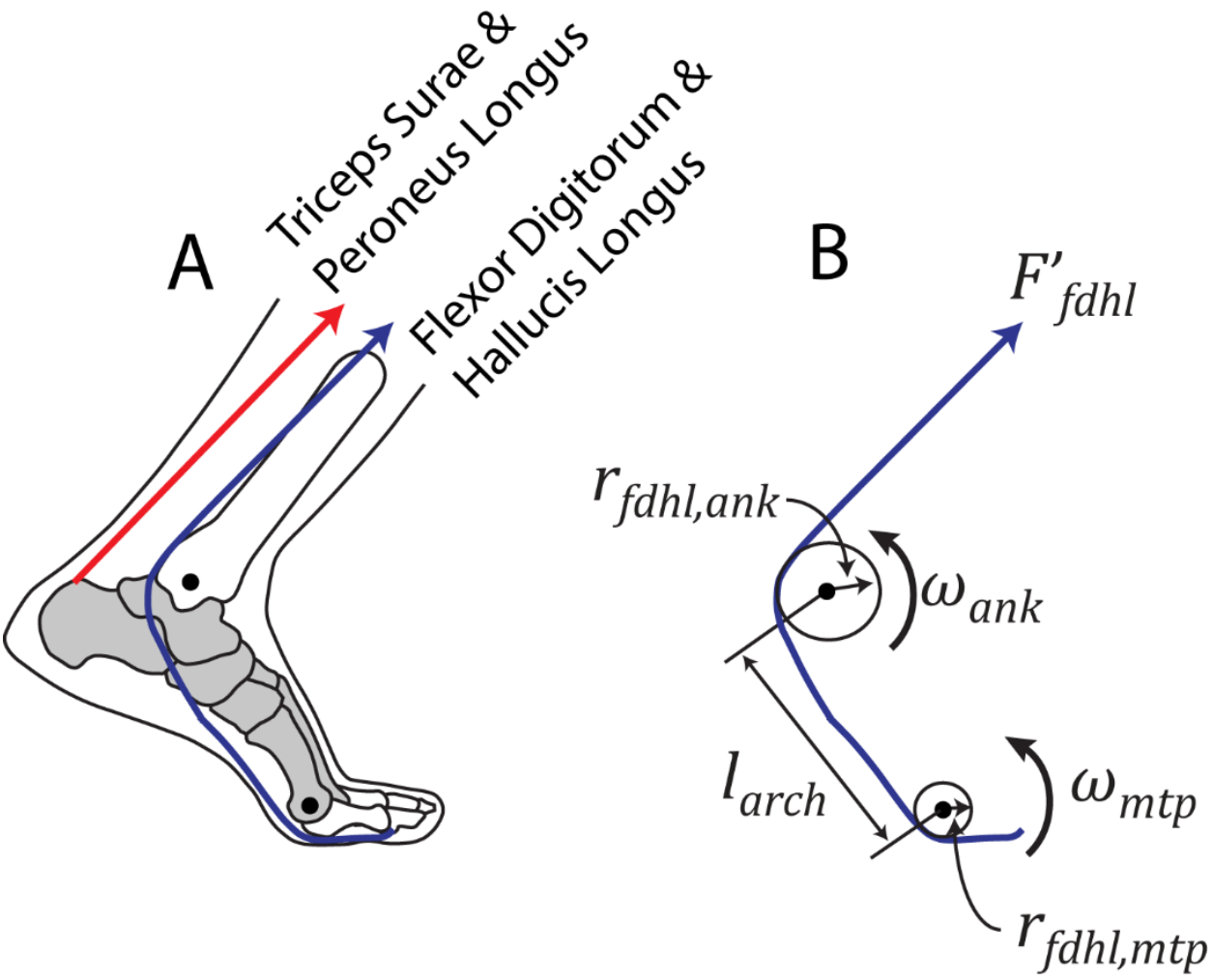


**Figure 2.2 Simplified representation of ankle-foot musculoskeletal model.** This simplified model was used to investigate the ankle plantarflexor muscles during the Push-off phase of walking. (A) The main ankle plantarflexor MTUs were included in the model: triceps surae (soleus and gastrocnemius), the peroneus longus, and the flexor digitorum and hallucis longus (FDHL). See 2.6 Appendix for more details on muscles that were included/excluded. (B) Kinematic, anthropomorphic, and EMG data were used to estimate power contributions from each MTU. An example is depicted for the multiarticular FDHL MTUs. Anthropomorphic MTU moment arms about the ankle ($r_{fdhl,ank}$) and MTP joints ($r_{fdhl,mtp}$) were combined with kinematic estimates – angular velocities of the ankle ($\omega_{ank}$) and MTP joints ($\omega_{mtp}$), and longitudinal arch length ($l_{arch}$) – to estimate time-varying MTU length changes. MTU force was estimated using an EMG-to-force mapping algorithm (see 2.6 Appendix for full details). Force was then multiplied by the rate of MTU length change to compute MTU power.

$P'_{fdhl}$ can then be added to other plantarflexing MTU powers obtained through the

musculoskeletal model in order to estimate the net MTU plantarflexing power ($P'_{MTU}$, Eqn. 2.6). This assumes that power from each other plantarflexor MTU can be approximated by calculating $M'_m \cdot \omega_{ank}$; in other words, we assumed that $P'_{m,ank} = P'_m$ for each of the other MTUs. This is expected for monoarticular MTUs (e.g., soleus) acting only about the ankle joint. This is also reasonable for the gastrocnemii (multiarticular ankle-knee) MTUs during the Push-off phase of walking because the ankle is plantarflexing while the knee is flexing, which both contribute to MTU shortening (i.e., both motions indicate positive MTU power, so we would not predict positive power at one joint and offsetting negative power at the other).

$$P'_{MTU}(t) = \sum_m P'_{m,ank}(t) - P'_{fdhl,ank}(t) + P'_{fdhl}(t) \qquad \text{[Eqn. 2.6]}$$

## 2.3 Results

We found that the EMG-driven model estimated ankle power, $P'_{ank}$, correlated strongly with inverse dynamics ankle power ($P_{ank}$, $R^2 = 0.98 \pm 0.02$ at nominal speed of 1.25 m/s, Fig. 2.3). This finding was consistent across walking speeds tested ($R^2 = 0.97 \pm 0.02$ at 0.75 m/s, $R^2 = 0.97 \pm 0.04$ at 1 m/s). The values reported are inter-subject means and standard deviations.

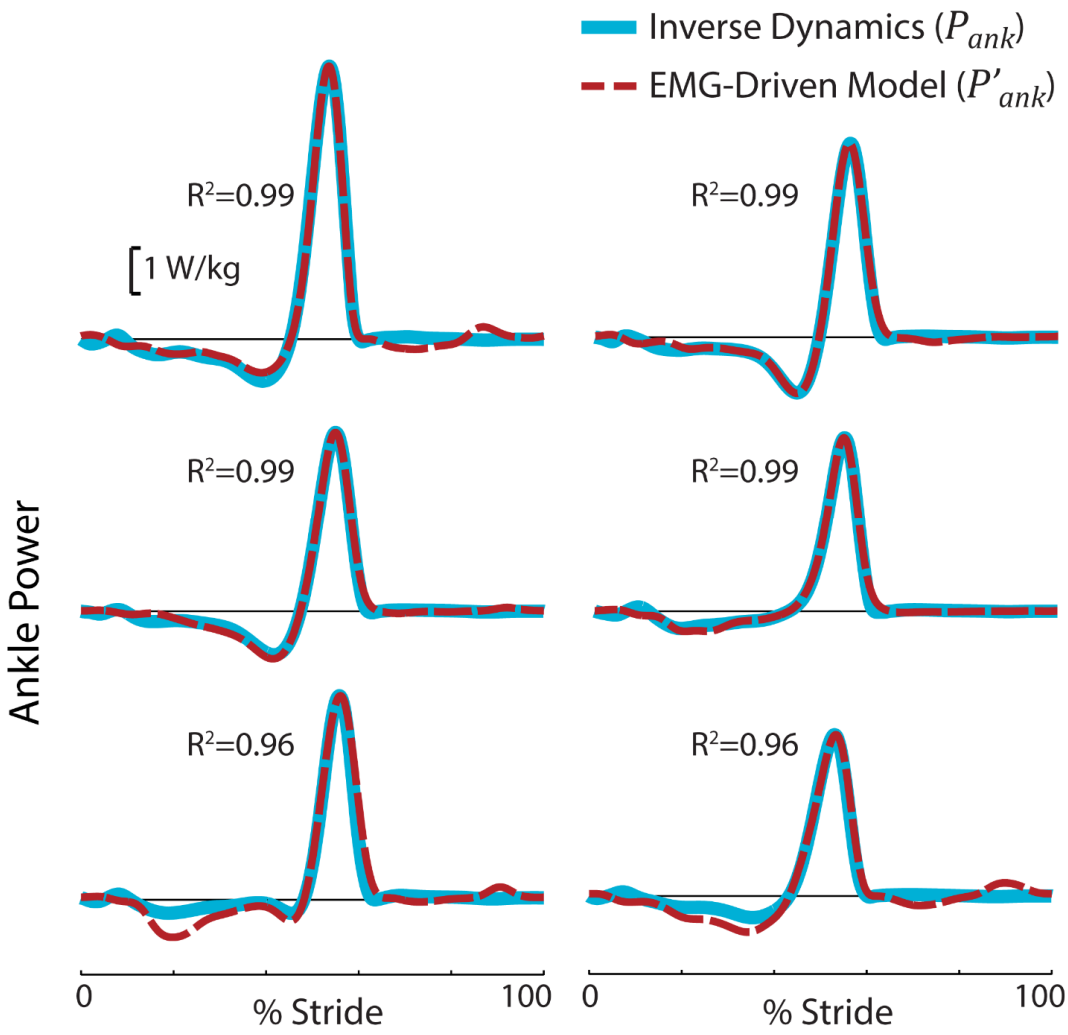


**Figure 2.3 EMG-driven musculoskeletal model was able to reproduce inverse dynamics sagittal plane ankle power.** Results are depicted for each individual subject at 1.25 m/s. The EMG-driven ankle joint power, $P'_{ank}$, (red dashed line) correlated strongly with inverse dynamics ankle power, $P_{ank}$, (blue solid line).

We computed individual MTU contributions, including contributions from the multiarticular FDHL MTUs (Fig. 2.4). The peak $P'_{ank}$ during Push-off was dominated by triceps surae power (89.0%) while the FDHL and peroneus longus MTUs contributed 6.9% and 4.1%, respectively.

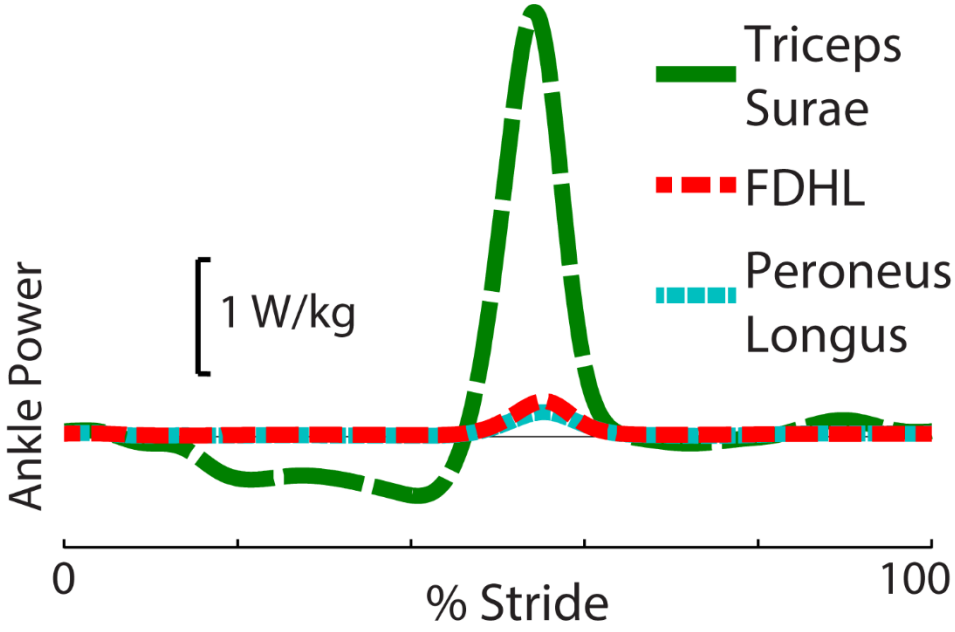


**Figure 2.4 Average MTU contributions to $P'_{ank}$ at 1.25 m/s.** Estimated MTU contributions are shown for the triceps surae, flexor digitorum and hallucis longus (FDHL), and peroneus longus (*N*=6).

Next, we estimated the minimum plantarflexing MTU power ($P'_{MTU,min}$) and work, by assuming isometric behavior of the FDHL MTUs during Push-off. We found that peak $P'_{ank}$ overestimated peak $P'_{MTU,min}$ by 7.0% (19.7 ± 10.5 W) at 1.25 m/s. This corresponded with Push-off work differences of 7.4% (1.7 ± 0.8 J, Fig. 2.5). Mean overestimates for peak Push-off power and Push-off work at 0.75 m/s were 4.8% and 5.0%, and at 1.00 m/s were 6.2% and 6.4%, respectively.

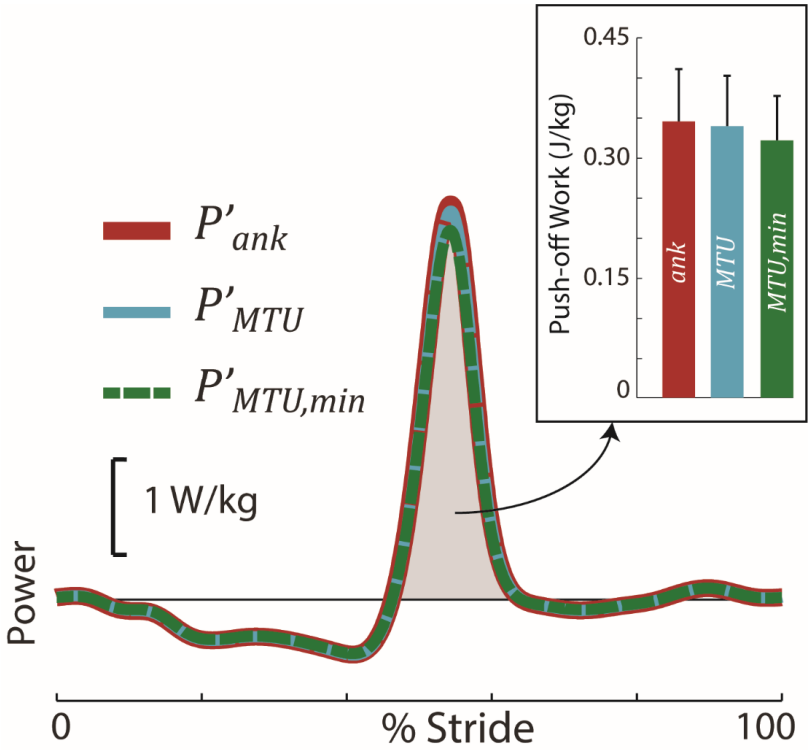


**Figure 2.5 Net ankle power vs. minimum MTU power vs. MTU power during human walking at 1.25 m/s (N=6).** Net ankle power overestimated MTU power and minimum MTU power by about 2% and 7%, respectively, due to multiarticular FDHL dynamics. Inset: Push-off work (area under the power curve within the shaded region) exhibited similar, relatively small differences.

We then relaxed the isometric MTU assumption and computed the net planarflexing MTU power ( $P'_{MTU}$). We found that the FDHL MTUs behaved nearly isometrically, but did lengthen and shorten slightly during Push-off. As such, we found that peak $P'_{ank}$ overestimated peak $P'_{MTU}$ by 1.7% (5.1 ± 2.9 W) at 1.25 m/s, which corresponded with 1.8% (0.4 ± 0.3 J) more Push-off work (Fig. 2.5). Mean overestimates for peak Push-off power and Push-off work at 0.75 m/s were 1.2% and 1.3%, and at 1.00 m/s were 1.6% and 1.7%, respectively.

## 2.4 Discussion

We developed an EMG-driven musculoskeletal model to investigate if net ankle joint power overestimates net plantarflexor MTU power during the Push-off phase of human gait due to neglected multiarticular MTU dynamics. Our EMG-driven model enabled us to estimate individual MTU kinetics during the walking cycle, and account for multiarticular contributions that are not captured by conventional inverse dynamics analysis. We found that ankle power only slightly overestimates net MTU power; nominally by about 2% at 1.25 m/s, but possibly as much as 7% if the FDHL MTUs behave more isometrically than we estimate from motion capture skin markers on the shank and foot. Therefore, the FDHL MTU dynamics do not substantially confound the interpretation of net MTU power from inverse dynamics during Push-off. This EMG-driven modeling approach may be useful for investigating larger multiarticular MTUs (e.g., hamstrings) and other locomotor activities, to improve our multi-scale understanding of movement biomechanics (i.e., linking joint-level biomechanical estimates to our understanding of underlying MTU dynamics).

Various approaches have been taken in the past to characterize muscle- or MTU-specific contributions. One approach assumes that inverse dynamics joint torques are distributed amongst muscles, proportional to their size (Farris and Sawicki 2012b). However, this approach does not account for muscle-specific activation patterns. A more complex approach involves the generation and analysis of musculoskeletal simulations (Hamner, Seth, and Delp 2010; Sartori et al. 2012; Thelen and Anderson 2006; Buchanan et al. 2004; Bogey, Perry, and Gitter 2005), which can examine a larger set of muscles, including small or deep muscles that are difficult to measure experimentally. Simulations can be developed using cost function optimizations to solve for muscle activation patterns (Hamner, Seth, and Delp 2010; Buchanan et al. 2004; Thelen and

Anderson 2006), or alternatively can be driven by bio-signals such as EMG (Sartori et al. 2012; Bogey, Perry, and Gitter 2005; Lloyd and Besier 2003). In the former case, the simulations require the researcher to define a cost function that approximates the subject-specific neural control strategy, which is difficult to identify, validate, and may not be generalizable across tasks. In the latter case, when simulations are bio-signal-driven, they typically require various muscle-specific input parameters (e.g., for Hill-type muscle models), which are generally not known empirically and which exhibit inter-subject variability. Both cases require high technical expertise to create these musculoskeletal simulations, which can be prohibitive for clinical research; although current efforts are being made to bridge this gap. To avoid these limitations we employed a simpler, empirically-driven approach, which we found to be adequate to estimate MTU-specific contributions about the ankle during the Push-off phase of human gait. Our method utilizes a simple EMG-to-force algorithm, and requires only one scaling and one time delay factor, which are automatically solved for based on empirical data.

Our EMG-driven model results compared favorably with inverse dynamics estimates and with previously published musculoskeletal model results. We observed a strong correlation between our model estimated power, $P'_{ank}$ , and inverse dynamics, $P'_{ank}$ (mean $R^2 \geq 0.97$ for all speeds). These correlations were similar to published $R^2$ values for a more complex ankle model using Hill-type muscles (Krishnaswamy, Brown, and Herr 2011). Additionally, the relative contributions from MTUs were similar to those estimated by musculoskeletal simulations based on Hill-type muscles. To draw this comparison, we used model-based force outputs published in Bogey et al. (2005) to estimate individual MTU power, then compared their relative MTU contributions to our model. This was accomplished by multiplying the published MTU forces by the ankle moment arms and ankle angular velocity used in our study. When comparing our

results versus those calculated from Bogey et al. (2005), we found that peak ankle Push-off power was dominated by triceps surae contributions (89.0% vs. 91.6%) and had similar FDHL contributions (6.9% vs. 6.1%).

There are several limitations to the modeling approach we employed, and its generalizability must be further explored and validated. Here we expound upon the limitations and assumptions detailed in the model derivation in the 2.6 Appendix. We assumed that MTU force production scaled linearly with EMG magnitude since the ankle-foot muscles are known to operate close to isometrically during Push-off (Fukunaga et al. 2002; Kirane, Michelson, and Sharkey 2008; Ishikawa et al. 2005). However, this linear relationship may breakdown for tasks involving more eccentric or concentric contractions. It may be necessary to develop new methods for empirically estimating MTU force from bio-signal or imaging modalities. Additionally, we implemented a simplified 2D (sagittal) analysis of forward walking, and further work would be needed to extend this approach to 3D analysis. Furthermore, this approach is dependent on estimates of maximal EMG activation, which are difficult to obtain and validate (Zhou, Suresh, and Rymer 2007). To better understand the implications of this limitation, we performed an informal Monte Carlo sensitivity analysis on maximum EMG activation. For each muscle we randomly varied maximum muscle activation from 50-150% of the measured max value, and then recomputed power variables during Push-off. We found that our quantitative power estimates were not substantially altered, and thus did not affect the conclusions drawn in this study. A final limitation to acknowledge is that our current model estimates net power from each MTU, but does not resolve mechanical power into contributions from muscle fibers vs. tendinous tissues. A grand challenge in the field remains to develop a unified, multi-scale biomechanical understanding, which for instance would enable us to confidently decompose

joint-level kinetics into individual MTU kinetics, and then to further decompose these into muscle vs. tendon contributions.

There may be other limitations of inverse dynamics that also cause it to overestimate net MTU power, aside from multiarticular FDHL dynamics. For instance, multisegment foot models have previously shown that the rigid-body foot assumption, common in most inverse dynamics calculations, can lead to an overestimate of peak ankle power by up to 53% (35% on average) due to unmodeled degrees-of-freedom within the foot (Bruening, Cooney, and Buczek 2012b). Similarly, deformable-body foot estimates indicate that when the ankle and foot are considered together that the peak power is reduced by 25-40% (Takahashi and Stanhope 2013; Zelik, Takahashi, and Sawicki 2015). These empirical estimates suggest that the foot may dissipate a significant portion of the Push-off power performed about the ankle, or that peak ankle power is simply overestimated by rigid-body inverse dynamics. Based on the results of this current study, which indicate relatively small contributions from the FDHL MTUs, it does not appear that the previously observed foot absorption can be explained away by unmeasured multiarticular dynamics. The functional role of this apparent foot absorption during Push-off in walking remains an open question; and it remains unclear if or how this behavior should be integrated in assistive technologies such as foot prostheses.

Moving forward, the EMG-driven modeling approach presented here may be applied to additional segments and joints within the body to further examine multiarticular MTU contributions during movement. In this study we investigated contributions from relatively small multiarticular MTUs that cross the ankle and toes joints, but further study is needed to understand how larger multiarticular MTUs affect our empirical biomechanical estimates. We focused this study on the FDHL MTUs in order to examine whether their unmodeled dynamics

affect our ability to infer net MTU power from joint power during a key phase of the human gait cycle. Muscles such as the gastrocnemius and biceps femoris are larger than the FDHL muscles (in terms of PCSA, (Ward et al. 2008), and are expected to contribute more significantly to joint kinetics (van Ingen Schenau, Bobbert, and Rozendal 1987), which may lead to larger discrepancies between joint-level and MTU-level kinetics estimates. This could affect our biomechanical understanding of walking, or other movement tasks. EMG-driven modeling may be a useful tool for future investigations and could be extended using complementary measurement modalities. For instance, incorporating B-mode ultrasound could potentially enable us to parse biomechanical contributions from muscles vs. tendons, or ultrasound elastography could provide an alternative way to estimate MTU-specific force (Killian Bouillard, Nordez, and Hug 2011).

## 2.5 Conclusion

In summary, we developed and applied an EMG-driven musculoskeletal model to investigate the degree to which net ankle power overestimates net MTU power during the Push-off phase of human walking, due to neglected multiarticular dynamics. The presented EMG-driven model reproduced ankle joint power with high fidelity, and provided insight on mono- and multi-articular MTU contributions. We found that the behavior of the FDHL MTUs may cause inverse dynamics ankle power to slightly overestimate the net positive power generated by plantarflexion MTUs during Push-off, but only by ~2-7%. This data-driven modeling approach could be applied to better account for other multiarticular MTU contributions, such as from the gastrocnemius or biceps femoris, to improve our multi-scale biomechanical understanding of human locomotion.

## 2.6 Appendix: EMG-Driven Musculoskeletal Model

We employed a musculoskeletal model similar to an approach taken by Farris and Sawicki (2012), except that we used an EMG-to-force mapping algorithm rather than assume force was distributed proportionally to muscle size. This modeling approach was used rather than a more complex musculoskeletal simulation (e.g., based on Hill-type muscles), because it required the selection/calibration of fewer unknown parameters. The model was used to gain insights into ankle plantarflexor MTU contributions during the Push-off phase of walking.

We utilized a simple EMG-to-force mapping algorithm to estimate MTU-specific contributions to ankle plantarflexion. For each muscle, $m$, we used the EMG envelope, muscle size and fiber pennation angle to estimate an unscaled, time-varying force profile, $F'_{m,unsc}$. $EMG_m$, the normalized EMG signal for each muscle, was defined as a function of time, $t$, and EMD, $\tau$. Next, the EMG envelope was scaled by the muscle physiological cross sectional area, $PCSA_m$, to account for size differences between muscles (Ward et al. 2008, Table 2.1). Then the EMG envelope was scaled by the cosine of the pennation angle, $\theta_m$, to account for muscle fiber direction, assuming a constant $\theta_m$ for each muscle (Ward et al. 2008, Table 2.1). The unscaled force profile ($F'_{m,unsc}$, Eqn. 2.a1) was assumed to be proportional to MTU force (A. L. Hof 1984), but not yet in units of force (e.g., Newtons per kilogram). To obtain a MTU force estimate, $F'_m$, in units of Newtons per kilogram, we needed an additional subject- and speed-specific scaling factor, $C$ (Eqn. 2.a2).

$$F'_{m,unsc}(t) = PCSA_m \cdot \cos(\theta_m) \cdot EMG_m(t-\tau) \quad [2.a1]$$

$$F'_m(t) = PCSA_m \cdot \cos(\theta_m) \cdot EMG_m(t-\tau) \cdot C \quad [2.a2]$$

**Table 2.1 Ankle plantarflexion muscle properties and maximum plantarflexion torque.** The maximum achievable muscle torque ("Maximum Torque" above) was assumed to be

proportional to the muscle moment arm (McCullough et al. 2011) multiplied by physiological cross sectional area (PCSA) (Ward et al. 2008) and the cosine of the pennation angle (Ward et al. 2008). Percentages reflect the relative contributions if all muscles were simultaneously maximally contracting.

| Muscle | Moment Arm ($r_m$) (mm) (McCullough et al. 2011) | PCSA ($cm^2$) (Ward et al. 2008) | Pennation Angle ($\theta_m$) (°) (Ward et al. 2008) | Maximum Torque (%) |
|---|---|---|---|---|
| Soleus | 53.1 | 51.8 | 28.3 | 51.9 |
| Medial Gastrocnemius | 53.1 | 21.1 | 9.9 | 23.6 |
| Lateral Gastrocnemius | 53.1 | 9.7 | 12.0 | 10.8 |
| Flexor Hallucis Longus | 24.0 | 6.9 | 16.9 | 3.4 |
| Flexor Digitorum Longus | 15.3 | 4.4 | 13.6 | 1.4 |
| Peroneus Brevis | 16.7 | 4.9 | 11.5 | 1.7 |
| Peroneus Longus | 20.8 | 10.4 | 14.1 | 4.5 |
| Tibialis Posterior | 8.9 | 14.4 | 13.7 | 2.7 |
| Total | - | - | - | 100.0 |

This simplified EMG-to-force mapping algorithm has several limitations. This analysis ignores the effects of other muscle properties such as the force-velocity and force-length relationships on EMG (Buchanan et al. 2004). Additionally, this analysis ignores the passive structures within the ankle, since structures such as ligaments act primarily at the limits of the range of motion of the ankle (David A. Winter 2009). These angular limits are not reached during normal walking.

We then estimated the unscaled moment profile that each MTU creates about the ankle joint. The unscaled muscle moment , $M'_{m,j,unsc}$ (Eqn. 2.a3, Fig. 2.6), was obtained by multiplying the unscaled force profile, $F'_{m,unsc}$, with the sagittal plane plantarflexion moment arm ($r_{m,j}$, for joint $j$), estimated from prior cadaveric observation (McCullough et al. 2011). Moment arms were assumed to be constant, which prior studies suggest is a reasonable first-order approximation given the ankle's range of motion during walking (Zelik and Kuo 2010; McCullough et al. 2011). This simplified estimate treats the ankle as a single degree-of-freedom rotational joint, which captures the majority of ankle kinetics during forward walking (Buczek et

al. 1994).

$$M'_{m,j,unsc}(t) = r_{m,j} \cdot F'_{m,unsc}(t) \quad [2.a3]$$

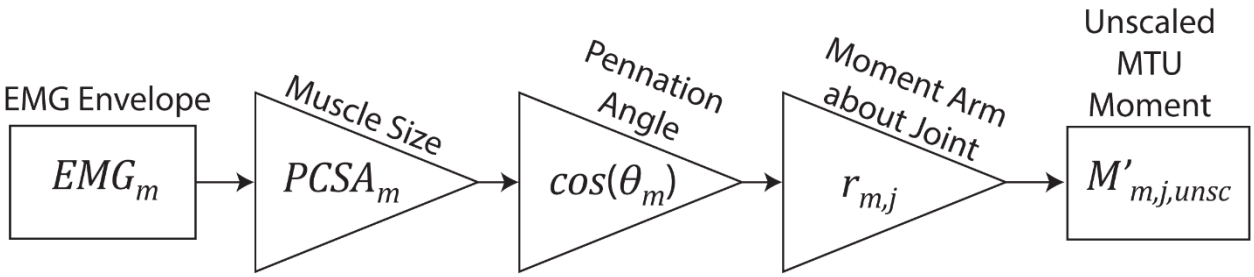


**Figure 2.6 EMG-Driven Model Stage I.** For each muscle (or group of muscles) the EMG envelope was multiplied by its physiological cross sectional area ($PCSA_m$), the cosine of the pennation angle ($\theta_m$), and the muscle moment arm about the joint of interest ($r_{m,j}$) – the ankle – to estimate the unscaled MTU moment profile about the ankle ($M'_{m,j,unsc}$). Scaling of this moment profile into units of Nm/kg was performed in Stage II of the model. The boxes indicate a measurement/outcome, the arrows represent a signal/waveform, and the triangles indicate multiplication.

We estimated the net MTU power profile, by summing the MTU-specific moments about the ankle ($\sum M'_{m,j,unsc}$) then multiplying the resultant profile with ankle angular velocity ($\omega_{ank}$), obtained from motion capture (see Fig. 2.7). First, we needed to account for the EMD between muscle activity and mechanical force production (Viitasalo and Komi 1981; Dieën et al. 1991). To do so, we computed $P'_{ank}$ for varying values of $\tau$ (Eqn. 2.a1), then found the EMD that yielded the maximum correlation with sagittal ankle power from inverse dynamics, $P_{ank}$. We termed this maximally correlated profile as the unscaled ankle plantarflexor power profile ($P'_{ank,unsc}$, Eqn. 2.a4). This power profile is equivalent to summing power estimates form each individual muscle about the ankle ($P'_{m,ank,unsc}$). We assumed the same (constant) EMD for all muscles.

$$P'_{ank,unsc}(t) = \sum M'_{m,ank,unsc}(t) \cdot \omega_{ank}(t) = \sum P'_{m,ank,unsc}(t) \quad [2.a4]$$

Next we scaled the magnitude of this model-estimated ankle power, so that it could be directly compared to mass normalized inverse dynamics based estimates (in Watts per kilogram, see Fig. 2.7). We computed the subject- and speed-specific scaling factor, $C$, by dividing the peak inverse dynamics sagittal plane ankle power ($P_{ank}$) by the peak unscaled ankle plantarflexor power profile ($P'_{ank,unsc}$). We assumed that the antagonistic dorsiflexor MTUs perform negligible power during Push-off, which is consistent with the absence of tibialis anterior EMG activity during this phase of gait (David A. Winter and Yack 1987; Zelik, Scaleia, et al. 2014b). We assumed that joint friction and foot inertia were also negligible. Additionally, we assumed that our plantarflexor muscle recordings adequately reflected the total plantarflexor contributions, which seemed reasonable given that the set of muscles recorded account for greater than 95% of the plantarflexion moment generating capabilities (see Table 2.1). Unmeasured plantarflexor muscles were the tibialis posterior, peroneus brevis, and plantaris. The tibialis posterior does have a moderate PCSA (Ward et al. 2008), but acts at a small (sagittal plane) moment arm (McCullough et al. 2011) compared to the other plantarflexor muscles and exhibits a relatively low EMG activation during gait (Murley et al. 2009; Ringleb et al. 2007), suggesting that its torque contributions are small (Table 2.1). Similarly, the peroneus brevis is expected to have a relatively small maximum torque contribution to plantarflexion (Zelik, Scaleia, et al. 2014b, Table 2.1). Finally, the plantaris is a small muscle that is only expected to contribute weakly to the ankle plantarflexion moment. It is rarely reported in literature and is in fact a muscle that is absent in about 10% of the population (Danforth 1924). The resultant model outcome, $P'_{ank}$, is an EMG-based estimate of ankle power (Eqn. 2.a5); however, as opposed to inverse dynamics, this model-based estimate enables us to parse ankle power into contributions

from individual MTUs.

$$P'_{ank}(t) = P'_{ank,unsc}(t) \cdot C = \sum \left( P'_{m,ank,unsc}(t) \cdot C \right) = \sum P'_{m,ank}(t) \qquad [2.a5]$$

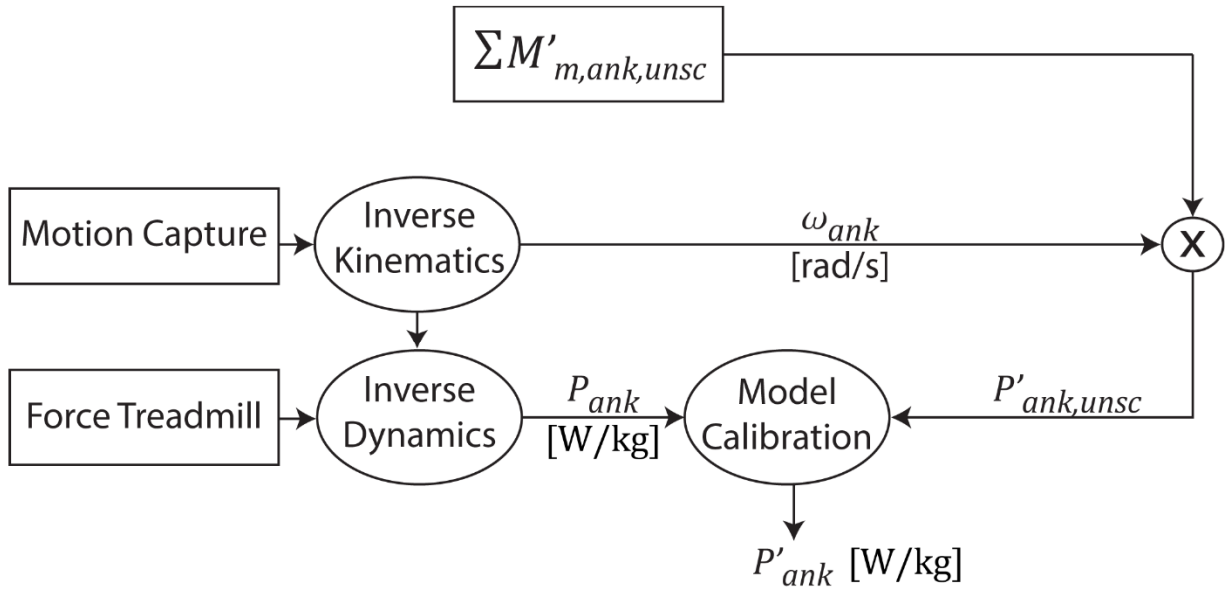


**Figure 2.7 EMG-Driven Model Stage II.** The sum of the unscaled muscle moments about the ankle from Stage I was multiplied by sagittal plane ankle angular velocity ($\omega_{ank}$) resulting in an unscaled ankle plantarflexor power profile ($P'_{ank,unsc}$). This profile was then scaled appropriately by matching peak inverse dynamics ankle power ($P_{ank}$); part of the model calibration. This resulted in an EMG-based estimate of ankle power ($P'_{ank}$) in units of W/kg. The boxes indicate a measurement/outcome, the arrows represent a signal/waveform, and the ovals represent an algorithm.

# Chapter 3

# Ankle and Foot Power in Gait Analysis: Implications for Science, Technology and Clinical Assessment

## 3.1 Introduction

Muscles and tendons about the ankle, knee and hip are typically considered the main mechanical power producers during human gait. Using inverse dynamics to estimate net power generated about these joints has become ubiquitous in human gait analysis studies (David A. Winter 1991; D. G. E. Robertson et al. 2013; David A. Winter 2009). Substantial effort has gone into characterizing how ankle, knee and hip kinetics are adapted during different locomotor tasks and varying task intensities (e.g., Farris and Sawicki 2012a; David A. Winter 1984, 1983a; Zelik and Kuo 2010), and understanding how power about each of these three joints contributes functionally to movement biomechanics (e.g., (Mann and Hagy 1980; Inman, Ralston, and Todd 1981; Perry 1992; Levine, Richards, and Whittle 2012; Zelik and Adamczyk 2016). However, in gait analysis studies, far less attention has been given to power contributions from the foot.

Foot power, the rate of mechanical work performed collectively by active and passive structures of the foot (sometimes including the shoe), is not typically estimated in gait analysis studies (Zelik, Takahashi, and Sawicki 2015). The standard convention in the gait analysis field is to model the entire foot as a single rigid-body segment, which neither absorbs nor generates mechanical power. This convention is found throughout biomechanics textbooks (Ranchos Los Amigos National Rehabilitation Center 2001; Baker 2013; Whittle 2014; David A. Winter 2009; Inman, Ralston, and Todd 1981; D. G. E. Robertson et al. 2013), and is reflected in commonly-

used motion capture marker sets. However, there is compelling evidence that foot power contributes meaningfully to walking (Takahashi and Stanhope 2013; Takahashi, Kepple, and Stanhope 2012; Siegel, Kepple, and Caldwell 1996; Zelik, Takahashi, and Sawicki 2015; Bruening, Cooney, and Buczek 2012b; MacWilliams, Cowley, and Nicholson 2003) and running (Stefanyshyn and Nigg 1997; Riddick and Kuo 2016; Kelly, Lichtwark, and Cresswell 2015; McDonald et al. 2016; Stearne et al. 2016), due to a complex biomechanical interplay between muscles and passive structures (Kelly et al. 2014; Ker et al. 1987; Venkadesan et al. 2017; Zelik, Scaleia, et al. 2014b).

Currently there remains a lack of clarity in the scientific literature regarding if, when and how foot power should be calculated in the study of gait biomechanics. A critical question looms: is modeling the entire foot as one rigid-body segment, which neither absorbs nor generates mechanical power, adequate for addressing the types of the scientific questions that are commonly investigated in gait analysis studies, or adequate for obtaining biomechanical estimates that properly inform the design, prescription and evaluation of clinical interventions (e.g., foot prostheses)? Here we present experimental evidence and analytical arguments suggesting that, in many cases, neglecting foot power is inadequate for scientific studies and may be inappropriate (misleading) for clinical gait analysis or informing technology development.

The purpose of this article is two-fold: (i) to use case study examples in conjunction with analytical arguments and prior literature to highlight *why* foot power should be estimated within the context of whole-body or lower-limb gait analysis studies, and then (ii) to discuss *how* to experimentally estimate (and interpret) foot and ankle power. This article is principally intended for individuals who employ conventional gait analysis methods (e.g., 3 degree-of-freedom (3DOF) rigid-body inverse dynamics) to understand bio- or neuro-mechanical aspects of human

locomotion, to inform device design, or to evaluate clinical interventions. Some of the observations contained within this article may be banal or obvious to foot experts and enthusiasts. But if so, this is all the more reason to resolve the discontinuity between scientists, engineers and clinicians focused specifically on the foot, and those who use gait analysis methods such as inverse dynamics to more broadly investigate how constituents of the body (e.g., individual joints, segments, muscles or tendons) contribute to whole-body movement.

## 3.2 Methods

We performed two gait analysis case studies that exemplify how and why to compute foot power, and implications on ankle power. The first case study was on a healthy individual during treadmill walking at fixed speed. We used an extended marker set to compute and contrast various estimates of ankle power, foot power, and combined ankle plus foot (termed *anklefoot*) power. The second case study involved a person with unilateral transtibial amputation walking sequentially on eight different prosthetic feet. We computed anklefoot power for each of the prostheses, and also for the biological limb. We contrasted estimates of anklefoot power against one of the most commonly-used ankle estimates (3DOF rotational Ankle power, which neglects foot power contributions). Power calculations are summarized below, followed by a discussion of key terminology, then experimental protocol details.

### 3.2.1 Power Calculations

Figure 3.1 summarizes the various power estimates computed in this study: two estimates of ankle power and four estimates of anklefoot power. See Supplementary Material (3.6-8 Appendices) for comprehensive details on calculations. All estimates are based on inverse dynamics analysis, but each estimate uses a slightly different model and/or different underlying assumptions. To maximize generalizability of our conclusions, we focused on a subset of analyses that can be estimated from ground reaction forces and motion capture measurements, which are common in many gait analysis studies. Estimation methods that require additional measurement modalities (e.g., pressure, (MacWilliams, Cowley, and Nicholson 2003b) or specialized data collection protocols (e.g., Bruening et al., 2012a; Scott and Winter, 1993; Takahashi et al., 2017) were not included in our present study, nor were *in vitro* approaches.

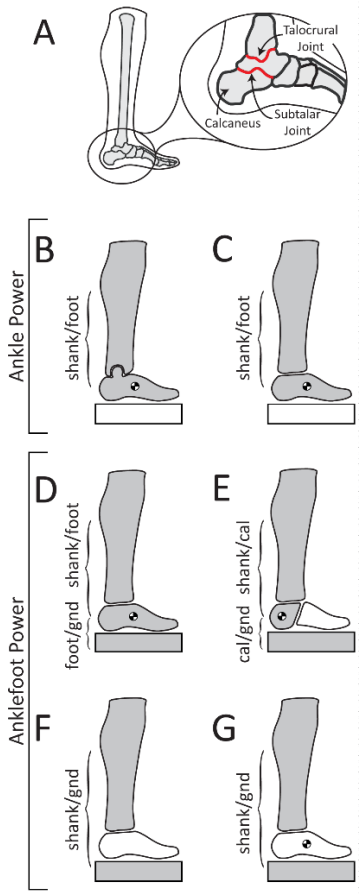


**Figure 3.1 Methods to compute ankle and anklefoot power.** (A) Biological ankle joint complex (AJC), comprised of the talocrural and subtalar anatomical joints. (B) 3DOF Ankle: rotational power between the shank and foot. All other power estimates are 6DOF (capturing rotational and translational power). (C) Ankle: rotational and translational power between the shank and foot. Methods (B) and (C) only estimate ankle dynamics, assuming a single rigid-body foot segment, but do not estimate power due to the motion of the foot relative to the ground (gnd). (D) Ankle + Distal Foot: anklefoot power computed by summing power of shank relative to foot plus power of foot relative to the ground. This method also assumes a single rigid-body foot segment. (E) AJC + Distal Calcaneus: anklefoot power computed by summing power of the shank relative to the calcaneus (cal) plus power of the calcaneus relative to the ground. This method does not treat the entire foot as a single rigid-body segment; rather it only assumes a portion of the foot, the calcaneus, is rigid. (F) Distal Shank: anklefoot power due to motion of the shank relative to the ground. This estimate assumes negligible foot mass and inertia. (G) Intersegmental: power flow in/out of a given landmark; in this case, the distal end of the shank. This estimate can be formulated to include (or not include) effects due to foot mass and inertia. Gray signifies segments (and the ground in anklefoot cases) used to compute power. Brackets indicate power calculated between two grey segments. White indicates that power was not explicitly computed relative to a given segment or the ground. The center-of-mass symbol on a segment signifies that the mass and moment of inertia of this segment were used in the calculation of power. See Supplementary Material (3.6 Appendix A) for detailed explanations and equations for each method.

### 3.2.2 Terminology

Here we define and clarify key terminology. First, we distinguish an *anatomical joint* vs. the model of an anatomical joint. Anatomical joint is used to specify the physical interface between two adjacent anatomical structures in the body. The term anatomical ankle joint refers specifically to the talocrural joint (Wu et al. 2002), located between the talus bone in the foot and the bones of the shank (tibia and fibula, see Fig. 3.1A). The term anatomical *ankle joint complex* (*AJC*) describes, collectively, the subtalar joint (talus-calcaneus anatomical joint, Fig. 3.1A) and the anatomical ankle joint. In effect, the AJC describes the interaction between the shank and the calcaneus (Wu et al. 2002). In contrast, the term *joint* is used in this manuscript to signify the modeled biomechanical interaction between two body segments (or between one body segment and the ground). Note that two segments need not be adjacent to each other to model a joint between them. For instance, the AJC is comprised of two anatomical joints, but the net relative motion between the shank and calcaneus can nonetheless be modeled/quantified as a single equivalent 6 degree-of-freedom (6DOF) joint. Also note that a joint can be modeled in various other ways, such as assuming a 1DOF rotational hinge, or a 3DOF ball-in-socket joint (Fig. 3.1B). 1DOF and 3DOF joints are the most prevalent models used in the gait analysis literature, while 6DOF joints provide the most comprehensive estimates (Buczek et al. 1994; Duncan, Kowalk, and Vaughan 1997; Zelik, Takahashi, and Sawicki 2015). Unless otherwise specified, joints (and thus joint powers) modeled in this study are 6DOF (3 rotational, 3 translational).

The lower-case term *ankle power* is used, colloquially and in a general manner, to signify the net power due to all structures – muscle-tendon units and other passive tissues – acting about the anatomical ankle joint. This is necessary because there is no consistent usage of the term ankle power in literature. Lower-case terms *foot power* and *anklefoot power* are used in an

analogous colloquial manner.

Capitalized power terms refer to specific experimental estimates, as detailed hereafter. The capitalized term *Ankle power* refers to estimates that model the interaction between a rigid-body shank and rigid-body foot (Fig. 3.1 B,C). Typically, skin-mounted markers are distributed over the shank, and also over the foot (e.g., from the calcaneus to the metatarsal heads). The foot is tracked in space as if it were a single rigid-body segment. These data are then used to compute either 3DOF (rotational) Ankle power, or 6DOF (rotational and translational) Ankle power. *AJC power* refers to estimates that model the interaction between a rigid-body shank and rigid-body calcaneus segment. In other words, the calcaneus is treated as its own rigid-body, separate from the rest of the foot. The calcaneus bone is sufficiently large and superficial that it can typically be tracked reasonably well with skin-mounted markers (MacWilliams, Cowley, and Nicholson 2003b; Reinschmidt et al. 1997; Stebbins et al. 2006). AJC power (or a similar hindfoot power) is often estimated in multi-segment foot modeling studies (Bruening, Cooney, and Buczek 2012b, 2012a; Dixon, Böhm, and Döderlein 2012; Leardini et al. 2007; Stebbins et al. 2006; Westblad et al. 2002); however, AJC power is otherwise uncommon in gait analysis studies. As detailed in the Discussion and 3.6 Appendix A, AJC power likely provides a better estimate of plantarflexor muscle-tendon contributions (than Ankle power), given that the soleus and gastrocnemius muscles insert onto the calcaneus, and that the mid-foot is known to undergo substantial motion during locomotion (Bruening, Cooney, and Buczek 2012b; Kelly, Lichtwark, and Cresswell 2015; MacWilliams, Cowley, and Nicholson 2003).

*Distal Segment power* refers to the power due to 6DOF motion of a rigid-body segment relative to the ground, thereby estimating the combined contributions from all structures and anatomical joints distal to a given segment. In other words, Distal Segment power describes

6DOF joint power between a given segment and the ground (see 3.7 Appendix B for detailed derivation). For instance, *Distal Foot* power signifies net power due to the 6DOF motion of the rigid-body foot segment relative to the ground. Similarly, *Distal Calcaneus* power signifies the power due to 6DOF motion of the calcaneus relative to the ground. Distal Foot power and Distal Calcaneus power are sometimes referred to as deformable-body estimates because they are often interpreted to reflect power due to deformation of structures within the foot segment (Takahashi, Kepple, and Stanhope 2012). However, it is important to note that methodologically these Distal Segment estimates do not directly measure or model soft tissue deformations (e.g., using finite element analysis). Rather, each method is simply a type of rigid-body inverse dynamics analysis that estimates mechanical power due to the relative motion of two bodies which are each assumed to be rigid (analogus to prior work on human-exosuit interface dynamics, Yandell et al., 2017). Distal Segment power estimates can then, in certain situations, be used to infer the kinetics of deformable structures located between the two rigid bodies (Fig. 3.1, see 3.7 Appendix B for further details), circumventing the need to apply more complex finite element methods from continuum mechanics.

The term anklefoot power encompasses a variety of different estimates of power due to relative motion between the shank and ground (Fig. 3.1). The names of specific anklefoot power estimates are capitalized: Ankle + Distal Foot (Fig. 3.1D), AJC + Distal Calcaneus (Fig. 3.1E), Distal Shank (Fig. 3.1F) and Intersegmental (Fig. 3.1G, Prince et al., 1994). See 3.6 Appendix A for further explanation of each anklefoot estimate.

Finally, note that our preferred terminology throughout the article is principally in relation to the assumed rigidity of the entire foot: we discuss the consequences of modeling the entire foot as a single rigid body (Fig. 3.1B-D) vs. not assuming the entire foot is a single rigid

body (Fig. 3.1E-G). An alternative way of phrasing this same distinction is in terms of *foot segmentation*: in essence, here we are discussing the consequences of estimating power when modeling the foot as a single segment (Fig. 3.1B-D) vs. assuming multiple segments of the foot (Fig. 3.1E), and vs. being segmentally-agnostic (in which we make no assumptions about how the foot is modeled/segmented, Fig. 3.1F-G).

### 3.2.3 Case Study 1

The purpose of this case study was to present an example of each of the ankle and anklefoot power estimates during normal walking, with a focus on biological limb function. A healthy female participant (23 years, 1.73 m tall, 61 kg) walked on a level, instrumented treadmill at 1.25 m/s (a typical walking speed) barefoot and then at the same speed with shoes (New Balance Fresh Foam 1080, a common running shoe). Twenty-two steps were analyzed from each walking condition. Prior to the study, the subject gave informed consent to the protocol which was approved by the Vanderbilt University Institutional Review Board. The subject had 24 passive reflective markers attached to her lower limbs (Fig. 3.2A). Markers were placed on the pelvis (4), and unilaterally on the thigh (4), knee (2), shank (4), ankle (2), calcaneus (5), and forefoot (3). We collected ground reaction forces (Bertec) and motion capture data (Vicon) at 1000 and 200 Hz, respectively. Force data were low-pass filtered at 10 Hz, and motion data at 6 Hz, using a 3rd order, zero-lag Butterworth filter. We then computed each ankle and anklefoot power estimate (Fig. 3.1, 3.6 Appendix A). We compared 6DOF Ankle power and each of the 4 anklefoot power estimates vs. a commonly-used gait analysis estimate, 3DOF Ankle power. This comparison highlights the importance of including foot power in gait analysis. We also compared the two methods that partition ankle vs. foot power (i.e., Ankle +

Distal Foot power vs. AJC + Distal Calcaneus power, Fig. 3.1). This comparison exemplifies how the choice of inverse dynamics method can affect scientific interpretations of foot and ankle function.

### 3.2.4 Case Study 2

The purpose of this case study was to apply ankle and anklefoot power estimates to a variety of prostheses, then to show how methodological choices can affect comparisons between (and interpretations of) different feet. This case study exemplifies the importance of including foot power (i.e., computing anklefoot power rather than just ankle power) when comparing clinical interventions like prosthetic feet, and when assessing the degree to which they restore biological limb function. An individual with unilateral, transtibial amputation (37 years, 1.78 m tall, 81 kg, male) walked sequentially on 8 different prosthetic feet (Table 3.1) at 1.25 m/s. Eight walking trials (one per prosthesis) were performed on a split-belt, force-instrumented treadmill (Bertec). For each trial, 14-19 strides were analyzed (after removing unusable data due to cross-over steps). The subject provided written, informed consent prior to participation. Each prosthetic foot was aligned by a certified prosthetist, and worn inside the same shoe. The same prosthetic socket was used for all conditions, and no adjustments to the socket were made after beginning the study. The subject was given a few minutes to acclimate to each foot; most of which he was already accustomed to wearing since he had worn them at home prior to participating in this experiment. Ground reaction forces and lower-body kinematics were simultaneously recorded during walking trials, at 2000 Hz and 100 Hz, respectively. 34 retroreflective motion capture markers were placed on the subject (Fig. 3.2B): pelvis (4), right/left thigh (8), right/left knee (4), right shank (4), left socket (4), right ankle (2), right foot

(3), left prosthesis/shoe (5). Force data were low-pass filtered at 10 Hz, and motion data at 6 Hz, using a 3rd order, zero-lag Butterworth filter. We then computed each ankle and anklefoot power estimate, except AJC + Distal Calcaneus power (since many prostheses either do not have, or differ considerably from, the calcaneus morphology of the human foot). Although the past decade has seen an increase in the use of anklefoot power analysis for prosthetic studies (Adamczyk, Roland, and Hahn 2017; Collins and Kuo 2010; De Asha et al. 2013; Ebrahimi, Goldberg, et al. 2017; Morgenroth et al. 2011; Segal et al. 2012; Takahashi, Horne, and Stanhope 2014; Wezenberg et al. 2014; Zelik et al. 2011a), the use of conventional 3DOF Ankle power is still the *de facto* standard (e.g., Crimin et al., 2014; Sawers and Hahn, 2011). Therefore, we compared conventional 3DOF Ankle power estimates vs. 6DOF Ankle power, and vs. each anklefoot power estimate (besides AJC + Distal Calcaneus power). For the Intersegmental power calculation, we did not include the inertial terms because we did not measure the moment of inertia for each individual prosthesis.

Statistical comparisons were not performed on the case study results. Case studies were intended to serve as clear, tangible examples of how methodological choices can affect estimates of ankle and foot biomechanics. All generalized conclusions and recommendations are based on analytical arguments and/or corroborated by previously published, multi-subject gait analysis studies.

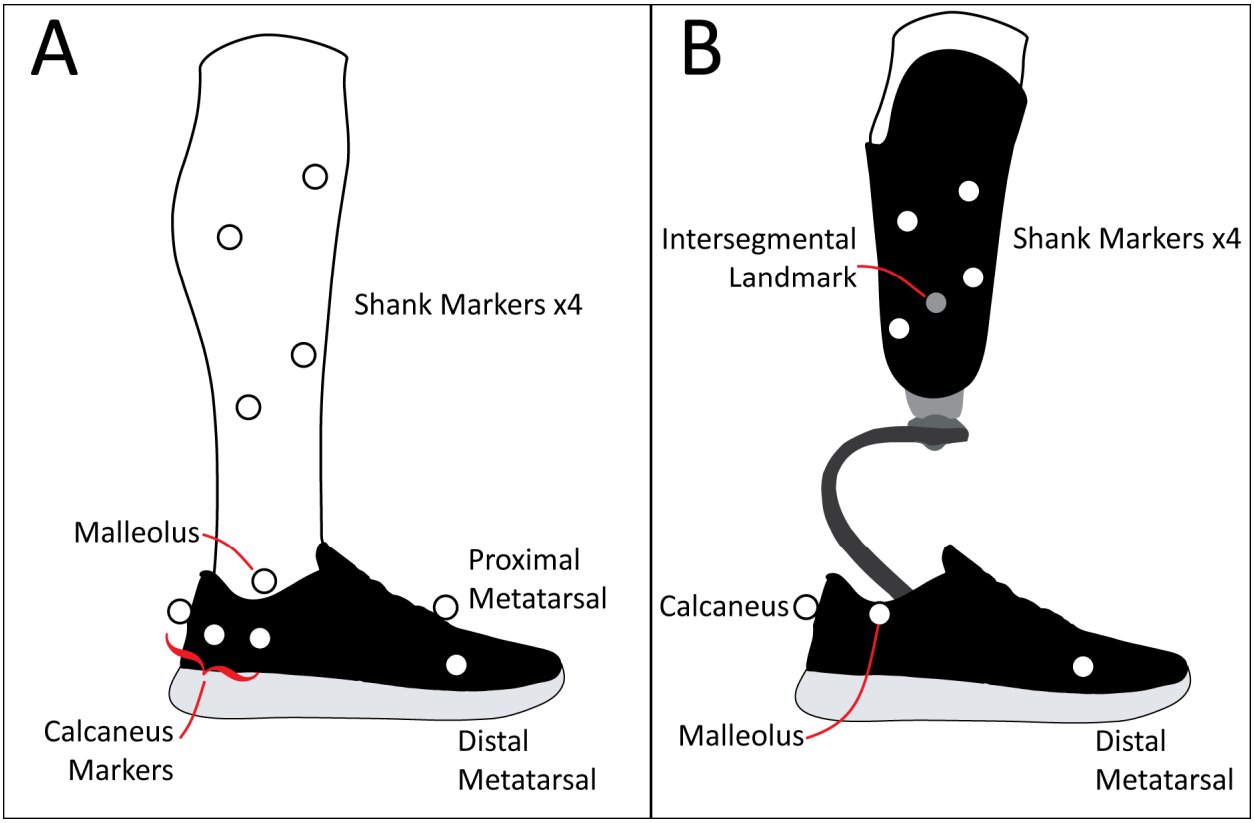


**Figure 3.2 Motion capture marker sets.** Lateral view shown for case study 1 (A) and case study 2 (B). (A) This marker set was used to track the shank, calcaneus and foot. Shown here is the shod case. The marker set for the barefoot case was identical. Shank motion was determined from the four shank markers. Ankle joint center was approximately midway between the medial malleolus (not shown, behind foot) and lateral malleolus markers. The calcaneus motion was determined from five markers: one on the posterior of the shoe/foot, one on the sustsentaculum tali (ST, on medial side of the foot), one on the peroneal trochlea (PT, the most anterior of the calcaneus markers shown), one between the posterior calcaneus and the ST (on medial side of the foot), and one between the posterior calcaneus and the PT. Foot segment motion was determined by four markers: one posterior on the calcaneus, two on the distal heads of 1st and 5th metatarsals (one shown) and one on the proximal head of the 1st metatarsal. (B) Prosthesis side marker set used to track the shank and the foot. Four markers on the socket were used to track the motion of the shank. The Intersegmental landmark (virtual marker, gray) was defined to be midway between the two most distal shank markers. The ankle joint center was defined as midway between the medial and lateral malleolus markers (lateral one shown). On the intact limb these markers were placed on the malleoli and on the affected limb, these markers were placed on the shoe. Foot motion was estimated by the motion of three markers: one posterior on the calcaneus and two on the approximate location of distal heads of 1st and 5th metatarsals (one shown). The intact foot mirrored this marker placement.

**Table 3.1 Prosthetic feet in case study 2.** Reported weight is the prosthesis inside the foot shell and shoe.

| Prosthesis | Weight (kg) |
|---|---|
| Rush | 1.12 |
| All-Pro | 0.81 |
| Vari-Flex XC | 1.06 |
| Soleus | 1.07 |
| Panthera | 0.92 |
| Kinterra | 1.07 |
| Game Changer | 1.09 |
| Raize | 1.58 |

## 3.3 Results

### 3.3.1 Case Study 1

Ankle power estimates were similar with both 3DOF and 6DOF methods in terms of peak power and positive work (Fig. 3.3). These findings are consistent with prior studies, each on 10 subjects (Buczek et al., 1994; Zelik et al., 2015). Anklefoot power estimates were also similar to each other (Fig. 3.3). This result is consistent with Takahashi et al. (2012), who previously demonstrated strong similarity between Distal Shank power and Ankle + Distal Foot power. However, Ankle power and positive work were substantially greater than anklefoot power and work, for all anklefoot estimation methods. This result is consistent with Zelik et al. (2015, N=10) and Takahashi and Stanhope (2013, N=11).

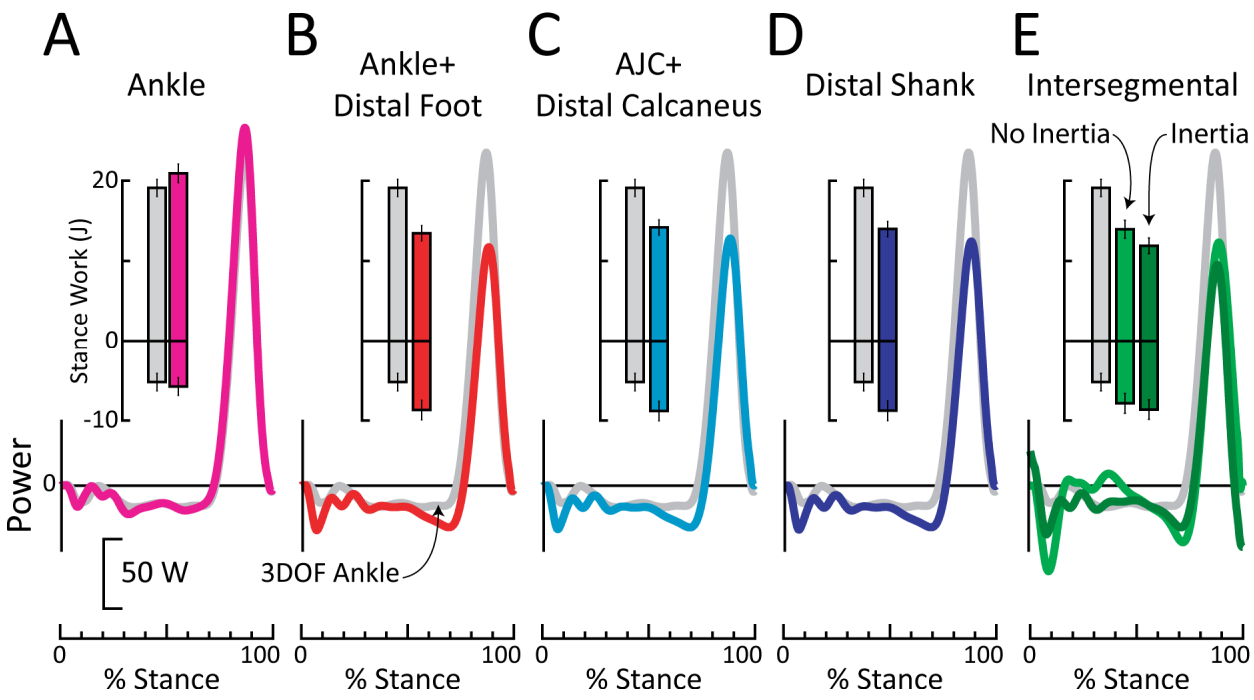


**Figure 3.3 Ankle and anklefoot power and work for barefoot walking of able-bodied individual at 1.25 m/s.** Each Ankle or anklefoot power is plotted over the stance phase of gait, relative to conventional 3DOF Ankle power (gray curve, representing power due to rotation of the shank relative to the foot). Inset bars represent positive and negative work over stance phase of gait. Standard deviation bars represent inter-step variability. (A) 6DOF (rotational + translational) Ankle power (pink) was similar to 3DOF (rotational) Ankle positive power (grey). (B-E) Peak 3DOF Ankle power was ~40% (~70 W) higher than peak anklefoot power estimates, and positive 3DOF Ankle work was ~40% (~6 J) higher than anklefoot positive work estimates. (B) Ankle + Distal Foot power (red). (C) AJC + Distal Calcaneus power (cyan). (D) Distal Shank power (blue). (E) Intersegmental power (green), assuming zero foot mass and inertia. When foot mass and inertia were included into the calculation of Intersegmental power (dark green), then peak power was decreased by 16 W and positive work decreased by 2 J over stance phase, relative to Intersegmental power calculation that neglected foot mass and inertia.

Ankle + Distal Foot power was nearly identical to AJC + Distal Calcaneus power (Fig. 3.4); however, there were substantial differences between Ankle vs. AJC power, and Distal Foot vs. Distal Calcaneus power (Fig. 3.4).

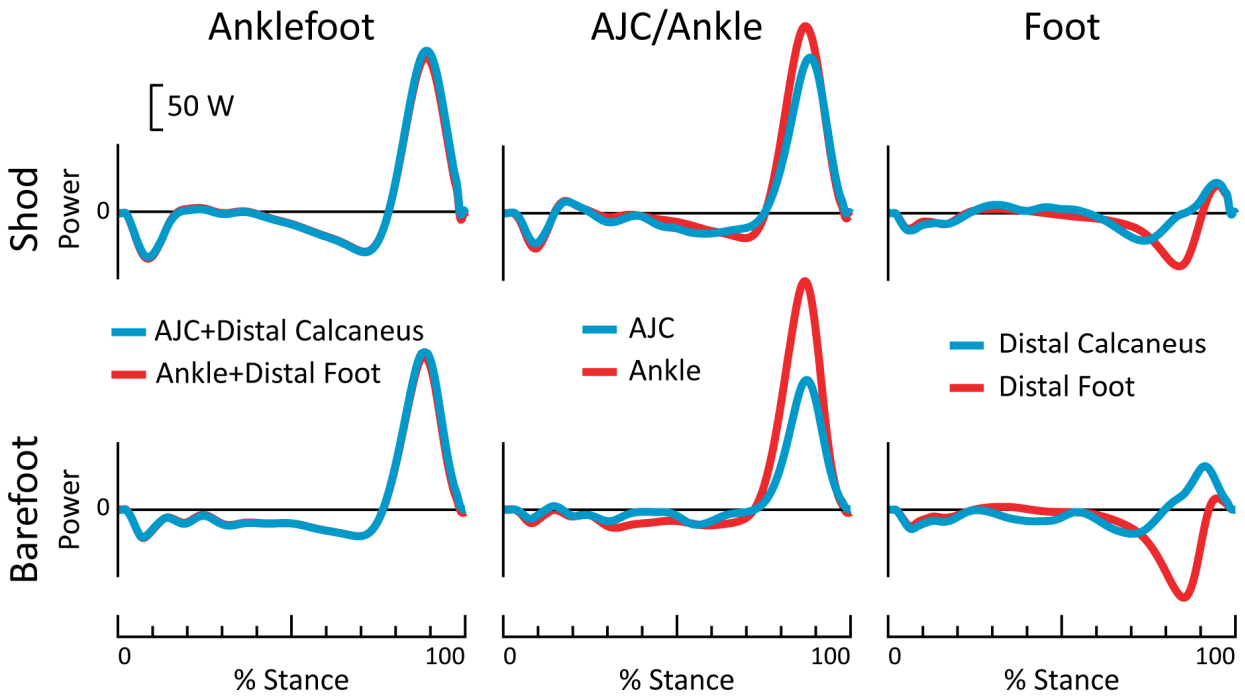


**Figure 3.4 Power calculations relative to foot vs. relative to calcaneus, for able-bodied individual during shod (top row) and barefoot (bottom row) walking at 1.25 m/s.** Both methods yielded very similar anklefoot power. However, large differences were observed in the partitioning Ankle/AJC vs. foot power sources. Peak Ankle (shank-foot) power was 20% (35 W) higher than peak AJC (shank-calcaneus) power during shod walking, and 77% higher (112 W) during barefoot walking. Positive Ankle work was 21% (3 J) and 79% (9 J) higher than positive AJC work during shod and barefoot walking, respectively. The magnitude of Distal Foot negative work was 53% (3 J) and 77% (5 J) more than the magnitude of Distal Calcaneus work during shod and barefoot walking, respectively. The magnitude of Distal Foot positive work was 45% (1 J) and 81% (3 J) less than the magnitude of Distal Calcaneus work during shod and barefoot walking, respectively.

### 3.3.2 Case Study 2

Anklefoot power estimates generally yielded similar results to each other when applied to prosthetic feet. An example is depicted in Fig. 3.5. For most prostheses, anklefoot power estimates differed substantially from 3DOF Ankle power, in terms of positive and/or negative power. However, the sign and magnitude of this difference was prosthesis-specific. For instance, three of eight prostheses showed fairly similar positive work (energy return) when comparing Distal Shank power estimates to 3DOF Ankle power, one prosthesis showed considerably more

positive work, and four prostheses showed substantially less positive work for the Distal Shank estimate (Fig. 3.6). Prosthesis-specific variability was also observed for negative work (energy absorption, Fig. 3.6).

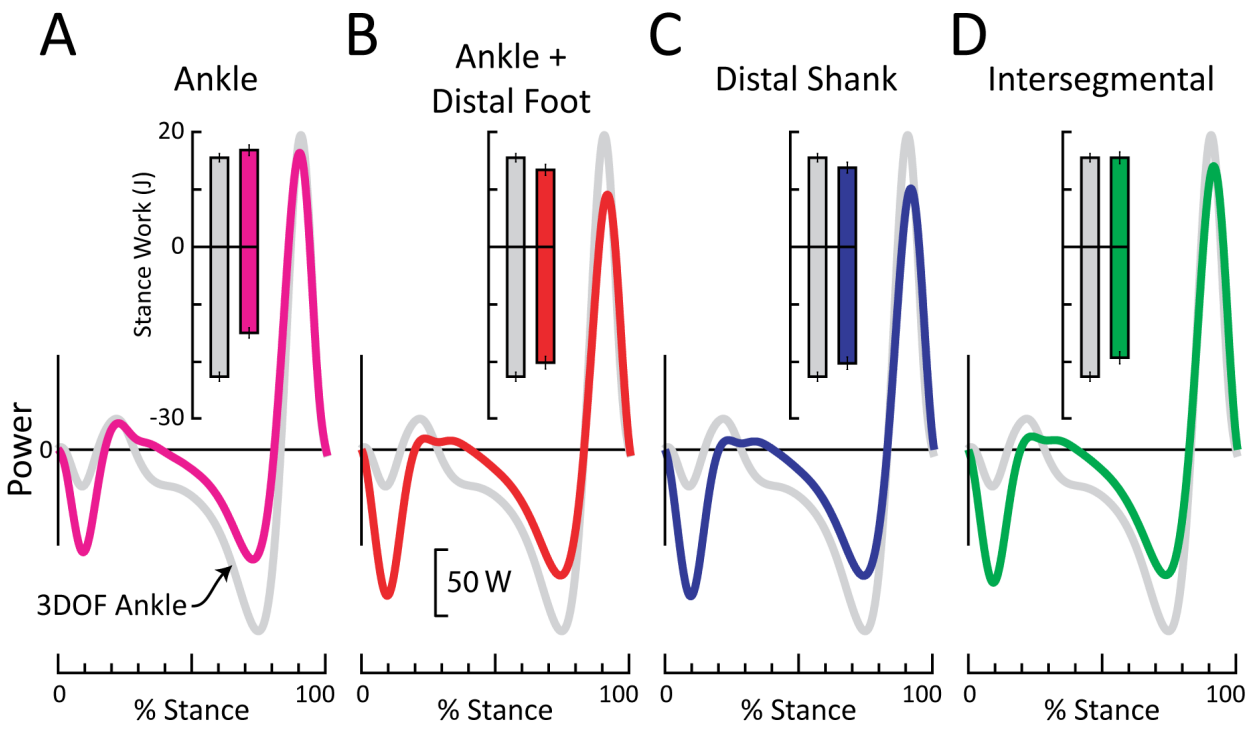


**Figure 3.5 Ankle and anklefoot power for an example prosthesis (All Pro) during walking at 1.25 m/s.** Each ankle or anklefoot power is plotted over the stance phase of gait, relative to conventional 3DOF Ankle power (gray curve, representing power due to rotation of the shank relative to the foot). Inset bars represent positive and negative work over stance phase of gait. Standard deviation bars represent inter-step variability. (A) 6DOF Ankle power (pink). When comparing 6DOF vs. 3DOF Ankle estimates, this particular prosthesis exhibited less negative work, slightly more positive work and similar peak power. (B) Ankle + Distal Foot power (red). (C) Distal Shank power (blue). (D) Intersegmental power (green), assuming zero foot mass and inertia. These different anklefoot estimates yielded power curves similar to each other. However, compared to 3DOF Ankle power, the anklefoot powers exhibited more negative power after foot contact (0-20% of stance), less negative power in mid-stance (40-85% stance), and slightly less positive power at the end of stance.

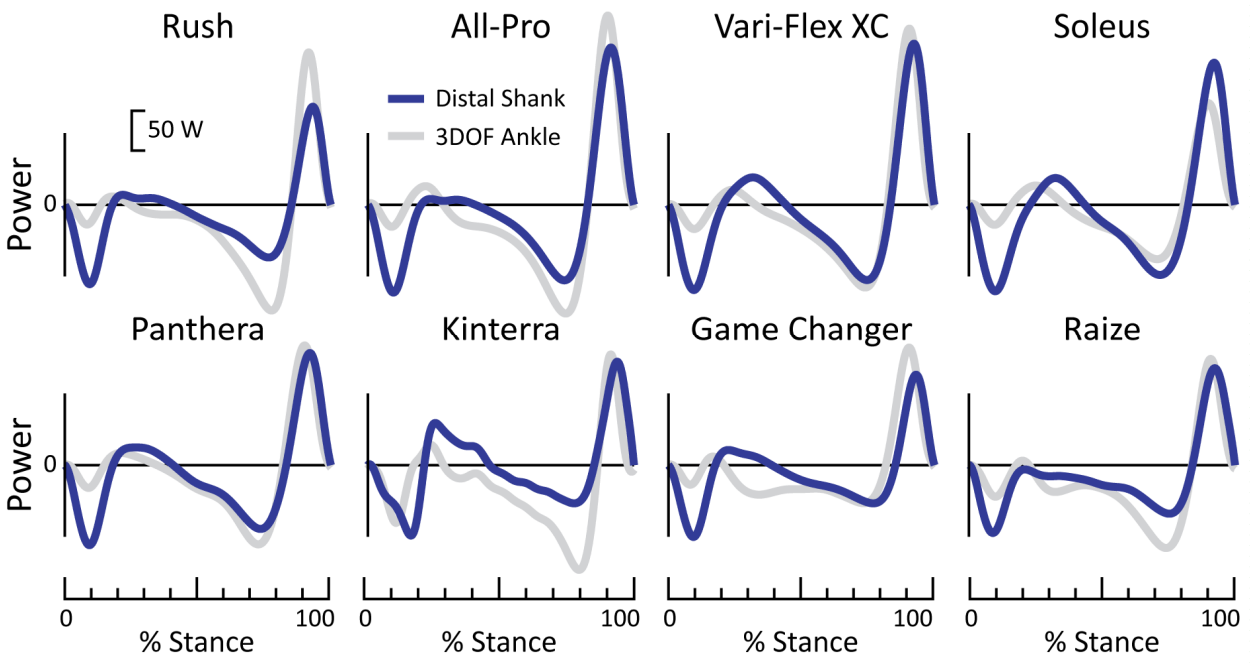


**Figure 3.6 Anklefoot (Distal Shank) power vs. 3DOF Ankle power for all 8 prostheses during walking at 1.25 m/s.** For all prostheses, the anklefoot power exhibited more negative power after foot contact (0-20% stance), relative to 3DOF Ankle power. For most prostheses, anklefoot power exhibited less negative power in mid-stance (~40-85% stance). Peak anklefoot power was notably less than 3DOF Ankle power for 4 of 8 prostheses (Rush, All Pro, Vari-Flex XC and Game Changer), roughly equivalent for 3 of 8 prostheses (Panthera, Kinterra and Raize), and greater for one prosthesis (Soleus).

Intact vs. prosthetic limb power differences were generally larger when using conventional 3DOF Ankle power analysis, than when estimating anklefoot power. A striking example was with the Soleus foot (Fig. 3.7). Based on 3DOF Ankle power analysis, the peak prosthetic Ankle power and positive Ankle work were 193 W and 12 J lower than the intact limb. However, when Distal Shank power was computed, these differences decreased by ~60-70% to 78 W and 4 J, indicating much more symmetry between intact and prosthetic limbs. On average (across all 8 feet), intact limb 3DOF peak Ankle power was 147 W higher than the prosthetic

limb; however, peak Distal Shank power was only 100 W higher. Similarly, intact limb 3DOF positive Ankle work was 13 J higher than the prosthetic limb, whereas this difference was only 8 J when computing Distal Shank power.

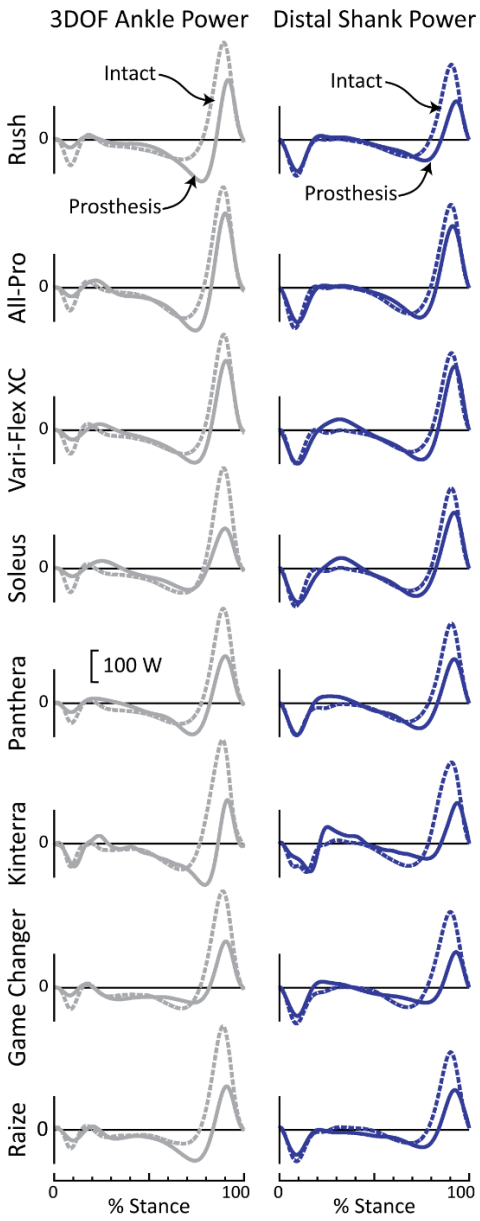


**Figure 3.7 Ankle and anklefoot power for intact (dashed) vs. prosthetic (solid) limb, while an individual walked on 8 different prostheses at 1.25 m/s.** 3DOF Ankle power estimates (left column) showed greater asymmetry between intact vs. prosthetic limb power generation, as compared to anklefoot power (Distal Shank, right column).

## 3.4 Discussion

These case studies exemplify problems that can arise when the entire foot is treated as a single rigid-body segment. Below we discuss scientific, clinical and technological implications, which highlight *why* it is important to include foot power in gait analysis studies; either explicitly by computing it, or implicitly by taking the (non-rigid) anatomy of the foot into account when estimating power about the ankle. Based on these empirical examples, analytical arguments and corroborating evidence from prior literature, we then recommend *how* to estimate biological and prosthetic power. In short, we recommend against computing conventional Ankle (shank-foot) power, and instead suggest AJC (shank-calcaneus) power as a more physiologically-relevant alternative. We also recommend estimating foot power, either using Distal Calcaneus (calcaneus-ground) power in addition to AJC (shank-calcaneus) power, or within a combined anklefoot power calculation (Fig. 3.1). Relaxing the assumption that the entire foot is a rigid body and including foot power in gait analysis is expected to enhance the quality and completeness of biomechanical estimates, help ensure proper evaluation of clinical interventions, and better inform the design of biomimetic devices.

### 3.4.1 Scientific Implications

Here we highlight two specific scientific implications, one related to the foot, and one to the ankle. First, treating the entire foot as a rigid body can skew our understanding of biological foot function. In the extreme, yet common case when only Ankle power is computed, the foot is implicitly assumed to contribute negligible power; however, there is substantial evidence to the contrary (Bruening, Cooney, and Buczek 2012b; Dixon, Böhm, and Döderlein 2012; Ker et al. 1987; MacWilliams, Cowley, and Nicholson 2003; Takahashi, Worster, and Bruening 2017;

Zelik, Takahashi, and Sawicki 2015). The more critical point to bring to bear is that even if Distal Foot power is computed, scientific interpretations of biological foot function may still be skewed because the entire foot is assumed to be a single rigid body. This is evident when comparing Distal Foot vs. Distal Calcaneus power (Fig. 3.4). Distal Foot power indicates a large amount of energy absorption, particularly during the Push-off (end-of-stance) phase of gait (Takahashi, Kepple, and Stanhope 2012; Zelik, Takahashi, and Sawicki 2015). Interpreting Distal Foot power to signify net power due to structures within the foot is (and has been) perplexing because: (i) such foot energy absorption would undermine the beneficial Push-off power generated about the ankle (A. D Kuo 2002; Arthur D. Kuo and Donelan 2010; Zelik and Adamczyk 2016), and (ii) this dissipative behavior of the foot is inconsistent with the more spring-like behavior of the foot arch and plantar fascia observed in prior *in vivo* and *in vitro* studies (Ker et al. 1987; Stearne et al. 2016). However, both these issues are resolved by computing Distal Calcaneus power instead, which does not model (or track) the entire foot as a single rigid-body segment (Fig. 3.1E, see 3.6 Appendix A). Functionally, the foot appears to be returning substantial energy in late Push-off (see Distal Calcaneus positive power in Fig. 3.4) and not dissipating large amounts of energy (per Distal Foot negative power in Fig. 3.4). Takahashi et al. (2017, $N$=14) provides more extensive corroborating evidence. We interpret these results to signify that Distal Foot power overestimates net energy dissipation by structures in the foot during the Push-off phase of gait. Thus it is not recommended to assume the entire foot is a single rigid-body segment in gait analysis; particularly when the goal is to understand net power contributions from the foot.

Second, treating the entire foot as a rigid body can distort our understanding of the ankle plantarflexors. Our results suggest that Ankle power (both 3DOF and 6DOF) overestimates

Push-off power generated by calf muscle-tendon units (MTUs). Figure 3.4 shows that Ankle power (which assumes a rigid foot) was 77% higher than AJC power (which only assumes the calcaneus is rigid) during barefoot walking, and 20% higher during shod walking. These findings are corroborated by multi-subject studies using multi-segment foot models. Various studies have found that Ankle (shank-foot) Push-off power was substantially overestimated – by an average of 66% (MacWilliams, Cowley, and Nicholson 2003b), 74% (Dixon, Böhm, and Döderlein 2012), 35% (Bruening, Cooney, and Buczek 2012b) and 27% (Segal et al. 2018) – as compared to an estimate of AJC (shank-calcaneus) power that is based on a multi-segment modeling approach. Ankle power tends to overestimate power generated by the ankle plantarflexor MTUs for the following reason: When the foot is modeled as a single rigid body, then motion within the foot (e.g., articulation at the mid-foot joint) bleeds over into the experimental ankle kinematics estimate, appearing as extra rotation of the foot segment relative to the shank. Thus, there appears to be more ankle joint rotation (and angular velocity), than is really occurring physiologically (Leardini et al. 2007). When this overestimate of Ankle angular velocity is multiplied by the estimated Ankle moment, then it yields an overestimate of Ankle power, relative to power generated by biological structures that cross the ankle. There are likely no physiological structure(s) crossing the ankle that actually generate the magnitude of peak power estimated via 3DOF or 6DOF Ankle analysis. Likewise, there may not be any physiological structure(s) in the foot that actually generate the peak (negative) powers estimated by Distal Foot calculations. Rather these high peak powers are due in large part to methodological choices (i.e., assuming the entire foot is one rigid body). In contrast, AJC power provides a more physiologically-relevant estimate of power generated by the ankle plantarflexors, since the Achilles tendon inserts on the calcaneus and the AJC model mitigates errors due to mid-foot or

forefoot articulation (see 3.6 Appendix A for extended explanation).

Compounding the overestimation problems described above is the fact that experimentally-estimated Ankle kinetics (e.g., power) are often used to infer the functional role of individual muscles and tendons. For instance, inverse dynamics Ankle power has been paired with B-mode ultrasound to infer Achilles tendon function (e.g., Farris and Sawicki, 2012b; Lichtwark and Wilson, 2006). Overestimating Ankle power may cause elastic energy return from tendons to be overestimated as well (Zelik and Franz 2017), though this warrants further investigation. Also, musculoskeletal simulations often use optimization procedures that seek to match experimental kinematics such as ankle angle or kinetics such as ankle power (Bogey, Perry, and Gitter 2005; At L. Hof et al. 1993; Honert and Zelik 2016; Neptune, Kautz, and Zajac 2001). Therefore, errors in experimental Ankle estimates could lead to quantitative, and potentially even qualitative errors, in simulation-based predictions of muscle and tendon dynamics. Finally, overestimating Ankle power may cause us to overvalue contributions from the plantarflexors, relative to muscles about other joints (e.g., knee, hip, or within the foot). This can distort our understanding of how power is distributed amongst various sources in the body.

### 3.4.2 Clinical Implications

Figures 3.6-8 highlight how treating the entire foot as a rigid body (and thereby neglecting foot power) can impair our ability to reliably compare different interventions (e.g., prosthetic feet) to each other, or to a biological norm. Ankle power estimates impose a rigid-shank/rigid-foot model onto prosthetic feet which, in large part, do not contain an explicit ankle joint and do not mechanically resemble this rigid-body model (Geil et al., 2000; Prince et al., 1994; Sawers and Hahn, 2011). In contrast, anklefoot power estimates can capture power (the

rate of prosthetic energy storage and return) that occurs along the entire prosthesis. Figures 3.6-7 highlight the discrepancy between a conventional 3DOF Ankle power estimate vs. a more complete anklefoot estimate. For some prosthetic feet (e.g., Rush), 3DOF Ankle power overestimated the prosthetic anklefoot Push-off power (e.g., via Distal Shank estimate, Fig. 3.6). For other prosthetic feet (e.g., Soleus) 3DOF Ankle power underestimated prosthetic anklefoot Push-off power. And for yet other feet (e.g., Panthera), 3DOF Ankle power was similar to anklefoot Push-off power. As such, for a given prosthesis we may be unable to predict a priori how 3DOF Ankle power is related to anklefoot power. If we were to compare Push-off power generated by the Rush vs. Soleus based on 3DOF Ankle power, then we would conclude that the Rush provided ~30% higher peak Push-off power (162 W vs. 120 W peak, Figs. 3.7-8). However, if we were to compare these same two feet using a more complete anklefoot estimate (Distal Shank power), then it becomes apparent that the conclusion based on Ankle power was incorrect. Distal Shank power indicates exactly the opposite: Soleus exhibited ~50% greater peak Push-off than the Rush (170 W vs. 114 W, Figs. 3.7-8). This example highlights the danger of relying on Ankle power estimates alone. Moreover, if we were to compute the mechanical efficiency of these passive prosthetic feet (i.e., energy returned relative to energy absorbed), we see that the choice of estimation method can have a tremendous effect. For instance, for the Kinterra, mechanical efficiency was estimated to be 29% vs. 89% when using 3DOF Ankle vs. Distal Shank power. Computing anklefoot power is also important when comparing between intact vs. prosthetic limb biomechanics, for example, to assess gait symmetry. The Soleus provides a compelling example. Based on 3DOF Ankle power, the intact vs. prosthetic limb contributions appeared to be highly asymmetric (Fig. 3.7); however, Distal Shank power revealed a much higher level of symmetry – the Soleus actually generated ~85% of the positive

work performed by the intact anklefoot.

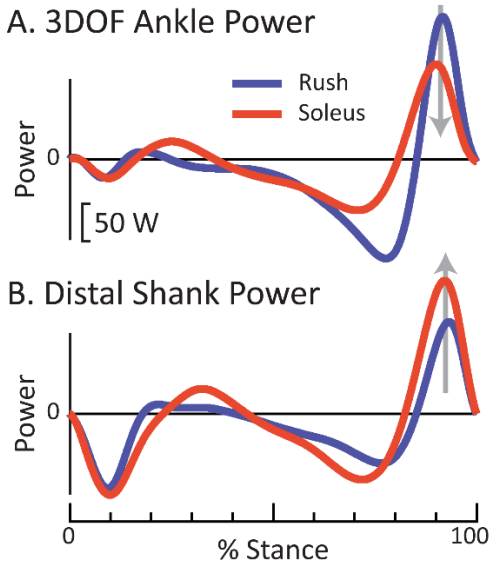


**Figure 3.8: Example of how choice of method can mislead conclusions when comparing two prosthetic feet.** (A) Conventional 3DOF Ankle power indicates that peak Push-off power from the Soleus foot (red) was decreased relative to the Rush foot (blue); however, (B) the more complete Anklefoot power estimate indicates the opposite, that peak Push-off power with the Soleus was increased relative to the Rush foot. Power curves are for walking at 1.25 m/s, for one individual with transtibial amputation.

Using Ankle power is also expected to skew comparisons of other clinical interventions such as footwear and orthoses. Figure 3.4 shows how interventions affecting the rigidity of the foot (e.g., shoe, in-shoe orthosis, foot plate, exoskeleton) will also affect the quality of the Ankle power estimate, relative to anklefoot or AJC power estimates. Imagine a person generated exactly the same amount of Push-off power with their plantarflexor muscle-tendon units during both shod and barefoot walking. Figure 3.4 suggests that experimental Ankle power estimates would nonetheless appear higher for barefoot walking simply because the foot is less rigid without shoes, and thus more motion within the foot bleeds over into the Ankle estimate. To visualize this effect, look at the peak power magnitude difference between Ankle vs. AJC power for barefoot walking, and then look at this same comparison for shod walking. During barefoot walking, Ankle power grossly overestimated AJC power (by 77%). When shoes (or other

interventions) are worn, which increase rigidity of the foot segment, then the magnitude of overestimation is reduced. Note that Distal Foot vs. Distal Calcaneus power estimates are similarly skewed when comparing barefoot vs. shod (Fig. 3.4). A variety of supporting evidence is found in prior literature. For example, Arch and Fylstra (2016) found that peak Ankle power was higher while walking barefoot than with a rigid footplate, even though combined anklefoot power was similar. Likewise, Bregman et al. (2012) found that peak Ankle power (and work) was higher when walking shod than with an ankle-foot orthosis (with a carbon-composite foot plate). Finally, Desloovere et al. (2006) found peak 3DOF Ankle power was highest barefoot (least rigid foot condition), next highest while shod, and the lowest while wearing an ankle-foot orthosis (most rigid foot condition) during gait. In all these cases, the critical danger is that one might interpret changes in Ankle power (with vs. without an intervention) as a reflection of how the intervention is benefitting or degrading biomechanical performance. In actuality, some of the estimated changes simply reflect methodological errors inherent in conventional Ankle power estimates. Thus, observed differences may have little to do with biomechanical adaptations by the user. This highlights why Ankle power should not be used to compare interventions that affect the rigidity of the foot.

One final example: imagine we had sought in this study to test the hypothesis that our subject generated more Push-off power with her calf musculature when walking barefoot, relative to shod. Based on 3DOF Ankle power (Fig. 3.9) we would have concluded that plantarflexor Push-off power *increased* by 20% when barefoot (supporting our hypothesis). However, AJC power contradicts this conclusion, suggesting that plantarflexor Push-off power actually *decreased* by 17% while barefoot (Fig. 3.9). This again exemplifies how Ankle power can potentially lead to the wrong conclusion when evaluating different conditions/interventions,

and not simply inaccuracies in numerical estimates.

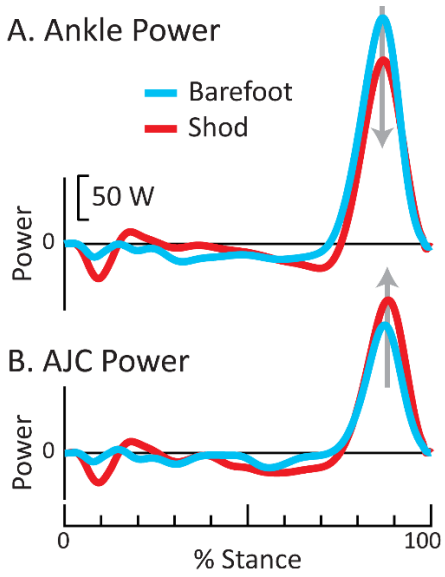


**Figure 3.9. Example of how choice of method can mislead conclusions when comparing shod vs. barefoot walking.** (A) Ankle power indicates that Push-off decreased while shod (red) relative to barefoot (blue); however, (B) AJC power indicates the opposite, that Push-off increased while shod. Power curves are for walking at 1.25 m/s, for one able-bodied person.

The comparison of 8 prosthetic feet (Figs. 6-7) highlights why it is problematic to assume that the foot is a single rigid-body, or to rely solely on Ankle power for interpretation. The subsequent discussion then shows how similar problems can occur with studies involving different footwear and orthoses. In short, conventional Ankle power – absolute power magnitudes and also relative power differences between conditions – can potentially mislead conclusions as a result of assuming the entire foot is a single rigid body. Based on these findings, it is recommended to compute anklefoot power when comparing lower-limb clinical interventions, and to avoid Ankle power.

### 3.4.3 Technological Implications

Treating the entire foot as a rigid segment can also result in inaccurate engineering design specifications for devices that aim to mimic or restore natural limb function. For instance, if we

sought to design a new prosthetic foot, then relying on conventional 3DOF Ankle power would result in a substantial overestimate of the mechanical power generation requirements for our device. This is because prosthetic feet replace the entire anklefoot, not simply Ankle power. Overestimating power requirements could affect selection of motors, gears, batteries and control parameters, and ultimately impact device weight, cost and complexity. This overestimation problem is evident in Figure 3.3, which shows that peak biological Ankle power (and work) tends to be much larger than anklefoot power (and work); consistent with prior multi-subject studies (Takahashi, Worster, and Bruening 2017; Takahashi and Stanhope 2013; Zelik, Takahashi, and Sawicki 2015). This same issue is also evident in Figure 3.7, where 3DOF Ankle power provides a skewed perspective on the degree to which existing prosthetic feet mimic intact anklefoot power. Another potential problem is that we may perceive functional deficiencies that do not actually exist, then use them as motivation to design new technology. From the perspective of 3DOF Ankle power, all 8 prosthetic feet tested were highly deficient in terms of positive Push-off power (Fig. 3.7), resulting in large asymmetry between limbs. This may suggest the need for a dramatically different foot design to restore natural anklefoot function. However, once the more complete anklefoot power estimate is computed then it becomes evident that some of the prostheses tested actually came quite close to replicating intact anklefoot power for this individual at this speed. These observations highlight why it is inadvisable to assume the entire foot is a rigid body if the goal is to use biomechanical estimates of the biological limb to identify design requirements for biomimetic devices.

### 3.4.4 Selecting an Appropriate Method

It is important to select an appropriate method to capture both ankle and foot power

contributions in gait analysis. However, method selection is nuanced, and depends on the precise objective of a given gait analysis study. In some cases it is beneficial to estimate ankle and foot power separately, though as shown in Fig. 3.4, the assumed model (shank-foot vs. shank-calcaneus) can substantially affect interpretation. In other cases it is more appropriate to estimate combined anklefoot power via Distal Shank power or Intersegmental calculations (e.g., when analyzing prostheses that do not contain an articulating ankle joint). Below we briefly summarize general recommendations. Conventional 3DOF Ankle power (shank-foot) is not recommended because it consistently overestimates net power produced by plantarflexing muscle-tendon units during walking (Zelik, Takahashi, and Sawicki 2015) and ignores foot power contributions (Fig. 3.4). 6DOF Ankle power also neglects important foot power contributions; however, it can be summed with Distal Foot power to provide a complete estimate of anklefoot power. The critical caveat here is that interpretation of biological ankle vs. foot power via this method may be misleading (Fig. 3.4). Summing AJC (shank-calcaneus) and Distal Calcaneus power is preferred because it provides: (i) a more physiologically-relevant partitioning of ankle vs. foot power in the biological limb, and (ii) sums to provide an estimate of anklefoot power that is nearly identical to Ankle + Distal Foot (Fig. 3.4). Power sources within the foot can be further decomposed using previously-published multi-segment foot modeling approaches (Bruening, Cooney, and Buczek 2012a; Dixon, Böhm, and Döderlein 2012; MacWilliams, Cowley, and Nicholson 2003; Takahashi, Worster, and Bruening 2017). AJC + Distal Calcaneus power estimates provide some of the same benefits as multi-segment foot models, except with fewer foot markers required, and without the need to track/model mid- or fore-foot segments, or to partition ground reaction forces amongst various foot segments. Finally, combined anklefoot power estimates are also recommended using either Distal Shank or Intersegmental power

calculations; though these do not allow for partitioning of power between ankle and foot. These two methods yield similar results to each other, and also to Ankle + Distal Foot power, and to AJC + Distal Calcaneus power (Figs. 3.3 & 3.5).

### 3.4.5 Limitations

There are well-understood limitations to case studies; however, there are also benefits. The purpose of this article was to provide concrete examples as to why it is important to compute foot power. Case studies here were intended to provide clear and unambiguous evidence of what *can* happen when the foot is treated as a single rigid-body segment. There is no uncertainty related to inter-subject variability or confounding factors. We also cited corroborating evidence from previously-published multi-subject studies, which further substantiate our main findings and conclusions. We focus on walking, but prior studies suggest that foot power is also meaningful in other locomotor tasks such as running (Kelly, Lichtwark, and Cresswell 2015; Wager and Challis 2016). Methods detailed here may help elucidate the puzzlingly large energy absorption estimated within the foot during running (10-25 J, (McDonald et al. 2016; Stefanyshyn and Nigg 1997) and sprinting (25-70 J, (Stefanyshyn and Nigg 1997). Calcaneus motion is generally well approximated by skin-mounted markers; however, may still slightly overestimate AJC rotation based on bone pins (Reinschmidt et al. 1997). Further research is warranted to understand confounds due to placing markers on the shoe vs. skin. Relatively low cut-off frequencies were used to process force and motion data (10 Hz and 6 Hz, respectively) based on the typical frequency content of human walking (Antonsson and Mann 1985). When higher cut-off frequencies were applied to our data (e.g., 25 Hz and 10 Hz, respectively) we found that this had no effect on any key trends, conclusions or interpretations. We acknowledge

that there are limitations to all experimental estimates, include anklefoot estimates presented. Each estimate is an imperfect approximation based on a simplified biomechanical model. For instance, none of the estimates presented explicitly model or account for multiarticular muscles crossing the ankle and metatarsophalangeal joints (Honert and Zelik 2016). And many of the estimates depend on foot mass and inertia being relatively small. Nevertheless, the critical point is that some models (i.e., used to estimate anklefoot power) are more complete and more physiologically-relevant than other models (e.g., that only estimate Ankle power, assuming a single rigid-body foot segment). These more complete models highlight why certain body dynamics, most notably foot power due to having a non-rigid foot, should not be neglected when performing gait analysis or interpreting results.

## 3.5 Conclusion

Treating the entire foot as a single rigid-body segment can result in obscuring (or even completely missing) important dynamics, re-affirming conclusions from prior multi-segment foot modeling studies. Here we overview *why* this is important to the gait analysis community, and *how* to better estimate anklefoot dynamics experimentally. Specifically, we highlight how neglecting foot power can hinder our scientific understanding of movement, confound our ability to make robust clinical comparisons (e.g., between prosthetic feet), and mislead the design of assistive devices aimed at mimicking or restoring biological limb function. To mitigate these problems, it is recommended to compute foot power in gait analysis using one or more of the methods outlined, and not to rely on conventional estimates of Ankle power.

## 3.6 Appendix A

Here we summarize each individual power calculation.

### 3.6.1 3DOF Ankle: Rotational Power

3DOF Ankle power ($P_{rot\_ank}$, Eqn. 3.A1) captures power due to rotation of the shank about the foot (Fig. 3.1B). Rotational power is obtained by multiplying the ankle joint moment ($\vec{M}_{ank}$) by the relative angular velocity of the shank with respect to the foot ($\vec{\omega}_{shank} - \vec{\omega}_{foot}$) (Elftman 1939; D. G. E. Robertson et al. 2013; Whittle 2014). Rotational power terms are summed about all 3 body planes (i.e., sagittal, frontal, transverse) to obtain net 3DOF Ankle power. The foot is typically modeled as a single rigid body, and tracked in 3D space via markers distributed along the hindfoot and forefoot (Buczek et al. 1994; Honert and Zelik 2016; D. G. E. Robertson et al. 2013; Takahashi, Horne, and Stanhope 2014; David A. Winter 1991; Zelik, Takahashi, and Sawicki 2015). This estimate fails to fully capture power due to the interaction between the foot and ground.

[3.A1] $$P_{rot\_ank} = \vec{M}_{ank} \cdot \left(\vec{\omega}_{shank} - \vec{\omega}_{foot}\right)$$

### 3.6.2 Ankle: Rotational + Translational Power

6DOF Ankle power ($P_{ank}$) captures power due to both rotation and translation of the shank relative to the foot (Eqn. 3.A2, Fig. 3.1C). 6DOF Ankle power is computed by summing 3DOF rotational Ankle power (Eqn. 3.A1) with 3DOF translational Ankle power. The translational power is defined as the dot product of net ankle force on the shank segment ($\vec{F}_{ank}$) and the relative translational velocity of the distal shank with respect to the proximal foot at the ankle (Buczek et al. 1994). Distal shank velocity and proximal foot velocities are defined here as the velocity of the ankle joint center based on rigid-body motion of the shank ($\vec{v}_{ank,shank}$) and foot ($\vec{v}_{ank,foot}$), respectively. Note that this formulation accounts for (i.e., captures) power due to relative segment endpoint displacement (Ebrahimi, Collins, et al. 2017). The addition of the translational power term helps account for imperfect joint modeling as well as any physical compression or translation that occurs at the ankle (Buczek et al. 1994; Zelik, Takahashi, and Sawicki 2015). As with 3DOF Ankle power, the foot is typically modeled as a single rigid body. This estimate also fails to fully capture foot power, due to the interaction between the foot and ground.

[3.A2] $$P_{ank} = \vec{F}_{ank} \cdot \left(\vec{v}_{ank,shank} - \vec{v}_{ank,foot}\right) + P_{rot\_ank}$$

### 3.6.3 Anklefoot: Ankle + Distal Foot Power

This approach estimates power due to both the ankle and foot, by summing 6DOF Ankle power (summarized above) with Distal Foot power ($P_{distal\_foot}$, Eqn. 3.A3). This combined power estimate ($P_{ank+distal\_foot}$, Eqn. 3.A4) represents power due to motion of the shank relative to the foot (Ankle power) plus power of the foot relative to the ground (Distal Foot

power, Fig. 3.1D). Both power terms are still based on calculations that assume the foot is a single rigid-body segment. Distal Foot power is sometimes interpreted to reflect deformation of structures within/around the foot, such as compression of the heel pad, foot arches or shoe, and rotation about the metatarsophalangeal joints (see Discussion for why this must be done cautiously and is often not recommended since it only models/captures a portion of foot power). Also note that Distal Foot power (and all other Distal Segment powers) captures power due to any ground deformation or foot slippage relative to the ground. Distal Foot power calculations also assume that mass and inertia distal to the foot segment is negligible (e.g., due to the toes). Distal Foot power is computed as:

[3.A3] $$P_{distal\_foot} = \vec{F}_{grf} \cdot \left( \vec{v}_{foot} + \vec{\omega}_{foot} \times \vec{r}_{cop/foot} \right) + \vec{M}_{free} \cdot \vec{\omega}_{foot}$$

where $\vec{F}_{grf}$ is the ground reaction force, $\vec{v}_{foot}$ is the velocity of the foot's center-of-mass (COM), $\vec{\omega}_{foot}$ is the angular velocity of the foot, $\vec{r}_{cop/foot}$ is the position of the COP relative to the foot's COM, and $\vec{M}_{free}$ is the free moment (Siegel, Kepple, and Caldwell 1996; Takahashi and Stanhope 2013; Zelik, Takahashi, and Sawicki 2015).

[3.A4] $$P_{ank+distal\_foot} = P_{ank} + P_{distal\_foot}$$

### 3.6.4 Anklefoot: AJC + Distal Calcaneus Power

This combined anklefoot power estimate ($P_{ajc+distal\_cal}$) is analogous to the preceding method (Ankle + Distal Foot power), except that it uses calcaneus instead of foot motion.

Experimentally, a cluster of markers is placed on the calcaneus (Fig. 3.2a) and used to estimate motion of this portion of the foot, based on rigid-body assumptions. AJC power ($P_{ajc}$, Eqn. 3.A5) is defined as the power due to motion (translation and rotation) of the shank relative to the calcaneus. Distal Calcaneus power ($P_{distal\_cal}$, Eqn. 3.A6) then captures power due to motion between the calcaneus and ground, reflecting translation and rotation of various foot structures (e.g., heel pad, foot arch, metatarsophalangeal joints, Takahashi et al., 2017). Again, mass and inertia due to structures distal to the calcaneus (e.g., forefoot, toes) is neglected.

AJC power is define as:

[3.A5] $$P_{ajc} = \vec{F}_{ank} \cdot \left(\vec{v}_{ank,shank} - \vec{v}_{ank,cal}\right) + \vec{M}_{ank} \cdot (\vec{\omega}_{shank} - \vec{\omega}_{cal})$$

where $\vec{v}_{ank,cal}$ is the ankle joint center velocity based on motion of the calcaneus, and $\vec{\omega}_{cal}$ is angular velocity of the calcaneus. Distal Calcaneus power is then defined as:

[3.A6] $$P_{distal\_cal} = \vec{F}_{grf} \cdot \left(\vec{v}_{cal} + \vec{\omega}_{cal} \times \vec{r}_{cop/cal}\right) + \vec{M}_{free} \cdot \vec{\omega}_{cal}$$

where $\vec{v}_{cal}$ is the velocity of the calcaneus' COM and $\vec{r}_{cop/cal}$ is the position of the COP relative to the calcaneus' COM.

[3.A7] $$P_{ajc+distal\_cal} = P_{ajc} + P_{distal\_cal}$$

Although AJC power (shank relative to calcaneus) is unconventional, it is appealing for several reasons. First, ankle power is often studied to understand the soleus, gastrocnemius and/or Achilles tendon; the main sources of plantarflexion power. These calf muscles (via the

Achilles tendon) insert directly onto the calcaneus. Thus, this approximation of shank-relative-to-calcaneus power seems more consistent with human anatomy than shank-relative-to-foot power (Ankle power). Second, prior studies indicate that the mid-foot joint undergoes substantial articulation during locomotor tasks like walking (Kelly, Lichtwark, and Cresswell 2015). If the foot is modeled as a single rigid body (as with Ankle power estimates), then this mid-foot articulation bleeds over into (i.e., appear as) ankle rotation causing ankle angle (and angular velocity, and thus power) to be overestimated (Leardini et al. 2007). Third, the calcaneus is a better approximation of a rigid-body than the entire foot. Again, this is due to motion of the mid-foot and other joints in the foot during walking and other locomotor tasks (Bruening, Cooney, and Buczek 2012b; Kelly, Lichtwark, and Cresswell 2015; MacWilliams, Cowley, and Nicholson 2003). Fourth, Figure 3.4 indicates that Distal Calcaneus power results were qualitatively consistent with cadaver studies on the foot arch (e.g., Ker et al., 1987), exhibiting energy storage and return by the foot. In contrast, Distal Foot power estimates are known to be highly inconsistent with these same cadaver studies, exhibiting large energy dissipation in late stance with little or no energy return. In summary, AJC + Distal Calcaneus power provides an appealing, more physiologically-relevant alternative to partition power sources within the body, which is more consistent with *in vitro* evidence of foot function than Ankle + Distal Foot power partitioning. As such, choice of methods can have important implications for how we interpret ankle vs. foot contributions in gait (see Discussion for further details and specific examples).

### 3.6.5 Anklefoot: Distal Shank Power

Distal Shank power ($P_{distal\_shank}$) provides a lumped estimate of anklefoot power, by directly computing the power due to 6DOF motion of the shank relative to the ground (see 3.7

Appendix B for detailed derivation). This estimate, described by Takahashi et al. (2012) as originating from a Unified Deformable segment model, has been applied to quantify net power contributions from prosthetic feet (more aptly called anklefeet). It is generally preferable to compute combined anklefoot power for prostheses since they often lack a clearly identifiable ankle joint and a well-defined foot segment that is distinct from the ankle. For prosthetic feet (or other interventions, e.g., anklefoot orthoses) where the ankle and/or foot deviate substantially from the anatomical norm, this Distal Shank power provides a means of capturing net power due to all structures distal to the shank. This approach assumes a rigid-body shank. However, it makes no assumptions about the rigidity or dynamics of the structures distal to the shank, except that these structures have negligible mass and inertia.

[3.A8] $$P_{distal\_shank} = \vec{F}_{grf} \cdot \left(\vec{v}_{shank} + \vec{\omega}_{shank} \times \vec{r}_{cop/shank}\right) + \vec{M}_{free} \cdot \vec{\omega}_{shank}$$

where $\vec{v}_{shank}$ is the velocity of the shank's COM, and $\vec{r}_{cop/shank}$ is the position of the center-of-pressure (COP) relative to the shank's COM.

### 3.6.6 Anklefoot: Intersegmental Power

Intersegmental power ($P_{interseg}$) is similar to the Distal Shank power estimate in that it provides a lumped estimate of anklefoot power. In fact, these two power estimates are analytically equivalent when foot mass and inertia are assumed to be negligible (see derivation in 3.8 Appendix C). The main difference is that Intersegmental power is nominally formulated to account for inertial effects of the foot (Prince et al. 1994), whereas Distal Shank power is not. Intersegmental power can be computed at any arbitrary point on a rigid-body segment (e.g., at the segmental center-of-mass, or at the segment's distal end), and it represents the net power flow into or out of that point. When computed for a point on the shank, Intersegmental power reflects an estimate of the net power flow to/from the combined anklefoot. Similar to Distal Shank power, this Intersegmental analysis is commonly used to analyze prosthetic power (Prince et al. 1994), when anatomically-inspired models of the ankle and foot may not be applicable or appropriate. Of note, the point at which Intersegmental power is computed must be proximal to all prosthetic foot components (e.g., located on the socket or rigid pylon), in order to fully capture prosthetic foot power. Below is an example of Intersegmental power, computed at the ankle joint center (i.e., distal end of the shank). Note, $\vec{F}_{ank}$ in [3.A9] represents the net force on the shank at the ankle.

[3.A9] $$P_{interseg} = \vec{F}_{ank} \cdot \vec{v}_{ank} + \vec{M}_{ank} \cdot \vec{\omega}_{shank}$$

where $\vec{v}_{ank}$ is the translational velocity of the ankle joint center.

## 3.7 Appendix B

The purpose of this Appendix is to demonstrate analytically that Distal Shank power provides an estimate of the 6DOF joint power between the shank and the ground.

In generalized form, the 6DOF power at/about a given joint ($j$), which is located between a proximal segment/body ($p$) and distal segment/body ($d$), is defined as:

[3.B1] $$P_{p/d} = \vec{F}_j \cdot \left(\vec{v}_{j,p} - \vec{v}_{j,d}\right) + \vec{M}_j \cdot \left(\vec{\omega}_p - \vec{\omega}_d\right)$$

where $\vec{F}_j$ is the net force at the joint on the proximal segment/body, $\vec{v}_{j,p}$ is the estimated velocity of the joint based on proximal segment/body motion, $\vec{v}_{j,d}$ is the estimated velocity of the joint based on distal segment/body motion, $\vec{M}_j$ is the net moment about the joint on the proximal segment/body, $\vec{\omega}_p$ is the angular velocity of the proximal segment/body, and $\vec{\omega}_d$ is the angular velocity of the distal segment/body, based on rigid-body assumptions.

The 6DOF power between the shank and the ground ($gnd$), both assumed to be rigid, using the ankle joint center to represent the modeled joint, is therefore:

[3.B2] $$P_{shank/gnd} = \vec{F}_{ank} \cdot \left(\vec{v}_{ank,shank} - \vec{v}_{ank,gnd}\right) + \vec{M}_{ank} \cdot \left(\vec{\omega}_{shank} - \vec{\omega}_{gnd}\right)$$

If we assume negligible foot mass and inertia, then the force and moment balances about the ankle joint center on the shank result in:

[3.B3] $$\vec{F}_{ank} = \vec{F}_{grf}$$

[3.B4] $$\vec{M}_{ank} = \vec{M}_{free} + \vec{r}_{cop/ank} \times \vec{F}_{grf}$$

where $\vec{F}_{grf}$ is the ground reaction force measured under the foot, $\vec{M}_{free}$ is the free moment and $\vec{r}_{cop/ank}$ is the position vector from the ankle joint center to the COP under the foot.

Furthermore, if the ground is not translating or rotating in the inertial frame (i.e., the ground is not moving relative to the motion of the Earth), then the velocity and angular velocity of the ground ($\vec{v}_{ank,gnd}$ and $\vec{\omega}_{gnd}$) are zero:

[3.B5] $$\vec{v}_{ank,gnd} = \vec{\omega}_{gnd} = 0$$

Plugging Eqns. 3.B3-B5 into Eqn. 3.B2 yields:

[3.B6] $$P_{shank/gnd} = \vec{F}_{grf} \cdot \vec{v}_{ank,shank} + (\vec{M}_{free} + \vec{r}_{cop/ank} \times \vec{F}_{grf}) \cdot \vec{\omega}_{shank}$$

Terms can be rearranged to:

[3.B7] $$P_{shank/gnd} = \vec{F}_{grf} \cdot \left(\vec{v}_{ank,shank} + \vec{\omega}_{shank} \times \vec{r}_{cop/ank}\right) + \vec{M}_{Free} \cdot \vec{\omega}_{shank}$$

Next, $\vec{v}_{ank,shank}$ and $\vec{r}_{cop/ank}$ can be written using vector addition:

[3.B8] $$\vec{v}_{ank,shank} = \vec{v}_{shank} + \vec{v}_{ank,shank}{}_{/shank}$$

[3.B9] $$\vec{r}_{cop}{}_{/ank} = \vec{r}_{cop}{}_{/shank} - \vec{r}_{ank}{}_{/shank}$$

where $\vec{v}_{shank}$ is the velocity of the shank's COM in the lab reference frame, $\vec{v}_{ank,shank}{}_{/shank}$ is the velocity of the ankle joint center relative to the shank's COM, $\vec{r}_{cop}{}_{/shank}$ is the position of the COP relative to the shank's COM, and $\vec{r}_{ank}{}_{/shank}$ is the position of the ankle joint center with respect to the shank's COM.

Assuming a rigid shank segment, then:

[3.B10] $$\vec{v}_{ank,shank}{}_{/shank} = \vec{\omega}_{shank} \times \vec{r}_{ank}{}_{/shank}$$

Plugging Eqns. 3.B8-B10 into Eqn. 3.B7, then simplifying, yields:

[3.B11] $$P_{shank}{}_{/gnd} = \vec{F}_{grf} \cdot \left(\vec{v}_{shank} + \vec{\omega}_{shank} \times \vec{r}_{cop}{}_{/shank}\right) + \vec{M}_{free} \cdot \vec{\omega}_{shank}$$

This is identical to Distal Shank power (Eqn. 3.A8), demonstrating that Distal Shank power represents 6DOF joint power due to motion (translation and rotation) between the rigid-body shank segment and ground.

Analogous derivations can be performed for any other Distal Segment powers (e.g., Distal Calcaneus power), showing that they are estimates of 6DOF power between the Segment and ground. However, note that the negligible mass and inertia assumption becomes increasingly

less valid as one moves up with leg (e.g., Distal Thigh power would be expected to include considerable errors due to neglected inertia). Also note that any power due to ground deformation, or to slippage of the foot relative to the ground, would also be captured by Distal Segment power calculations. Finally, care should be taken in treadmill studies because errors in treadmill belt speed (e.g., actual vs. assumed/programmed speed) can appear in the analysis as relative motion between the segment and ground, resulting in a misestimate of Distal Segment power.

## 3.8 Appendix C

The purpose of this Appendix is to demonstrate that Intersegmental power from Prince et al. (1994) computed at the ankle joint center is analytically equivalent to Distal Shank power, when foot mass and inertia are assumed to be negligible.

Intersegmental power ($P_{interseg}$) at the ankle joint center ($ank$), is defined as:

[3.C1] $$P_{interseg} = \vec{F}_{ank} \cdot \vec{v}_{ank} + \vec{M}_{ank} \cdot \vec{\omega}_{shank}$$

where $\vec{F}_{ank}$ is the net force at the ankle on the shank segment, $\vec{v}_{ank}$ is the translational velocity of the ankle, $\vec{M}_{ank}$ is the net moment about the ankle on the shank segment, and $\vec{\omega}_{shank}$ is the angular velocity of the shank based on rigid-body assumptions.

Assuming that foot mass and inertia are negligible, the force and moment balances about the ankle joint on the shank segment result in:

[3.C2] $$\vec{F}_{ank} = \vec{F}_{grf}$$

[3.C3] $$\vec{M}_{ank} = \vec{M}_{free} + \vec{r}_{cop/ank} \times \vec{F}_{grf}$$

where $\vec{F}_{grf}$ is the ground reaction force measured under the foot, $\vec{M}_{free}$ is the free moment and $\vec{r}_{cop/ank}$ is the position vector from the ankle joint center to the COP under the foot.

Plugging Eqns. 3.C2-C3 into Eqn. 3.C1, then simplifying yields:

[3.C4] $$P_{interseg} = \vec{F}_{grf} \cdot \left(\vec{v}_{ank} + \vec{\omega}_{shank} \times \vec{r}_{cop/ank}\right) + \vec{M}_{free} \cdot \vec{\omega}_{shank}$$

Next, the velocity of the ankle joint center ($\vec{v}_{ank}$) and the position of the COP relative to the ankle ($\vec{r}_{cop/ank}$), in the lab reference frame, can be written using vector addition:

[3.C5] $$\vec{v}_{ank} = \vec{v}_{shank} + \vec{v}_{ank/shank}$$

[3.C6] $$\vec{r}_{cop/ank} = \vec{r}_{cop/shank} - \vec{r}_{ank/shank}$$

where $\vec{v}_{shank}$ is the velocity of the shank's COM in the lab reference frame, $\vec{v}_{ank/shank}$ is the velocity of the ankle joint center relative to the shank's COM, $\vec{r}_{cop/shank}$ is the position of the COP relative to the shank's COM, and $\vec{r}_{ank/shank}$ is the position of the ankle joint center relative to the shank's COM.

Assuming a rigid shank segment, then:

[3.C7] $$\vec{v}_{ank/shank} = \vec{\omega}_{shank} \times \vec{r}_{ank/shank}$$

Plugging Eqns. 3.C5-C7 into Eqn. 3.C4, and simplifying, then yields:

[3.C8] $$P_{interseg} = \vec{F}_{grf} \cdot \left(\vec{v}_{shank} + \vec{\omega}_{shank} \times \vec{r}_{cop/shank}\right) + \vec{M}_{free} \cdot \vec{\omega}_{shank}$$

Eqn. 3.C8 is identical to the Distal Shank power calculation in Eqn. 3.A8.

Note that Takahashi et al. (2012) previously demonstrated that Ankle + Distal Foot power ($P_{ank+distal\_foot}$, Eqn. 3.A4) is also analytically equivalent to Distal Shank power when distal foot mass and inertia are negligible. Finally, see Figure 3.1 for conceptual visualizations of these anklefoot power equivalencies.

# Chapter 4

# Foot and Shoe Responsible for Majority of Soft Tissue Work in Early Stance of Walking

## 4.1 Introduction

Soft tissues located throughout the human body are known to passively perform mechanical work through wobbling and deforming, particularly following foot impacts with the ground. During the initial phase of walking after foot contact both active muscles as well as passive soft tissues perform negative work (often termed Collision phase). Previous studies have estimated ~60% of the negative work done was due to the deformation of distributed soft tissues, with the remaining ~40% being work performed by muscles and tendons acting about lower-limb joints (ankle, knee, hip, Zelik & Kuo, 2010). The magnitude of work performed by soft tissues has been found to increase with walking speed, and to be higher in obese individuals relative to non-obese (Fu et al. 2015). Soft tissue work has also been estimated to contribute to other tasks, such as running (Riddick and Kuo 2016) and jump landing (Zelik and Kuo 2012; Cazzola 2009).

It is not yet known which specific tissues in the body are responsible for the majority of the soft tissue work. Soft tissues capable of performing work (i.e., absorbing energy) during different activities include: intervertebral discs (Virgin 1951), viscera (Minetti and Belli 1994; Cazzola 2009), adipose tissue (Fu et al. 2015), wobbling muscle mass (Schmitt and Günther 2011; Pain and Challis 2002), and the subcalcaneal fat pad in the foot (termed the heel pad hereafter, Aerts, Ker, De Clercq, Ilsley, & Alexander, 1995; Bennett & Ker, 1990; Ker, Bennett, Alexander, & Kester, 1989; Whittle, 1999). For practical measurement reasons, the deformation

of footwear (Shorten 1993; Aerts and Clercq 1993; Klute, Berge, and Segal 2004; Whittle 1999) is often lumped in with the biological soft tissue estimates (i.e., experimental studies yield estimates of combined foot and shoe work, Zelik, Takahashi, and Sawicki 2015; Zelik and Honert 2018).

Recent studies suggest that the deformation of the foot and shoe may be responsible for a considerable amount of the soft tissue work during walking and running (Kelly, Cresswell, and Farris 2018; Takahashi, Worster, and Bruening 2017). The purpose of this study was to quantify how much of the soft tissue work after foot contact was due to the foot and shoe, versus from soft tissues elsewhere in the body, and how this distribution of work changed with walking speed and slope.

## 4.2 Methods

### 4.2.1 Summary

We collected ground reaction forces and whole-body kinematics while subjects walked at different speeds and on different slopes. We computed various estimates of mechanical power, then utilized a previously-published Energy-Accounting analysis, to estimate the amount of soft tissue work immediately following foot contact. Next we extended this prior analysis by parsing out how much of this soft tissue work was due to deformation of the foot (including the shoe) vs. work done by soft tissues elsewhere in the body.

### 4.2.2 Data Collection

Ten healthy subjects (5 male, 5 female, Age: 22±2 years, Height: 1.7±0.11 m, Weight: 68.5±13.7 kg) participated in an instrumented gait analysis study. All subjects provided written informed consent to the protocol, which was approved by the Institutional Review Board at Vanderbilt University. Each subject walked at five different speeds (0.8, 1.0, 1.2, 1.4, 1.6 m/s) on seven different slopes (0, ±3, ±6, ±9), for a total of 35 different trials, on a split-belt, force-instrumented treadmill (Bertec, Columbus, OH, USA). Seventy six retro-reflective markers were affixed to each subject (see 4.6 Appendix A) in order to track upper- and lower-limb motions during walking. Ground reaction forces and marker data were collected for each trial for 30 seconds at 2000 Hz and 100 Hz, respectively. The center-of-pressure of the instrumented treadmill was accurate to less than 5 mm under static loads. The motion capture system (Vicon T40S, Oxford, UK) image error was less than 0.3 mm for all subjects and trials.

### 4.2.3 Data Analysis

Analysis was performed using Visual3D software (C-Motion, Germantown, MD, USA) and a custom MATLAB (MathWorks, Natick, MA, USA) script. Marker and force data were low-pass filtered at 10 Hz and 15 Hz, respectively, with 3$^{rd}$ order, dual pass, Butterworth filters. These data were used to compute different power metrics (detailed in the subsequent paragraphs). After cross-over steps (e.g., left foot on right belt) were removed, each power metric was parsed into strides based on left foot contact. Mean intra-subject power metrics were computed for each subject and trial (i.e., combination of speed and slope). Then, mean inter-subject power and work metrics were computed for each trial.

### 4.2.4 COM & Peripheral Powers

We computed Center-of-Mass (COM) power for each lower-limb using the individual-limbs method (Donelan, Kram, and Kuo 2002) and the Peripheral power (i.e., rate of energy change, Zelik, Takahashi, and Sawicki 2015; van der Kruk et al. 2018) of the hands, forearms, upper arms, thighs, shanks and feet with respect to the body's COM. COM and Peripheral power terms were computed as detailed and derived in Zelik et al. (2015). The COM power reflects the time rate of change of kinetic and potential energy of the COM while the Peripheral power terms represent the time rate of change of segmental energies with respect to the COM of the body (Zelik, Takahashi, and Sawicki 2015). The summation of the COM and Peripheral powers from all limbs provides an estimate of whole-body power (rate of energy change), which we term here as the Total power (see Fig. 4.1). This summation of the COM and Peripheral powers is consistent with the rationale and interpretation described in van der Kruk et al. (2018).

### 4.2.5 Joint & Distal Foot Powers

Six degree-of-freedom (6DOF) joint powers for the lower-limb joints (i.e., ankles, knees, hips; Zelik, Takahashi, and Sawicki 2015) and upper-limb joints (i.e., wrists, elbows, shoulders; Riddick & Kuo, 2016) were estimated using rigid-body inverse dynamics calculations. Lower-limb joint powers were estimated using a bottom-up approach (starting calculations from the ground reactions forces, Robertson, Caldwell, Hamill, Kamen, & Whittlesey, 2013), whereas upper-limb joint kinetics were computed using a top-down approach (starting calculations from finger tips, Ashby, Vlietstra, Hickox, & Alderink, 2015; Cimolin et al., 2012). We did not estimate the lumbosacral joint power, which has been estimated to be very small during normal walking (Zelik and Kuo 2010). The power due to deformation of the foot and shoe was estimated using a Distal Foot power calculation (rationale discussed below, Siegel, Kepple, & Caldwell, 1996; Takahashi & Stanhope, 2013; Zelik & Honert, 2018). Note that for brevity we use the term foot to encompass both the biological segment and the shoe surrounding it.

### 4.2.6 Foot Absorption Phase of Gait

Distal Foot power was used to define the initial phase of the gait cycle over which we computed negative work (energy absorption) summary metrics. We term this part of the gait cycle *Foot Absorption* and it covers roughly 0-15% of the stride cycle (Fig. 4.1). It is formally defined from foot contact to when the Distal Foot power curve crossed -0.05 W/kg. This non-zero threshold was necessary as the Distal Foot power does not always cross zero during early stance, but comes close. Foot Absorption is used instead of the more traditional COM Collision phase (which is often used to study level ground walking, Zelik, Takahashi, and Sawicki 2015) because the individual-limb COM power curve often does not exhibit negative power after foot

contact during incline walking and Collision phase is thus ill-defined on these slopes (Franz, Lyddon, and Kram 2012).

### 4.2.7 Rest-of-Body (ROB) Soft Tissue Power and Work

The power curves summarized above were then used to compute estimates of Soft Tissue power for the rest-of-body (ROB). ROB Soft Tissue power includes contributions from jiggly, wobbly and deformable tissues throughout the body (e.g., fat/muscle around the thigh, the intervertebral disks and viscera, see Fig. 4.1, Fu et al. 2015; Zelik and Kuo 2010; Zelik, Takahashi, and Sawicki 2015), minus the foot (since this is captured by Distal Foot power, see below). Similar to prior literature (Zelik and Kuo 2010; Zelik, Takahashi, and Sawicki 2015; Fu et al. 2015), the term Soft Tissue is capitalized to distinguish that these are quantitative estimates of power and work that we attribute to the deformation of non-rigid tissues/materials (based on certain assumptions, as detailed below and in: Zelik and Kuo 2010; Zelik, Takahashi, and Sawicki 2015), as opposed to a colloquial discussion of (lower-case) soft tissues in the body.

The ROB Soft Tissue power was estimated using a previously-published Energy-Accounting analysis (Zelik, Takahashi, and Sawicki 2015), as the difference between the Total power of the body (sum of COM power from each lower limb plus Peripheral powers for all limbs and segments, Fig. 4.1) and Joint+Foot power (all 6DOF joint powers plus Distal Foot powers, see Fig. 4.1). Written out, this mechanical power balance, detailed in Zelik et al. (2015), is as follows:

$$\text{Joint+Foot power} + \text{ROB Soft Tissue power} = \text{Total power}$$

This equation is similar to the power balance presented in Aleshinsky (1986) and van der Kruk et al. (2018); however, there are a few notable differences because in our analysis of soft tissue contributions we relax the rigid-body and idealized articulating joint assumptions. For instance, relative to van der Kruk et al. (2018), we computed 6DOF joint power rather than 3DOF joint power on the left hand side of the equation, because the former is insensitive to the estimated joint center location (Zelik, Takahashi, and Sawicki 2015). We additionally computed the Distal Foot power, which is analogous to the environmental power term in van der Kruk et al. (2018), and we included an additional term called ROB Soft Tissue power on the left hand side of the equation to account for the relaxed rigid-body assumptions in our analysis. Finally, we computed whole-body rate of energy change (i.e., summed kinetic and gravitational power) on the right hand side of the equation in accordance with König's theorem, similar to Kruk et al. (2018). Experimentally, this allows us to forego rigid-body assumptions in the calculation of COM power (Zelik, Takahashi, and Sawicki 2015). In our analysis of treadmill walking, we also assumed negligible air resistance and ground deformation (i.e., frictional power terms defined in van der Kruk et al. (2018).

There were also a few notable differences in our methods relative to the Energy-Accounting analysis presented in Zelik, et al., (2015). First, the prior study only included lower-limb joint powers (ankle, knee, hip) and the Distal Foot power. Here we extend the analysis to also include the shoulder, elbow and wrist joint powers. Second, the prior study sought to examine the positive work during the Push-off phase of gait and therefore presented an individual-limb analysis (which requires some additional assumptions, Zelik, Takahashi, and Sawicki 2015). Here we apply a more complete whole-body analysis (i.e., summing contributions from all upper and lower-limbs), which is beneficial because it circumvents the

need for these additional assumptions. Next, ROB Soft Tissue work (in Joules) was computed by integrating under the negative portion of the ROB Soft Tissue power curve during Foot Absorption.

### 4.2.8 Foot Soft Tissue Power & Work

During Foot Absorption, we use the Distal Foot power of the leading limb as an estimate of Foot Soft Tissue power. The Distal Foot power represents the 6DOF power between the foot and the ground, meaning the translational power due to the motion of the COM of the foot relative to the ground plus the rotational power of the foot relative to the ground. In this model, the foot is modeled as a single, rigid body segment (Zelik and Honert 2018). Note that the Distal Foot power provides a lumped (i.e., net power) estimate from both passive (e.g., subcalcaneal fat pad, midsole shoe cushioning) and active (e.g., intrinsic foot muscle) power sources; in contrast to multi-segment foot modeling approaches that are employed to further parse out various power sources within the foot (e.g., due to metatarsophalangeal joint rotation).

Next, Foot Soft Tissue work (in Joules) was computed by integrating under the negative portion of the Distal Foot power curve during Foot Absorption. We should acknowledge that our own recent work indicates that it is preferable to use Distal Calcaneus power rather than Distal Foot power (Zelik and Honert 2018) in order to more fully capture foot dynamics. This is primarily important during mid- and late-stance (e.g., Push-off phase of gait). However, this recommendation was not known to us at the time of data collection for this current study, and thus in our current data set the markers used were insufficient to estimate Distal Calcaneus power (as it requires at least three markers on the hindfoot). Fortunately, Distal Foot power and Distal Calcaneus power appear to be very similar during early stance based on the data currently

available in the literature (Zelik and Honert 2018), thus Distal Foot power was deemed a reasonable surrogate measure here. For a full derivation of the Distal Foot power, see the appendix in Zelik & Honert, 2018.

### 4.2.9 Total Soft Tissue Work

We defined Total Soft Tissue work during Foot Absorption as the summation of the Foot Soft Tissue work and the ROB Soft Tissue work (Fig. 4.1).

### 4.2.10 Statistical Analysis

Statistical analyses were performed to determine the correlation of key outcome metrics with increasing speed and slope. The key outcome metrics computed during Foot Absorption were: (i) Foot Soft Tissue work, (ii) ROB Soft Tissue work, (iii) Total Soft Tissue work, and (iv) the percentage of the Total Soft Tissue work that was performed due to foot deformation (i.e., Foot Soft Tissue work divided by Total Soft Tissue work, multiplied by 100 to report as a percentage). We computed Spearman's rank correlations with a Holm-Sidak post-hoc error correction for each outcome metric. Significance was evaluated with a family-wise $\alpha$=0.05.

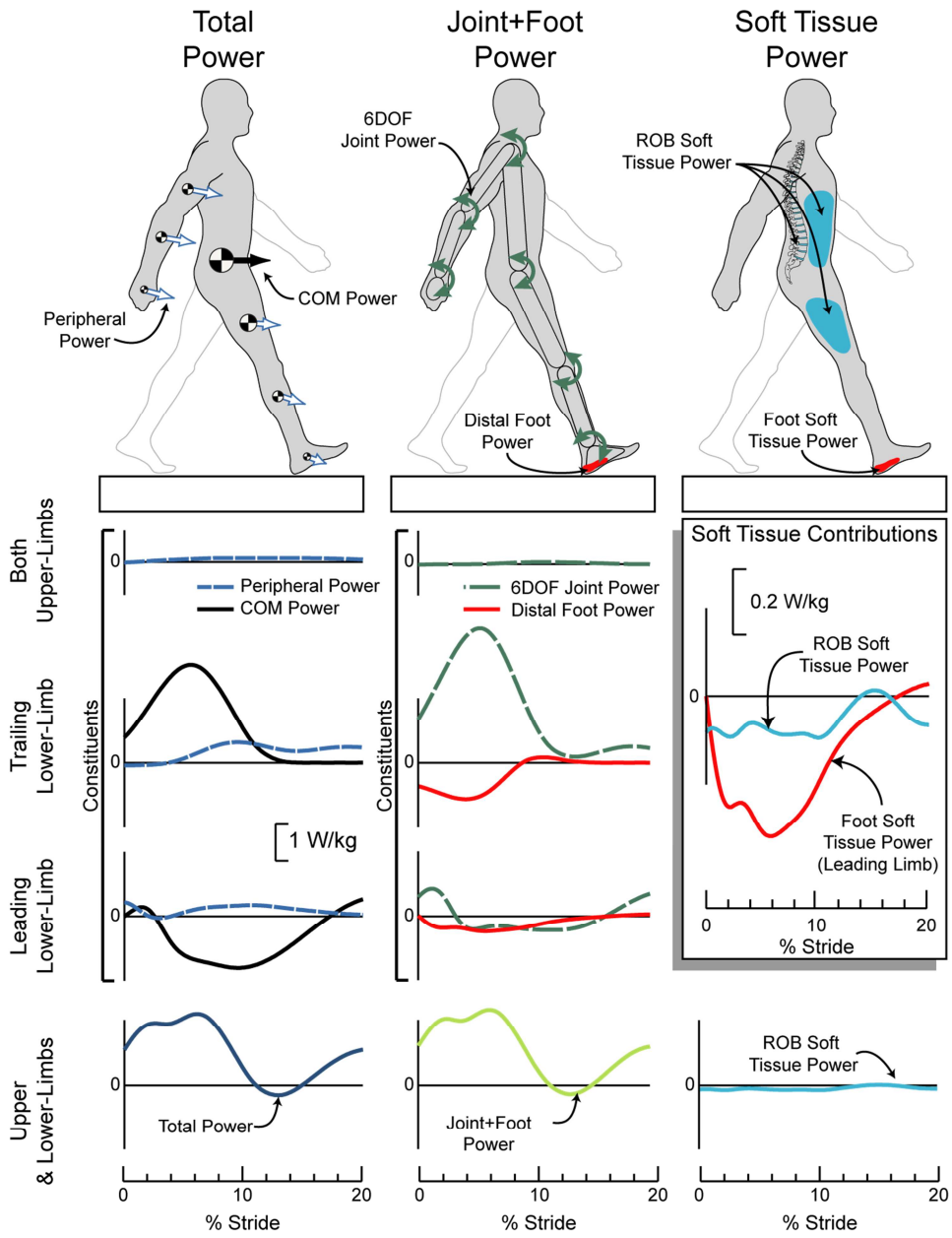


**Figure 4.1. Energy-Accounting analysis used to estimate soft tissue power contributions during early stance.** The Foot Soft Tissue power is estimated by computing the leading limb Distal Foot power during Foot Absorption (~0-15% of stride), and represents power due to deformation of the foot and shoe. The ROB Soft Tissue power is computed as the difference between the Total power and the Joint+Foot power curves, and is power attributed to soft tissues elsewhere in the body. Total power is the summation of the Peripheral power of the arms (i.e., hands, forearms, upper arms) and legs (i.e., feet, shanks, thighs) and the COM power from the leading and trailing limbs; collectively signifying the rate of energy change of the whole-body. The Joint+Foot power is the summation of the upper- (i.e., wrists, elbows, shoulders) and lower-limb (ankles, knees, hips) joint powers and the Distal Foot power from the leading and trailing foot. For aesthetic simplicity, the cartoons only depict the leading limb power contributions. The results shown here are study averaged (N = 10) at 1.2 m/s on level ground.

## 4.3 Results

The Total power of the body and the Joint+Foot power showed very strong qualitative agreement across the full range of speeds and slopes (Fig. 4.2). As a result, the difference between these two curves (i.e., the ROB Soft Tissue power) was relatively small across the entire gait cycle (on average < 0.7 W/kg, Fig. 4.2). During the Foot Absorption phase, the Foot Soft Tissue power typically exhibited greater power absorption (negative power) than the ROB Soft Tissue power (except when walking slowly uphill, Fig. 4.3).

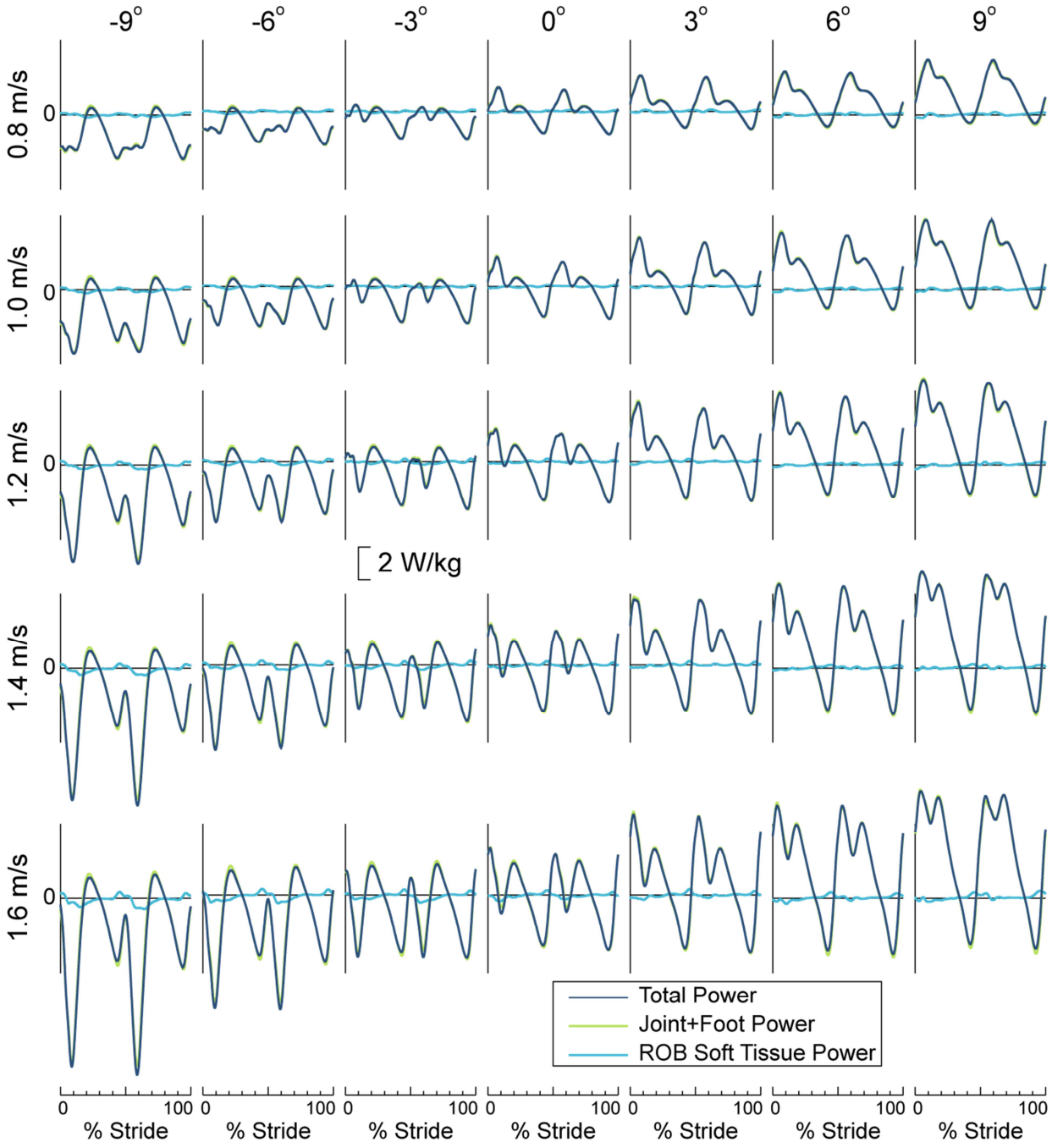


**Figure 4.2. Total power (dark blue), Joint+Foot power (light green), and ROB Soft Tissue power (light blue) for a wide range of walking speeds and slopes.** Uphill is denoted with positive slopes and downhill with negative slopes. The difference between the Total power and Joint+Foot power is defined as the ROB Soft Tissue power. Results shown are the inter-subject mean (N = 10).

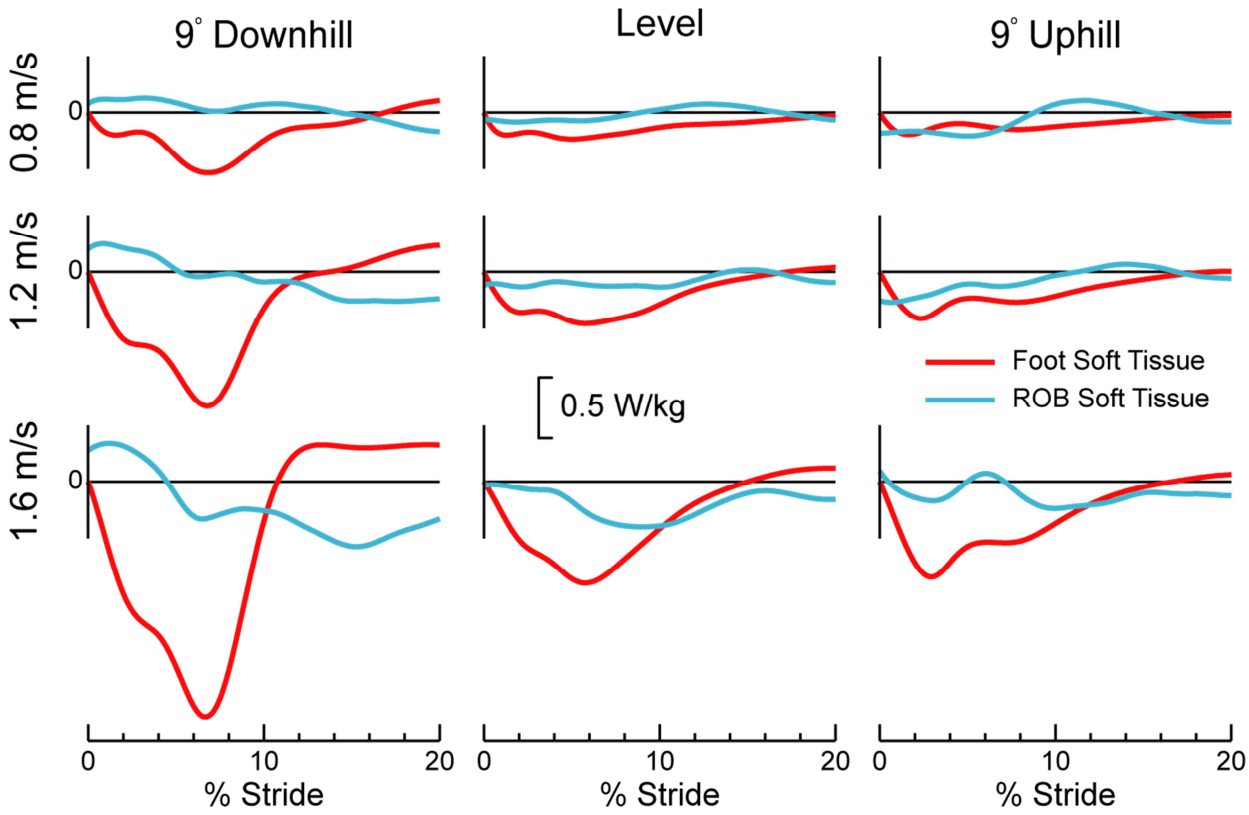


**Figure 4.3. Soft Tissue powers during early stance.** The leading limb Distal Foot power provides an estimate of Foot Soft Tissue power (due to deformations within the foot and shoe). ROB (rest-of-body) Soft Tissue power is an estimate of contributions from deformable tissues elsewhere in the body (minus the foot). Results depicted are the inter-subject mean (N = 10).

Increasing gait speed (from 0.8 to 1.6 m/s) led to an increasing trend in the magnitudes of Foot Soft Tissue work and Total Soft Tissue work during the Foot Absorption phase, regardless of slope ($p<0.0001$, see Table 4.1 and 4.3). The ROB Soft Tissue work magnitude increased with increasing speed during downhill walking ($p<0.006$, see Table 4.2) and during one uphill slope (3 degrees, $p<0.002$). The percentage of Total Soft Tissue work done by the foot varied up to 19% with increasing speed, on average, but no significant trends were found as a function of speed (Table 4.4, Fig. 4.4).

Increasing slope (from -9 to +9 degrees) led to a decreasing trend in the magnitude of Foot Soft Tissue work (Table 4.1) and in the percentage of Total Soft Tissue work done by the

Foot (Fig. 4.4, Table 4.4, $p<0.003$), regardless of speed. The ROB Soft Tissue work (Table 4.2) and Total Soft Tissue work (Table 4.3) did not exhibit consistent trends with increasing slopes, resulting in some statistically significant and some non-significant trends at different speeds (Tables 4.2-4.3).

**Table 4.1. Foot Soft Tissue work (J) during Foot Absorption at different speeds and slopes.** Negative slopes indicate downhill walking. P-values indicate the significance of the trend in work with increasing speed for each slope (at the bottom of each column), and with increasing slope for each speed (at the right of each row). Asterisks indicate significant trends. All results shown are the inter-subject mean ± one standard deviation (N=10).

| | | Slope (°) | | | | | | | |
|---|---|---|---|---|---|---|---|---|---|
| | | -9 | -6 | -3 | 0 | 3 | 6 | 9 | *p*-value |
| Speed (m/s) | 0.8 | -2.8±1.1 | -2.6±1.0 | -2.5±1.0 | -2.2±0.7 | -1.9±0.5 | -1.8±0.4 | -1.7±0.4 | <0.0001* |
| | 1.0 | -3.7±1.6 | -3.3±1.2 | -3.0±1.1 | -2.6±0.7 | -2.2±0.6 | -2.3±0.6 | -2.0±0.5 | <0.0001* |
| | 1.2 | -5.0±2.0 | -4.2±1.6 | -3.9±1.4 | -3.1±1.0 | -2.8±0.8 | -2.8±0.8 | -2.5±0.8 | <0.0001* |
| | 1.4 | -6.0±2.2 | -5.7±1.9 | -4.5±1.8 | -4.2±1.0 | -3.4±0.9 | -3.5±0.9 | -3.3±1.0 | <0.0001* |
| | 1.6 | -7.5±2.9 | -6.6±2.3 | -5.6±2.3 | -4.5±1.3 | -4.4±1.0 | -4.3±1.1 | -4.0±1.1 | <0.0001* |
| | *p*-value | <0.0001* | <0.0001* | <0.0001* | <0.0001* | <0.0001* | <0.0001* | <0.0001* | |

**Table 4.2. ROB (rest-of-body) Soft Tissue work (J) during Foot Absorption at different speeds and slopes.** Negative slopes indicate downhill walking. P-values indicate the significance of the trend in work with increasing speed for each slope (at the bottom of each column), and with increasing slope for each speed (at the right of each row). Asterisks indicate significant trends. All results shown are the inter-subject mean ± one standard deviation (N=10).

| | | Slope (°) | | | | | | | |
|---|---|---|---|---|---|---|---|---|---|
| | | -9 | -6 | -3 | 0 | 3 | 6 | 9 | *p*-value |
| Speed (m/s) | 0.8 | -0.4±0.4 | -0.6±0.5 | -0.6±0.7 | -1.0±0.9 | -0.8±1.0 | -1.2±1.3 | -1.9±2.2 | 0.009 |
| | 1.0 | -0.8±0.8 | -0.5±0.5 | -0.6±0.6 | -1.2±1.0 | -1.0±0.9 | -1.5±1.2 | -1.5±1.5 | 0.02 |
| | 1.2 | -0.9±0.8 | -0.7±0.7 | -0.8±1.0 | -1.3±1.0 | -1.7±1.7 | -1.5±1.0 | -2.1±1.4 | 0.0003* |
| | 1.4 | -0.9±0.5 | -0.9±0.6 | -1.4±1.5 | -1.7±1.3 | -1.9±0.9 | -1.7±1.3 | -1.7±1.4 | 0.03 |
| | 1.6 | -1.3±0.9 | -1.9±1.2 | -1.3±1.2 | -2.3±1.4 | -2.3±1.2 | -2.6±1.6 | -2.3±1.6 | 0.02 |
| | *p*-value | 0.006* | <0.0001* | 0.0006* | 0.01 | 0.002* | 0.06 | 0.6 | |

**Table 4.3. Total Soft Tissue work (J) during Foot Absorption at different speeds and slopes.** Negative slopes indicate downhill walking. P-values indicate the significance of the trend in work with increasing speed for each slope (at the bottom of each column), and with increasing slope for each speed (at the right of each row). Asterisks indicate significant trends. All results shown are the inter-subject mean ± one standard deviation (N=10).

| | | Slope (˚) | | | | | | | |
|---|---|---|---|---|---|---|---|---|---|
| | | -9 | -6 | -3 | 0 | 3 | 6 | 9 | *p*-value |
| Speed (m/s) | 0.8 | -3.2±1.3 | -3.2±1.2 | -3.1±1.4 | -3.2±1.2 | -2.8±0.8 | -3.0±1.2 | -3.6±2.2 | 0.4 |
| | 1.0 | -4.5±2.0 | -3.8±1.4 | -3.6±1.4 | -3.8±1.3 | -3.3±0.9 | -3.8±1.1 | -3.6±1.4 | 0.2 |
| | 1.2 | -5.8±2.2 | -5.0±1.8 | -4.6±2.1 | -4.5±1.5 | -4.5±1.8 | -4.3±1.4 | -4.7±1.5 | 0.05 |
| | 1.4 | -6.8±2.3 | -6.6±2.0 | -5.9±2.9 | -5.9±1.9 | -5.3±1.2 | -5.2±1.4 | -5.0±1.5 | 0.001* |
| | 1.6 | -8.9±3.2 | -8.5±2.5 | -6.9±3.1 | -6.8±2.1 | -6.7±1.7 | -6.9±2.0 | -6.3±1.9 | 0.002* |
| | *p*-value | <0.0001* | <0.0001* | <0.0001* | <0.0001* | <0.0001* | <0.0001* | 0.0009* | |

**Table 4.4. Percentage of Total Soft Tissue work performed by the Foot at different speeds and slopes.** Negative slopes indicate downhill walking. *P*-values indicate the significance of the trend in work with increasing speed for each slope (at the bottom of each column), and with increasing slope for each speed (at the right of each row). Asterisks indicate significant trends. All results shown are the inter-subject mean ± one standard deviation (*N*=10).

| | | Slope (˚) | | | | | | | |
|---|---|---|---|---|---|---|---|---|---|
| | | -9 | -6 | -3 | 0 | 3 | 6 | 9 | *p*-value |
| Speed (m/s) | 0.8 | 90±18% | 83±13% | 83±16% | 70±23% | 71±23% | 64±24% | 52±26% | 0.003* |
| | 1.0 | 82±21% | 89±9% | 85±12% | 69±22% | 70±23% | 63±23% | 62±24% | 0.002* |
| | 1.2 | 87±19% | 86±12% | 84±11% | 71±16% | 64±20% | 69±17% | 58±17% | <0.0001* |
| | 1.4 | 89±14% | 87±9% | 77±14% | 72±17% | 66±13% | 70±19% | 71±22% | 0.002* |
| | 1.6 | 86±9% | 79±15% | 81±12% | 67±16% | 67±14% | 64±19% | 68±20% | 0.0006* |
| | *p*-value | 0.4 | 0.1 | 0.06 | 0.9 | 0.3 | 0.9 | 0.1 | |

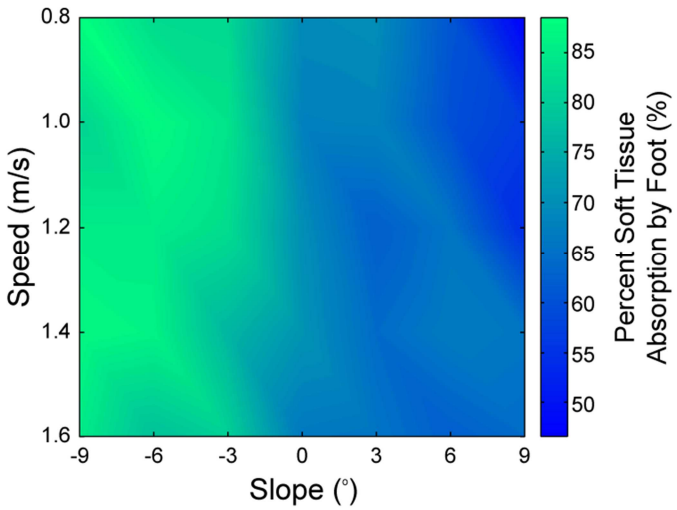


**Figure 4.4. Percentage of Total Soft Tissue work performed by the foot across speeds and slopes.** Increasing slope reduced the percentage of soft tissue energy absorption done by the foot, regardless of speed. Increasing speed has little effect on the percent soft tissue absorption performed by the foot. This heat map was created based on mean data from Table 4.4 for visualization purposes, using the default interpolated shading algorithm in MATLAB for aesthetic smoothing.

## 4.4 Discussion

The results indicate that deformation of the foot (which includes both biological and shoe structures in our study) is responsible for the majority of the energy absorption (negative work) done by soft tissues across a broad range of walking speeds and slopes during early stance. The foot absorbed as much as 7.5 J and contributed up to 90% of the Total Soft Tissue work after foot contact. During level and uphill walking the percentage of Soft Tissue work done by the foot was typically about 60-70%, and during downhill walking this was observed to increase to 80-90% (Table 4.3). The Foot Soft Tissue work increased by up to 3.5 J with decreasing slope (9 degrees uphill vs. 9 degrees downhill at 1.6 m/s, see Table 4.1) and increased by up to 4.7 J with increasing speed (0.8 m/s vs. 1.6 m/s at 9 degree downslope, Table 4.1). Kelly, Cresswell and Farris (2018) found a similar trend in running: more energy absorption by the foot at higher speeds.

The Foot Soft Tissue work observed here was in good agreement with energy absorption estimates reported in prior literature, including from impact studies, finite element models and gait analysis studies. We observed the Foot Soft Tissue absorption work to be 2.6-3.1 J for level ground walking at 1-1.2 m/s (Table 4.1). Impact studies with peak forces similar to walking at 1-1.2 m/s estimated foot absorption to be ~3-7 J (Aerts & Clercq, 1993; Kinoshita, Ogawa, Kuzuhara, & Ikuta, 1993). These studies estimated the foot energy absorption by fixating a person's lower-limb, dropping an instrumented mass onto their foot (and shoe) and then measuring the force and displacement of the mass (Aerts & Clercq, 1993; Bennett & Ker, 1990; Jørgensen & Bojsen-Møller, 1989; Ker et al., 1989; Kinoshita et al., 1993). Of note, these types of impact studies may overestimate foot absorption because other soft tissues (e.g., wobbling calf muscles) may also be responsible for a portion of the energy absorbed (Pain & Challis, 2001).

When just the foot and shoe were examined via finite element analysis, they were estimated to absorb ~2.5 J during locomotion, again with similar peak forces to the gait speeds mentioned above (Verdejo & Mills, 2004). In a barefoot gait analysis study, the heel pad was estimated to absorb 1.5 J at ~1.0 m/s. This was estimated by multiplying heel pad displacement (measured via radiographs) with heel forces (measured by a foot pressure sensor, Wearing, Hooper, Dubois, Smeathers, & Dietze, 2014). Another barefoot walking study estimated 3.8 J of heel pad energy absorption at 1.3 m/s, though they employed a calculation that captured the combined contribution from both the foot and the ankle (Baines, Schwab, & Soest, 2018). Overall, our estimate of Foot Soft Tissue work seems to be in reasonable agreement with the range of values reported in prior literature.

While most biomechanical studies historically focus on joint mechanics (e.g., ankle, knee, hip), the results here re-emphasize that soft tissues also provide substantial contributions to early stance gait dynamics. This is highlighted by comparing Total Soft Tissue work (Table 4.3) to the negative joint work from the leading limb (ankle+knee+hip) during Foot Absorption (Table 4.5). We observe that the Total Soft Tissue work (Table 4.3) greatly exceeded the joint work during the Foot Absorption phase (Table 4.5) in uphill walking. During level ground walking, the Total Soft Tissue work was ~150% of the magnitude of the joint work at slow speeds and ~50% of the joint work magnitude at fast speeds. During downhill walking the Total Soft Tissue work was ~20-50% of the magnitude of the joint work during Foot Absorption phase. These trends are consistent with those observed in our previous jump landing study (Zelik & Kuo, 2012), which showed that with increased Collision magnitudes there was a reduced percent contribution from soft tissues. Although it is possible for soft tissues to absorb a larger percentage of the negative work (e.g., by locking the knee into a fully extended position at foot

impact, (Zelik and Kuo 2012), this may be undesirable due to associated pain or risk of injury. In prior barefoot impact studies, experimenters limited their testing range because impacts that required ~3.7 J of heel pad absorption instigated pain in the subjects (Kinoshita et al., 1993).

**Table 4.5. Leading limb negative lower-limb joint (ankle+knee+hip) work performed during Foot Absorption at different speeds and slopes.** Negative slopes indicate downhill walking. All results shown are the inter-subject mean ± one standard deviation (N=10).

| | | Slope (˚) | | | | | | |
|---|---|---|---|---|---|---|---|---|
| | | -9 | -6 | -3 | 0 | 3 | 6 | 9 |
| Speed (m/s) | 0.8 | -18.1±5.6 | -12.1±3.1 | -7.7±2.4 | -2.1±1.3 | -0.2±0.3 | -0.1±0.1 | 0.0±0.0 |
| | 1.0 | -24.1±9.3 | -17.4±4.3 | -10.0±2.8 | -3.2±2.0 | -0.2±0.3 | 0.0±0.2 | 0.0±0.0 |
| | 1.2 | -32.4±12.2 | -20.4±5.8 | -13.6±4.1 | -5.5±2.8 | -0.6±0.7 | -0.1±0.1 | 0.0±0.0 |
| | 1.4 | -35.4±6.7 | -23.8±4.6 | -16.7±4.8 | -7.9±3.4 | -1.5±1.7 | -0.2±0.3 | 0.0±0.0 |
| | 1.6 | -41.1±11.5 | -30.0±7.0 | -20.7±5.5 | -11.1±4.5 | -2.8±2.3 | -0.7±0.9 | -0.1±0.1 |

The correspondence between Total power and Joint+Foot power – across all speeds and slopes – was frankly remarkable (Fig. 4.2). Despite the theoretical basis for expecting summed Joint+Foot power to match well with the Total (whole-body) power (Aleshinsky 1986; van der Kruk et al. 2018), to our knowledge this has never actually been shown experimentally for walking. For a variety of practical and methodological reasons, prior attempts have only yielded partial agreement over certain portions of the gait cycle (e.g., D. A. Winter 1979; Zelik, Takahashi, and Sawicki 2015), or when both estimates are derived from the same rigid body assumptions (Ebrahimi 2018). Our current findings suggest benefits to applying a whole-body approach when performing Energy-Accounting analysis, which enables inclusion of upper-limb joint powers, requires fewer assumptions (e.g., related to partitioning COM and Peripheral powers between limbs, Zelik, Takahashi, and Sawicki 2015), and reduces the discrepancies between Total power and 6DOF Joint+Foot power (Figs. 4.2 and 4.5). Collectively, these current findings give confidence in the empirical accuracy and methodological completeness of the power estimates computed in this study.

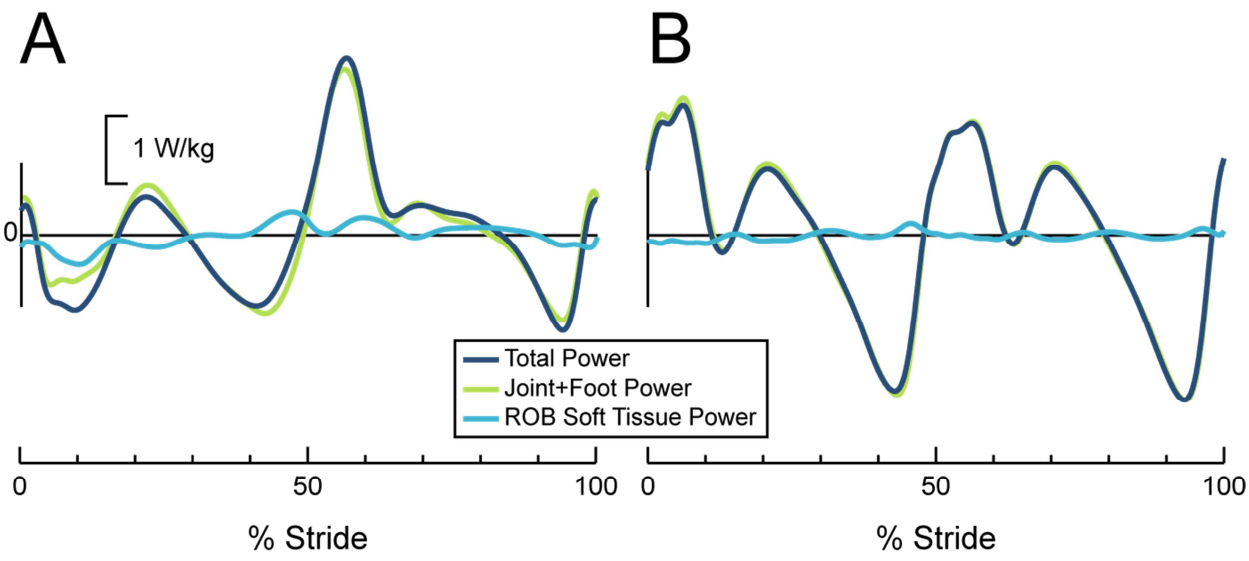


**Figure 4.5. Energy-Accounting analysis using a (A) individual-limb analysis and (B) whole-body analysis.** The whole-body analysis (summing together all upper- and lower-limb powers) provides a more complete estimate of Total power of the body. Whereas individual-limb analysis requires some additional assumptions related to partitioning COM and Peripheral powers between limbs.

There are several limitations to acknowledge with this study. Each of the subjects wore their own shoes which can affect the Distal Foot power (Aerts and Clercq 1993; Zelik and Honert 2018). This study was performed on a relatively young, non-obese population. As such, the results (e.g., percentage of Total Soft Tissue work done by the foot) should not be assumed to generalize to all other ages and body types. Of note, the properties of the heel pad change with age (Hsu et al. 1998) and the magnitude of Soft Tissue work after foot contact has previously been shown to increase in obese individuals (Fu et al. 2015). We interpret the ROB Soft Tissue power to be the net power contributions from deformable structures throughout the body (excluding the foot). However, this waveform may also be due, at least in part, to inaccuracies in model parameters (e.g., segment inertia) or imperfect measurements (e.g., ground reaction forces or moments, kinematics). Additionally, the marker and force data were filtered at different frequencies. Prior studies suggest this filtering approach may lead to transient peaks in joint

moment estimates during the first ~50 ms after foot contact in high impact movements (Kristianslund, Krosshaug, and Bogert 2012; McCaw et al. 2013; Roewer et al. 2014) and in running (Bezodis, Salo, and Trewartha 2013). To confirm that this effect was not skewing our results we applied the same marker and force filtering frequency (15 Hz) to our walking data in this study. We found no major effects on the key outcome metrics, trends, conclusions or interpretations. In general, when computing mechanical work and power metrics over longer periods of time (e.g., Foot Absorption was an average of 160 ms ), we have not found the use of different filtering cut-off frequencies (e.g,, 10 Hz motion vs. 15 Hz force) to substantially alter results or conclusions (Zelik and Honert 2018; Zelik and Kuo 2012). In our power balance we assumed rolling friction was negligible, and did not compute energy loss due to slight variations in treadmill belt speed. However, prior studies suggest this energy loss may be small; for instance Sloot et al. (2014) estimated ~0.25 J of treadmill energy loss in early stance of walking (1.3 m/s) due to variations in belt speed. Lastly, we did not compute the power contributions from the neck or spine joints. It is expected that these joints have small power contributions, as the neck and trunk (e.g., lumbosacral joint) generally undergo little rotation (Hirasaki et al. 1999) and have relatively small moments during walking (Callaghan, Patla, and McGill 1999).

## 4.5 Conclusion

In summary, we found that most of the Soft Tissue work that occurs after foot contact was due to deformation of the foot and shoe: ~60-70% of the Total Soft Tissue work during level and uphill walking, and 80-90% during downhill walking.

## 4.6 Appendix A

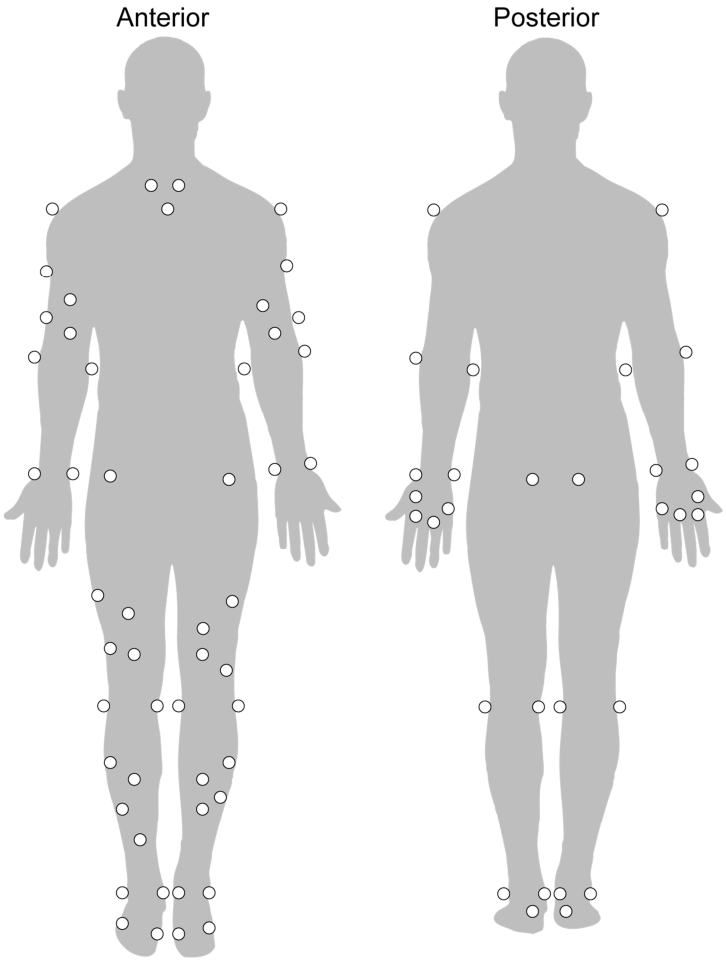


**Figure 4.6. Full-body marker scheme.** Each segment tracked had at least four markers tracking the motion.

Seventy six passive reflective markers were used to define the motion of the upper and lower-limbs along with the pelvis and trunk. Two markers were placed on the wrists, elbows, knees and ankles to help define joint centers. Four tracking markers were attached to each of the following segments: forearm, upper arms, thighs and shanks. An additional tracking marker was placed on the scapula acromium tip for the upper arm. Four tracking markers on each hand were placed on the following landmarks: $2^{nd}$, $3^{rd}$ and $5^{th}$ metacarpal head and base of the $2^{nd}$

metacarpal. Markers placed on the trunk were: right and left clavicle anterior sternoclavicular joints and sternal manubriosternal edge. The pelvis was defined by the right and left anterior and posterior iliac crests. The following markers that were placed on the exterior of the shoes: calcaneus, 1$^{st}$ and 5$^{th}$ metatarsal heads and the base of the 1$^{st}$ metatarsal. Each joint center was defined using a functional joint algorithm applied to movements that spanned the range of motion that occurs during walking (Ehrig et al. 2006; Taylor et al. 2010).

# Chapter 5

# Effect of Toe Joint Stiffness and Toe Shape on Walking Biomechanics

## 5.1 Introduction

During typical walking, the human metatarsophalangeal (MTP) joints undergo substantial flexion (sometimes termed the toe rocker phase of gait, Perry and Burnfield 2010), followed by extension. We refer to this MTP motion as *toe joint articulation*. It has been suggested that toe joint articulation may affect the gear ratio of the ankle extensor muscles, and thereby effect economy of locomotion (Carrier, Heglund, and Earls 1994; Takahashi et al. 2016). Simulations provide complementary evidence that toe joint articulation may be beneficial for walking dynamics (e.g., reducing mechanical cost-of-transport, Kumar et al. 2009; Huang et al. 2010). Further evidence that toe joint articulation can impact locomotor economy and other performance metrics is found in the fields of prosthetics (Grabowski, Rifkin, and Kram 2010; Zhu, Wang, and Wang 2014b), footwear (Takahashi et al. 2016; Oh and Park 2017), sport biomechanics (Oh and Park 2017; Nigg et al. 1998; Willwacher et al. 2013; Roy and Stefanyshyn 2006) and humanoid robotics (Ahn, Lee, and Go 2003; Buschmann, Lohmeier, and Ulbrich 2009). However, the effects of specific toe properties (e.g., joint stiffness, shape, length) have not been fully or systematically studied, and it remains unclear if or how we should be mimicking or augmenting biological toe joint behaviors in devices such as prostheses, exoskeletons and robot feet, or in the design of shoes.

A gap exists in our understanding of how various toe properties affect bipedal locomotion. For instance, a few studies have partially explored the effects of increasing toe joint stiffness (via orthoses inserted into the shoe, which act as springs in parallel with the biological

joints, Takahashi et al. 2016; Oh and Park 2017; Nigg et al. 1998; Willwacher et al. 2013; McDonald et al. 2016; Roy and Stefanyshyn 2006); however, these studies did not test the effects of reducing biological toe joint stiffness. Likewise, it is generally not practical to alter biological toe shape, or to artificially lengthen or shorten the biological toes. The purpose of this study was to address some of these knowledge gaps. We designed and built an adjustable foot prosthesis that enabled us for the first time to systematically investigate the effects of individual toe properties across a broad range of physiological and non-physiological values. Findings are expected to have implications for the design of devices (e.g., prosthetics, orthotics, robotics), footwear and other clinical interventions.

Bipedal walking simulations predict that toe joint articulation can impact locomotor performance (Yan Huang et al. 2012; Y. Huang et al. 2010; Kumar et al. 2009). However, the effects of toe joint articulation in simulation depend on specific model parameters such as ankle and toe stiffness, foot length and the ratio of toe to foot length. Huang et al. 2010 found that with foot and toe proportions similar to that of humans, having a toe joint improved the mechanical cost-of-transport (energy needed to traverse a given distance) by up to 20% relative to a purely rigid foot. The magnitude of this benefit depended on ankle and toe joint stiffness. For instance, if the ankle joint stiffness was relatively weak, the toe joint stiffness had little effect on the cost-of-transport (Yan Huang et al. 2012). In simulation, changes in mechanical cost-of-transport were due to how toe (and other ankle-foot) dynamics affected the redirection of the COM velocity during the step-to-step transition. Model parameters that reduced Collision losses at foot contact then reduced the energy input (positive work) necessary for the model to walk at fixed speed (Kumar et al. 2009). In humans, a reduction in mechanical work potentially signifies a reduction in muscular effort needed during gait (Arthur D. Kuo, Donelan, and Ruina 2005). In

biped robot simulations, inclusion of a toe joint has been found to increase walking speed (Kwon and Park 2012; Zhang et al. 2010; Sellaouti et al. 2006) and to reduce lower limb joint torques (Yoon et al. 2011; Zhang et al. 2010; Yamane and Trutoiu 2009). Although potential benefits of toe joint articulation have been predicted through simulation, complementary empirical studies are needed to test these predictions and to understand human responses to changes in toe properties.

Experimental footwear and prosthetic studies provide supporting evidence that toe joint dynamics can impact locomotor performance. Augmenting the bending stiffness of footwear (through orthotic shoe inserts) can increase the effective toe joint stiffness during walking and running (Takahashi et al. 2016; Oh and Park 2017; Nigg et al. 1998; Willwacher et al. 2013; McDonald et al. 2016; Roy and Stefanyshyn 2006), which has been shown to affect metabolic cost (Takahashi et al. 2016; Oh and Park 2017). Though the biomechanical reason(s) for the metabolically optimal toe joint stiffness are not yet fully understood, changes in shoe bending stiffness were accompanied by changes in ankle dynamics (e.g., Takahashi et al. 2016; Arch and Fylstra 2016). Complementary findings from studies on prostheses also suggest that the addition of a toe joint may aid locomotion for persons with amputation. One study found a 10% reduction in metabolic cost, on average, when four lower limb prosthesis users walked on a foot with an articulating toe joint, vs. a foot without a toe joint (Grabowski, Rifkin, and Kram 2010). A separate study on powered prosthetic feet found that toe joint articulation reduced ankle motor torque requirements by 15% (Zhu, Wang, and Wang 2014b).

In summary, evidence from experimental and simulation studies indicates the importance of toe joint dynamics. However, there remains a need to isolate and understand the effects of individual toe joint properties during human walking. The objectives of this study were to

characterize the effects of varying toe joint stiffness across different ankle joint stiffness conditions, and to characterize the effects of toe shape on level-ground walking biomechanics.

## 5.2 Methods

To isolate and examine individual toe properties, we designed and constructed an adjustable foot prosthesis, then tested able-bodied persons wearing this prosthesis bilaterally below simulator boots (which fixate the biological ankle). We tested ankle and toe joint stiffness above, at, and below physiological joint quasi-stiffness (Hansen et al. 2004; MacWilliams, Cowley, and Nicholson 2003; Rouse et al. 2013; Zhu, Wang, and Wang 2014a), while collecting biomechanical force and motion data. Additionally, we tested toe shapes that were anatomical and non-anatomical in form, in order to determine how this aspect of the foot affects gait.

### 5.2.1 Ankle-Toe Prosthesis

We designed and fabricated a pair of adjustable foot prostheses (Fig. 5.1). The key feature of the design was that it allowed us to independently vary individual foot properties (e.g., toe joint stiffness, ankle stiffness) to systematically characterize their effects on gait. Our prosthesis (width 6.8 cm; mass 1.23 kg) is comparable in size to commercially available prosthetic feet worn in shoes (Ozden et al. 2005; Gailey et al. 1997). Nominally, the prosthesis was 27 cm long (heel to toe) and measured 20 cm from heel to toe joint axis, reflecting approximate human foot anthropometrics (Fessler, Haley, and Lal 2005; Rolian et al. 2009). Below the prosthesis, attached via hook and loop, was 1.3 cm shoe crepe (durometer: 35-40A) with Vibram outsoling to mimic shoe-like tread.

The adjustable foot prosthesis has two sagittal degrees-of-freedom: one to approximate the ankle joint and another to approximate the transverse toe (MTP) joint axis (Fig. 5.1, Bojsen-Møller and Lamoreux 1979) in the biological foot. These rotational degrees of freedom were provided by pillow bearings and brass bushings, respectively. The extension stiffness at each of

these joints was adjusted by interchanging die springs at the ankle and 1095 steel cantilever springs at the toe joint. A 75A durometer rubber damper provided plantarflexion dampening of the ankle beyond neutral position (e.g., after heel contact), similar to commercially-available single-axis foot prostheses.

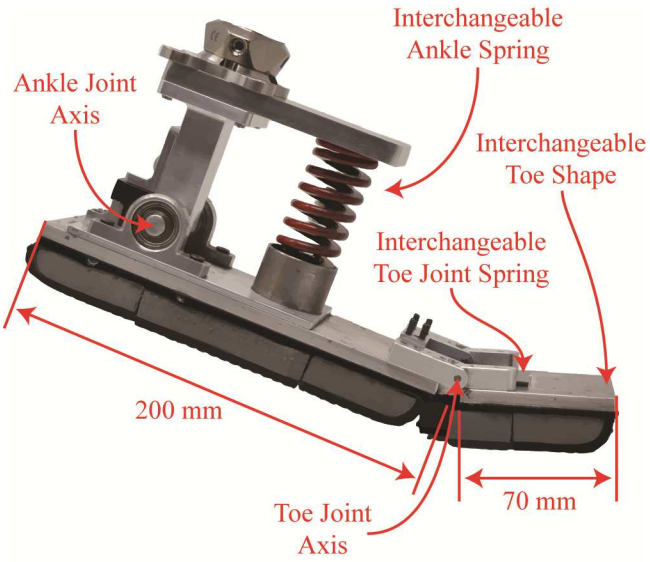


**Figure 5.1 Adjustable ankle-toe prosthesis.** The ankle-toe joint prosthesis has two degrees-of-freedom with interchangeable ankle and toe joint stiffness. The toe of this prosthesis can also be interchanged to test different shapes. Shown here is the Square toe shape.

### 5.2.2 Subject Enrollment

Ten healthy able-bodied subjects (5 males, 5 females, 23±3 yrs, 76.6±6.4 kg, 1.77±0.06 m) were recruited to participate in a two-day gait analysis study. All subjects gave informed consent to the protocol, which was approved by the Institutional Review Board at Vanderbilt University. We recruited subjects with a mass of 73 ± 10 kg to permit testing of roughly the same mass-normalized prosthetic ankle and toe joint stiffness conditions across all subjects. We recruited persons without amputation similar to previous studies (Zelik et al. 2011; Caputo and Collins 2014; Adamczyk, Collins, and Kuo 2006; Malcolm et al. 2015), in order to avoid amputation-specific variability (e.g., residual leg length, amputation type, amputation surgery) and common comorbidities (e.g., residual limb pain, osteoarthritic pain, scoliosis).

### 5.2.3 Training

On the first day, subjects were given time to acclimate to walking on the adjustable foot

prostheses. Subjects wore a pair of the adjustable foot prostheses below prosthetic simulator boots (modified Aircast boots which immobilize the biological ankles, Zelik et al. 2011; Caputo and Collins 2014; Adamczyk, Collins, and Kuo 2006; Malcolm et al. 2015). The simulator boots and prostheses increased the subject's leg length by 0.16 m. Subjects walked over-ground for at least one hour, with frequent breaks. This in-lab acclimation period enabled the subjects to experience six of the 25 conditions that would be tested during the data subsequent collection. These six conditions entailed three different ankle and six different toe conditions that included the least and most stiff ankle and toe joint conditions. Subjects returned within one week for experimental data collection.

### 5.2.4 Data Collection

We performed an experimental data collection the second day. Subjects donned the simulator boots bilaterally with the adjustable foot prostheses. They walked at 1.0 m/s on a split-belt instrumented treadmill (Bertec, Columbus, OH, USA) while we collected ground reaction forces (GRFs) and motion capture (Vicon T40, Oxford, UK) for 30 seconds. Forty-six passive reflective markers were affixed bilaterally to the lower limbs, simulator boots, and prostheses. The data collection consisted of 25 different conditions: 20 pseudo-randomized ankle and toe stiffness combinations, followed by five randomized toe shape conditions (see Fig. 5.2, Table 5.4). After data collection, we asked each subject if they preferred walking with or without an articulating toe joint. We did not ask subjects about each individual condition to avoid response fatigue (Egleston, Miller, and Meropol 2011).

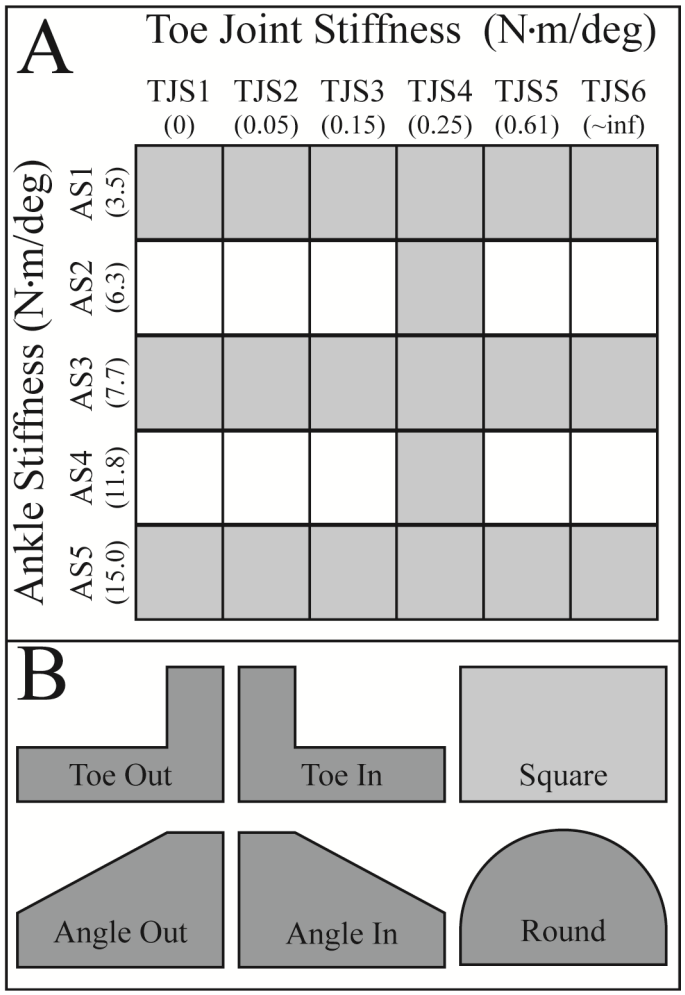


**Figure 5.2 (A) Ankle and toe joint stiffness sweep and (B) Toe shape sweep.** (A) Ankle stiffness (AS) and toe joint stiffness (TJS) combinations tested in this study are shown in gray. The stiffness value for each condition is in parentheses, in units of N·m/deg. The ankle spring was varied via die springs and toe joint stiffness was varied via spring steel cantilever springs (TJS2-TJS5). We completely removed the toe to achieve the zero stiffness condition (TJS1). An aluminum strut was used to provide a near-infinite toe joint stiffness, preventing the toe from articulating (TJS6). (B) The different toe shapes were interchanged on the ankle-toe prosthesis (depicted from a right foot perspective). The Square toe shape was only tested in the ankle and toe joint stiffness sweep. From the left foot perspective, all shapes are mirror of what is shown.

In addition to the training day, subjects were given time during the data collection to further acclimate to the different conditions. Initially, the subjects were given five minutes to re-acclimate themselves with the prosthesis while walking on the treadmill. A minimum of 30 seconds was given to the subjects each time the condition was changed during the data

collection. Data were then only collected when subjects visually appeared comfortable with the new condition, as assessed by a trained experimenter – thus we erred on the side of giving subjects more time to adjust to the new condition if they seemed as if they made need it.

### 5.2.5 Ankle and Toe Joint Stiffness Sweep

Prior to testing, ranges of ankle and toe joint stiffness were chosen to include stiffness below, at, and above the physiological quasi-stiffness for an individual of 73 kg (Hansen et al. 2004; MacWilliams, Cowley, and Nicholson 2003; Zhu, Wang, and Wang 2014a; Mager et al. 2018). Quasi-stiffness is commonly used characterize the relationship between net joint torque and angle during a certain portion of a movement cycle (Latash and Zatsiorsky 1993; Hansen et al. 2004). The physiological ankle has been approximated as having quasi-stiffness of between 5.5-11.0 N·m/deg during the entire stance phase of walking (Hansen et al. 2004). In this study we tested rotational ankle stiffness (AS) values of 3.5, 6.3, 7.7, 11.8 and 15.0 N·m/deg. This range of AS also corresponds roughly to the range of stiffness values reported for commercially-available prosthetic ankles (Sanderson and Martin 1997; Major et al. 2014; Ferris et al. 2012). Hereafter, these ankle stiffness values are labeled as AS1 through AS5, signifying softest to stiffest spring, respectively. These stiffness conditions were achieved by interchanging commercially-available die springs at the ankle (see Fig. 5.1). The physiological toe joint behavior during walking is also reasonably well characterized by quasi-stiffness, with reported values between 0.05-0.30 N·m/deg during the entire stance phase (Zhu, Wang, and Wang 2014a). In our study we tested toe joint stiffness (TJS) of 0, 0.05, 0.15, 0.25, 0.61, and ~infinite N·m/deg, labeled as TJS1 through TJS6, signifying softest to stiffest spring, respectively. TJS2 through TJS5 were obtained through interchanging thicknesses and number of spring steel cantilever springs (see

Fig. 5.1). TJS1 (zero stiffness) was achieved by completely removing the toe and toe joint of the prosthesis, which was necessary to avoid toe drop during leg swing which would be a tripping hazard. TJS6 was set by replacing the spring steel with a 6.5 mm thick aluminum strut for a near-infinite toe joint stiffness. The testing order of ankle springs was randomized and the toe joint stiffness was randomized within each different ankle spring condition (see Table 5.4). This pseudo-randomization was performed in order to limit the amount of time spent interchanging the prosthetic ankle springs (which was a more time-consuming operation than interchanging toe springs). The conditions TJS1-TJS6 were tested with AS1, AS3, and AS5. To keep total walking time reasonable for each subject, only TJS4 was tested with AS2 and AS4 (Fig. 5.2A). All stiffness sweep conditions were tested with the Square toe shape (Fig. 5.2B). Changes in ankle and toe joint stiffness resulted in minimal changes (±0.12 kg) in prosthesis mass (1.23 kg). The toe and ankle joint stiffness conditions that were tested here were selected prior to subject recruitment, as such we recruited subjects within a ±10 kg range of the 73 kg individual that the prosthesis was designed around.

### 5.2.6 Toe Shape Sweep

We designed the Square and Angle Out toe shapes to emulate two different biological forefoot shapes, the “intermediate foot” and the “Greek foot” respectively (Fig. 5.2B, Hefti 2007). The Angle In toe shape represents the opposite of the “Greek foot” shape. The Toe In shape was designed to emulate the presence of just the hallux (big toe) or lack thereof with the Toe Out shape (Fig. 5.2B). Lastly, we tested the Round shape because it is similar to many commercial prostheses (Fig. 5.2B). The Square toe was not tested within this sweep because it was already tested within the previous stiffness sweep. We completely randomized the testing of

the other five toe shapes (see Table 5.4). Changes in toe shape varied the mass of the foot ±0.02 kg.

### 5.2.7 Data Analysis

We computed joint kinematics and kinetics, and COM power. Marker and force data were low-pass filtered at 6 Hz and 15 Hz respectively with a third order, dual-pass, Butterworth filter. Joint kinematics and kinetics were calculated through Visual3D (C-Motion, Germantown, MD, USA). Data were divided into strides (from foot contact to ipsilateral foot contact), then averaged across strides. Foot contact was defined as when the vertical GRFs increased above 20 N. Cross-over steps (e.g., right foot landing on left belt of instrumented treadmill) were removed from analysis prior to averaging stride-based metrics. COM power was computed from the GRFs via the individual limbs method (Donelan, Kram, and Kuo 2002). COM work was computed during different phases of gait (Collision, Rebound, Preload, and Push-off, Fig. 5.3) by integrating under the power curve (similar to Zelik, Takahashi, and Sawicki 2015). For one subject the AS5-TJS6 condition exhibited unusual fluctuations in the COM power, such that Collision, Rebound, and Preload could not be defined. Work metrics were not computed for these phases for this subject. Net power from the prosthesis, in this manuscript termed *anklefoot power*, was also computed from established methods (defined in previous literature as Unified Deformable shank power, Takahashi and Stanhope 2013). This anklefoot power is a 6 degree-of-freedom joint estimate between the shank segment (in this case the simulator boot) and the ground (for full derivation see Zelik and Honert 2018), meaning it estimates the net power contributions from everything below the shank (i.e., the ankle and toe joints as well as the shoe crepe).

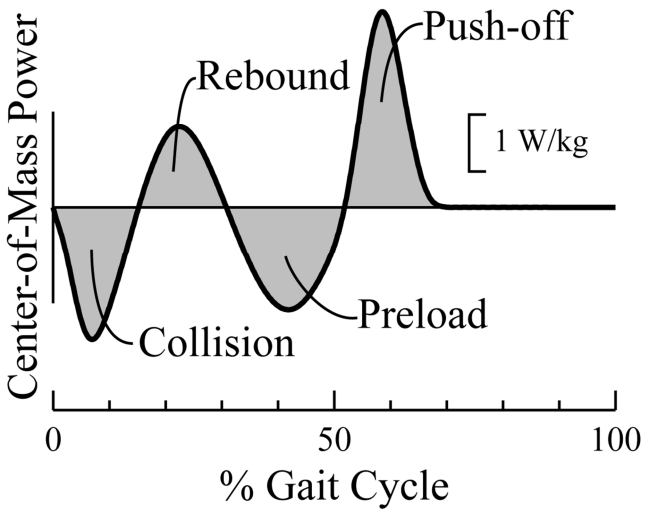


**Figure 5.3. Phases of gait as defined by the COM power.**

We examined 20 different combinations of ankle and toe joint stiffness (using the nominal Square toe shape), as well as five additional toe shape conditions. For brevity, we present only a subset of key outcome metrics. Kinematic and kinetic time series data show joint level trends. COM power and work during different phases of gait provide whole-body summary metrics (Zelik et al. 2011; Caputo and Collins 2014; Jackson and Collins 2015). We focus on the Push-off phase of gait because this is when the toe joint undergoes flexion/extension, and because Push-off is known to affect walking performance (Caputo and Collins 2014; Jackson and Collins 2015; Malcolm et al. 2015). We also summarize Collision phase outcomes because changes in Push-off work have been theorized (Arthur D. Kuo, Donelan, and Ruina 2005) and in some cases shown experimentally (e.g., Jackson and Collins 2015; Adamczyk, Roland, and Hahn 2017) to influence negative work during contralateral limb Collision, which occurs after foot contact during leading limb weight acceptance.

Statistical analysis was performed to determine the significance of trends in outcome metrics. We examined the significance in trends of different outcome metrics ($M$) with

increasing stiffness (*S*) with a one-way analysis of covariance (ANCOVA). We analyzed the following outcome metrics: peak toe joint flexion, peak ankle moment, peak ankle power, peak anklefoot power, peak COM power, peak knee moment, peak knee power during the Collision phase, peak COM power during the Collision phase, ankle Push-off work, anklefoot Push-off work, COM Collision work, COM Rebound work, COM Preload work, and COM Push-off work. For simplicity, we assumed a linear response, thus data were fitted to the relationship: $M=C*S+D$, where $C$ is the coefficient and $D$ is the offset. The stiffness and outcome metric variables were non-dimensionalized using gravity, subject-specific mass and leg length in order to account for size differences between subjects prior to averaging across subjects (to compute inter-subject study mean). In the toe joint stiffness sweep, the near-infinite stiffness toe joint (TC6) was not included in the regression analysis to avoid skewing of the slope coefficient. For the toe shape sweep, we performed a multiple comparison analysis of variance (ANOVA) with a Holm-Sidak correction. We did not perform an ANCOVA analysis with the toe shape sweep as these conditions do not fall along a continuum of values (as was the case in the stiffness sweep). We assessed if each toe shape caused a significant change in COM work during Collision, Rebound, Preload or Push-off, relative to each other toe shape. In all analyses, significance level of 0.05 was used.

## 5.3 Results

### 5.3.1 Effect of Toe Joint Stiffness

Increasing toe joint stiffness decreased peak toe joint extension angle during walking ($p$<0.001, Fig. 5.4), from a maximum at TJS2 of 52˚ to a minimum of 6˚ at TJS6. Increasing toe joint stiffness from zero (TJS1) to the stiffest condition (nearly-infinite, TJS6) resulted in: 53% (0.6 Nm/kg) greater peak ankle moment, 129% (11.6 J) greater ankle Push-off work, 91% (1.2 W/kg) greater peak anklefoot power, 181% (12.2 J) greater anklefoot Push-off work, and 48% (5.7 J) greater COM Push-off work. All these increasing trends were statistically significant ($p$<0.001, Fig. 5.4). With increasing toe joint stiffness, we also observed a 78% (1.2 W/kg) greater peak ankle power and 27% (0.5 W/kg) greater peak COM power, on average, though these were not significant trends ($p$=0.11 and $p$=0.21, respectively). On average, the lowest peak COM Push-off power was actually obtained with the second lowest stiffness (TJS2: 1.77 W/kg, vs. TJS1: 1.83 W/kg). Although the stiffest toe joint resulted in the highest Push-off power, 9 out of 10 subjects self-reported that they did not prefer this condition. Rather these subjects preferred having a toe joint that could articulate during walking. Changes to toe joint stiffness had smaller effects on knee and hip kinematics and kinetics. Knee angle over the stride was nearly unchanged for all toe joint stiffness values except for TJS1 (zero stiffness). TJS1 exhibited, on average, ~11˚ less knee flexion during swing phase than the other toe stiffness conditions. All trends and values summarized above were evaluated at AS3. AS1 and AS5 results are presented below.

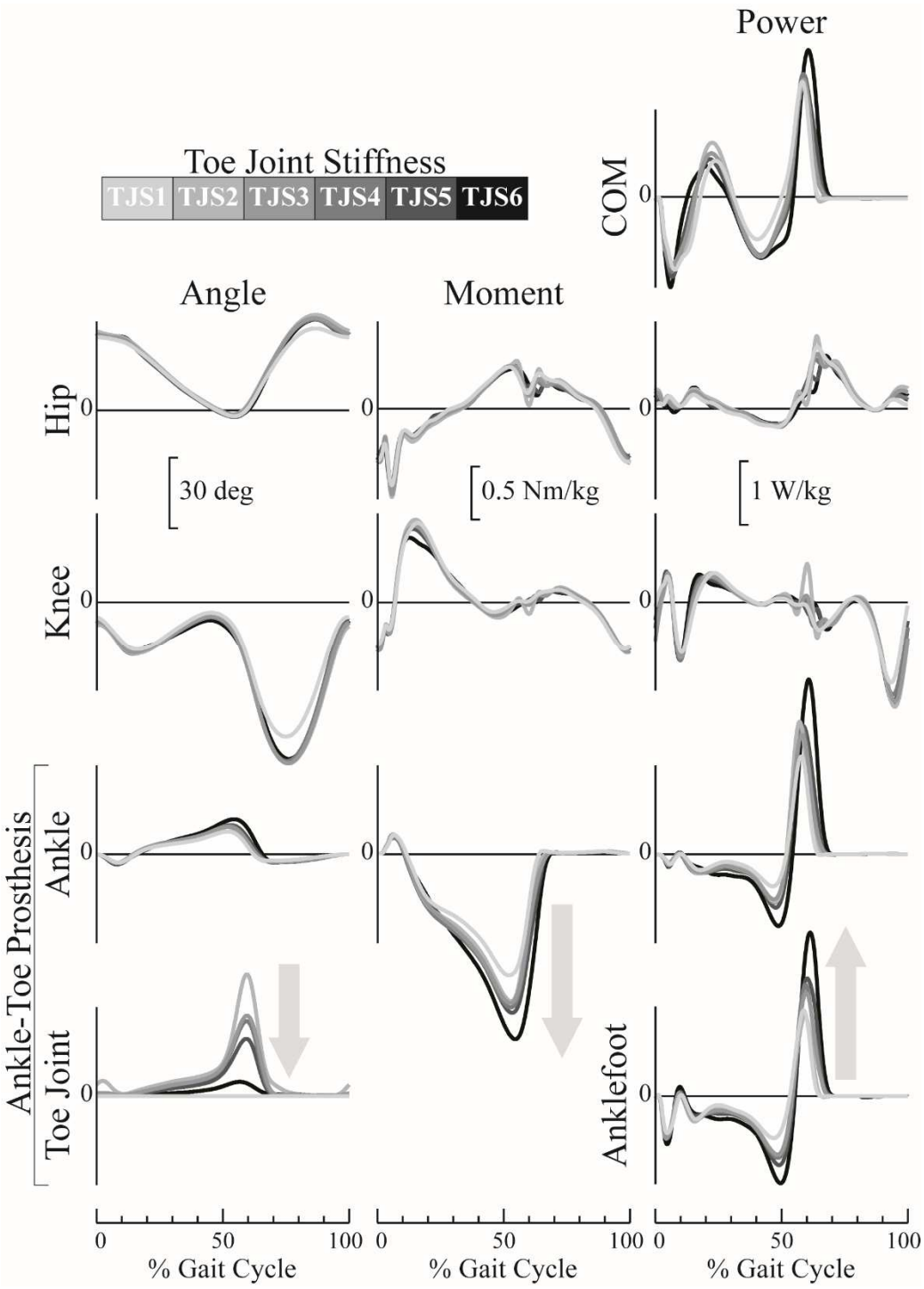


**Figure 5.4 Effects of varying toe joint stiffness on lower limb kinematics, kinetics and COM power.** Reported time series results are at Ankle Stiffness 3 (AS3, 7.7 N·m/deg), for all toe joint stiffness conditions when walking at 1.0 m/s. Shaded arrows indicate statistically significant trends ($p<0.001$) in peak values with increasing toe joint stiffness. Curves depict inter-subject means.

Changes to toe joint stiffness had the largest effects on gait biomechanics when the ankle was sufficiently stiff (see Fig. 5.5). With the softest ankle spring (AS1), changing toe joint stiffness had relatively small, and mostly not statistically significant, effects on COM work (Fig. 5.5). In contrast, toe joint stiffness effects were more pronounced with higher ankle stiffness (AS3, AS5). For instance, with the softest ankle spring (AS1), increasing toe joint stiffness from TJS1 (zero) to TJS6 (near-infinite) resulted in ~1 J increase in COM Push-off work ($p$=0.18). But for stiffer ankles (AS3, AS5) there was ~6 J increase in COM Push-off work as well as ~9 J increase in COM Preload work (both significant trends, $p$<0.001). For AS1 and AS3, there were no significant trends in Collision ($p$>0.07) and Rebound work ($p$>0.33). For AS5, there was a significant decreasing trend during Rebound ($p$<0.001), but not Collision ($p$=0.07, Fig. 5.5).

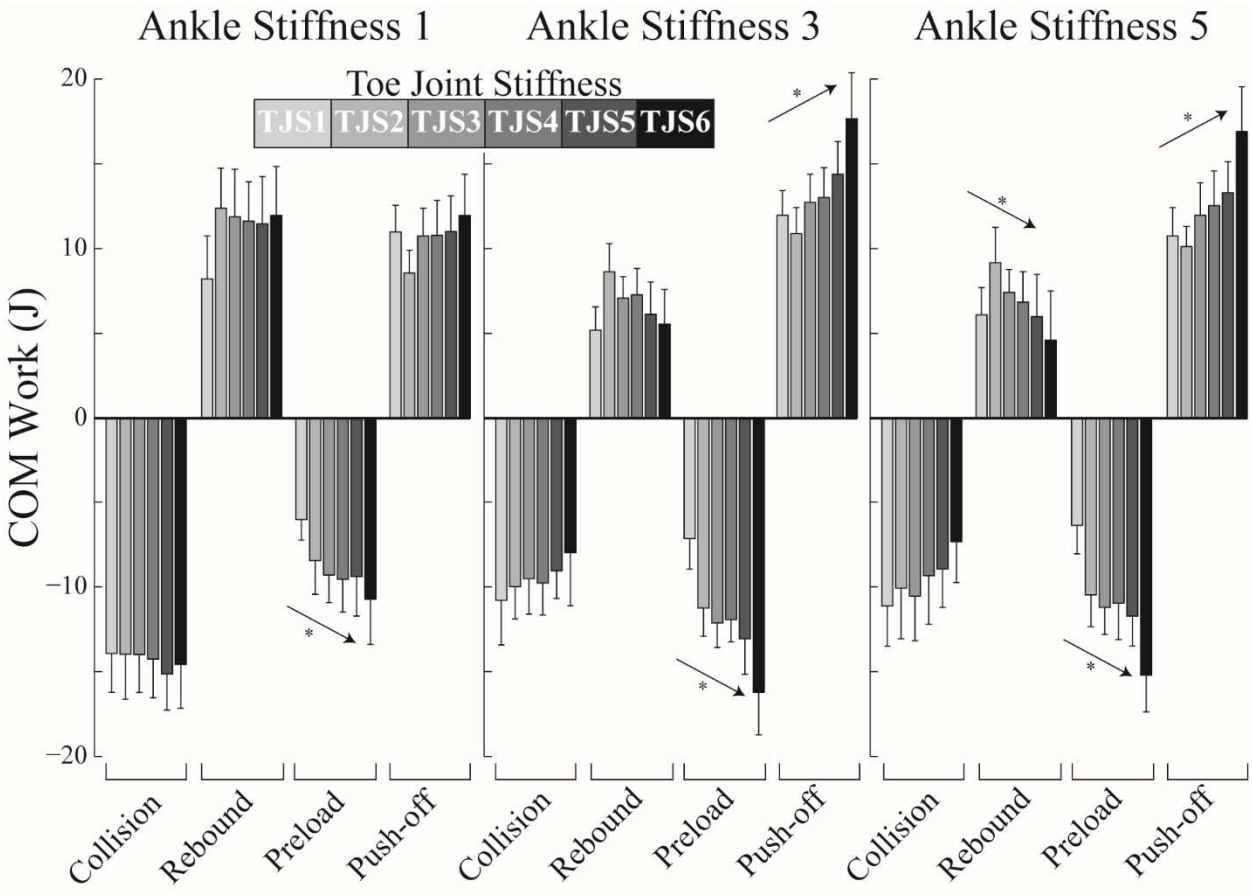


**Figure 5.5 COM work during different phases of gait for three different ankle stiffness conditions across all tested toe joint stiffness conditions.** Arrows with asterisks above indicate statistically significant trends ($p<0.01$). Inter-subject means and standard deviations are shown.

### 5.3.2 Effect of Ankle Stiffness

During Push-off, increasing ankle stiffness from AS1 to AS5 resulted in: 48% (7.9˚) decrease in maximum ankle dorsiflexion angle, 26% (0.6 W/kg) decrease in peak ankle Push-off power, and 25% (0.4 W/kg) decrease in anklefoot peak Push-off power (all significant trends, $p<0.01$). We also observed a 15% (2.0 J) decrease in ankle Push-off work and a 22% (2.3 J) decrease in anklefoot Push-off work though these were not significant trends ($p=0.14$ and $p=0.09$, respectively). However, increasing ankle stiffness led to a 38% (0.4 Nm/kg) increase in magnitude of peak ankle moment and a 12% (0.2 W/kg) increase in peak COM Push-off power

(both significant trends, $p<0.05$). Increasing ankle stiffness caused earlier peak ankle moment and earlier toe joint extension in the gait cycle (Fig. 5.6). Increasing ankle stiffness from the softest (AS1) to the stiffest spring (AS5) resulted in the following changes during early- to mid-stance (Collision and Rebound phases of gait): 17% (0.2 Nm/kg) decrease in peak knee moment (Fig. 5.6), 45% (0.5 W/kg) decrease in peak knee power magnitude, and 50% (0.5 W/kg) decrease in peak COM Collision power magnitude (all significant trends, $p<0.01$, Fig. 5.6). Varying ankle stiffness only resulted in relatively small changes in hip kinematics and kinetics (Fig. 5.6). All trends and values summarized above were evaluated at TJS4.

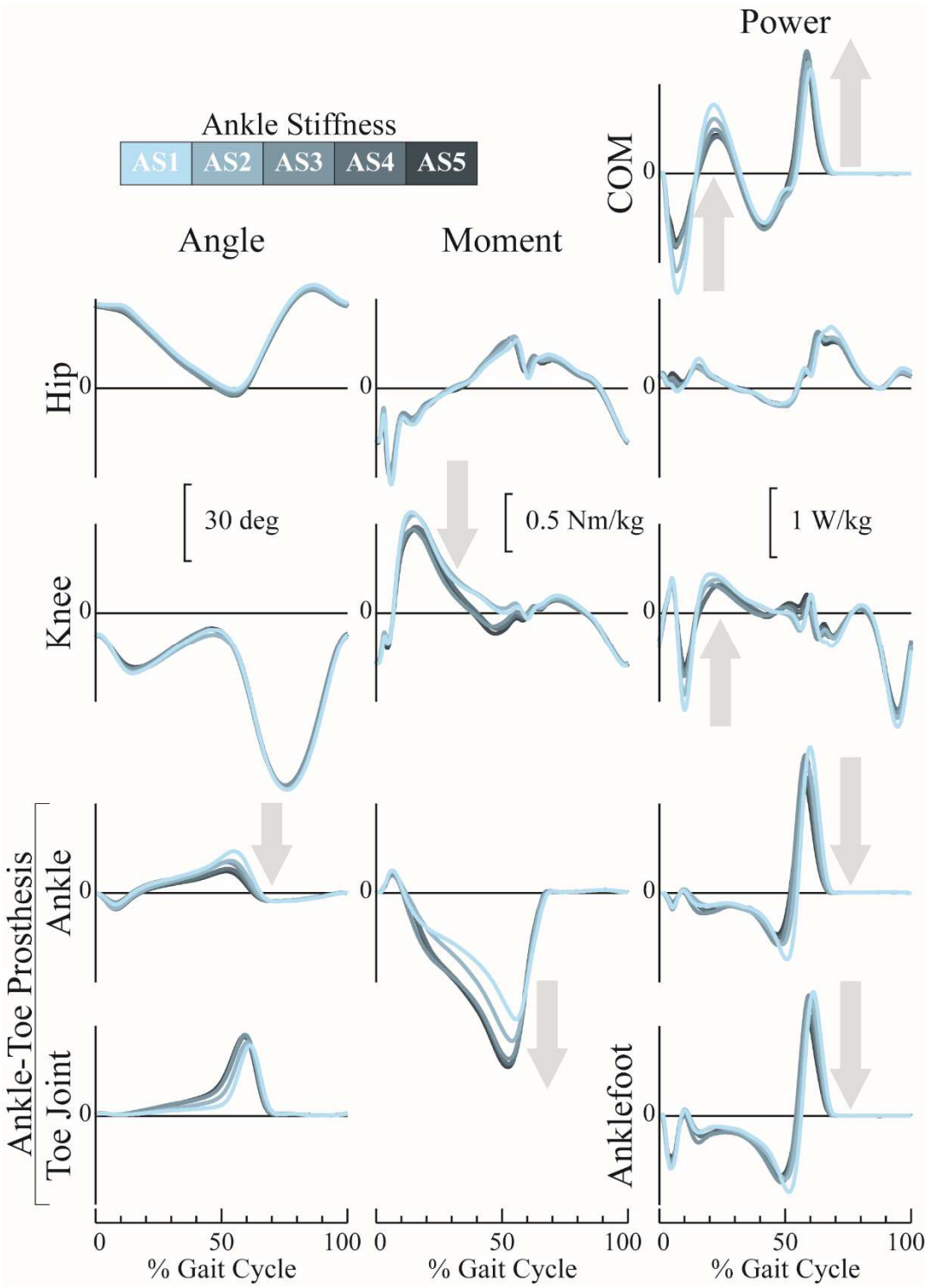


**Figure 5.6 Effects of varying ankle stiffness on lower limb kinematics, kinetics and COM power.** Reported time series results are at Toe Joint Stiffness 4 (TJS4, 0.25 N·m/deg) for all ankle stiffness conditions when walking at 1.0 m/s. Shaded arrows indicate statistically significant trends ($p<0.05$) in peak values with increasing ankle joint stiffness. Inter-subject means are shown.

Varying ankle stiffness affected COM work (Fig. 5.7) primarily during early- to mid-stance (Collision and Rebound), and to a lesser extent during mid- to late-stance (Preload and Push-off). Increasing ankle stiffness from AS1 to AS5 resulted in ~5 J decrease in the magnitude of COM Collision work ($p<0.001$), ~5 J decrease in COM Rebound work ($p<0.001$), ~1 J increase in magnitude of COM Preload work ($p=0.22$), and ~2 J increase in COM Push-off work ($p<0.05$, Fig. 5.7). However, for Preload and Push-off phases, the maximum COM work was observed at an intermediate ankle stiffness (AS3). For AS3, COM Preload and Push-off work magnitudes were ~2 J larger than for AS1, and ~0.5 J larger than for AS5 (Fig. 5.7). All trends and values summarized above were evaluated at TJS4.

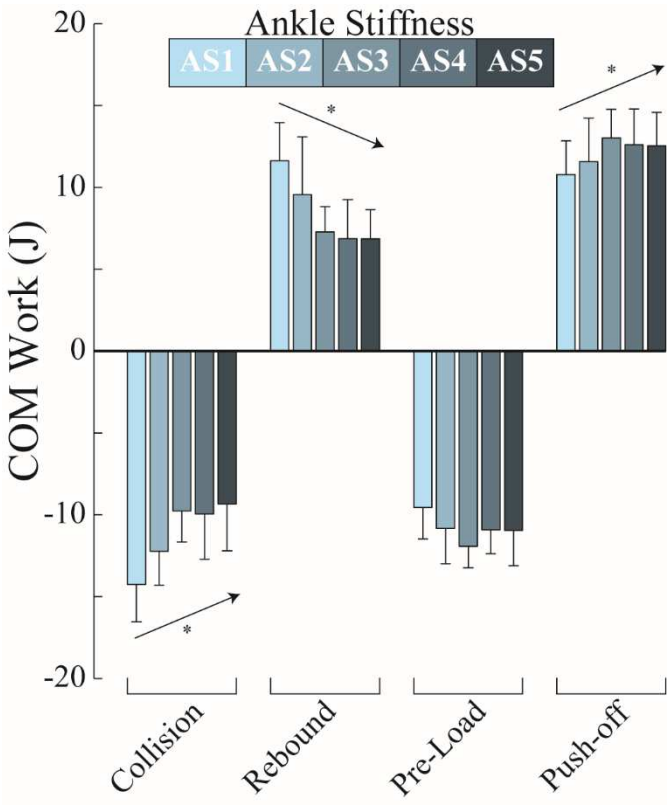


**Figure 5.7 COM work during different phases of gait for all tested ankle stiffness conditions.** Results are shown at a single toe joint stiffness (TJS4, 0.25 N·m/deg). Arrows with asterisks above indicate statistically significant trends ($p$<0.001). Inter-subject means and standard deviations are shown.

### 5.3.3 Effect of Toe Shape

Toe shape had minimal effect on ankle, knee, hip and COM outcome measures (kinematics and kinetics, Figs. 5.8-9). The only exception was with the Square toe shape, which exhibited visible differences in joint kinematics and kinetics (Fig. 5.8) and statistical differences in COM work performed during various phases of the gait cycle ($p$ < 0.05, Fig. 5.9); however, as detailed in Discussion, the Square toe was tested during a different part of the experiment than all the other toe shapes.

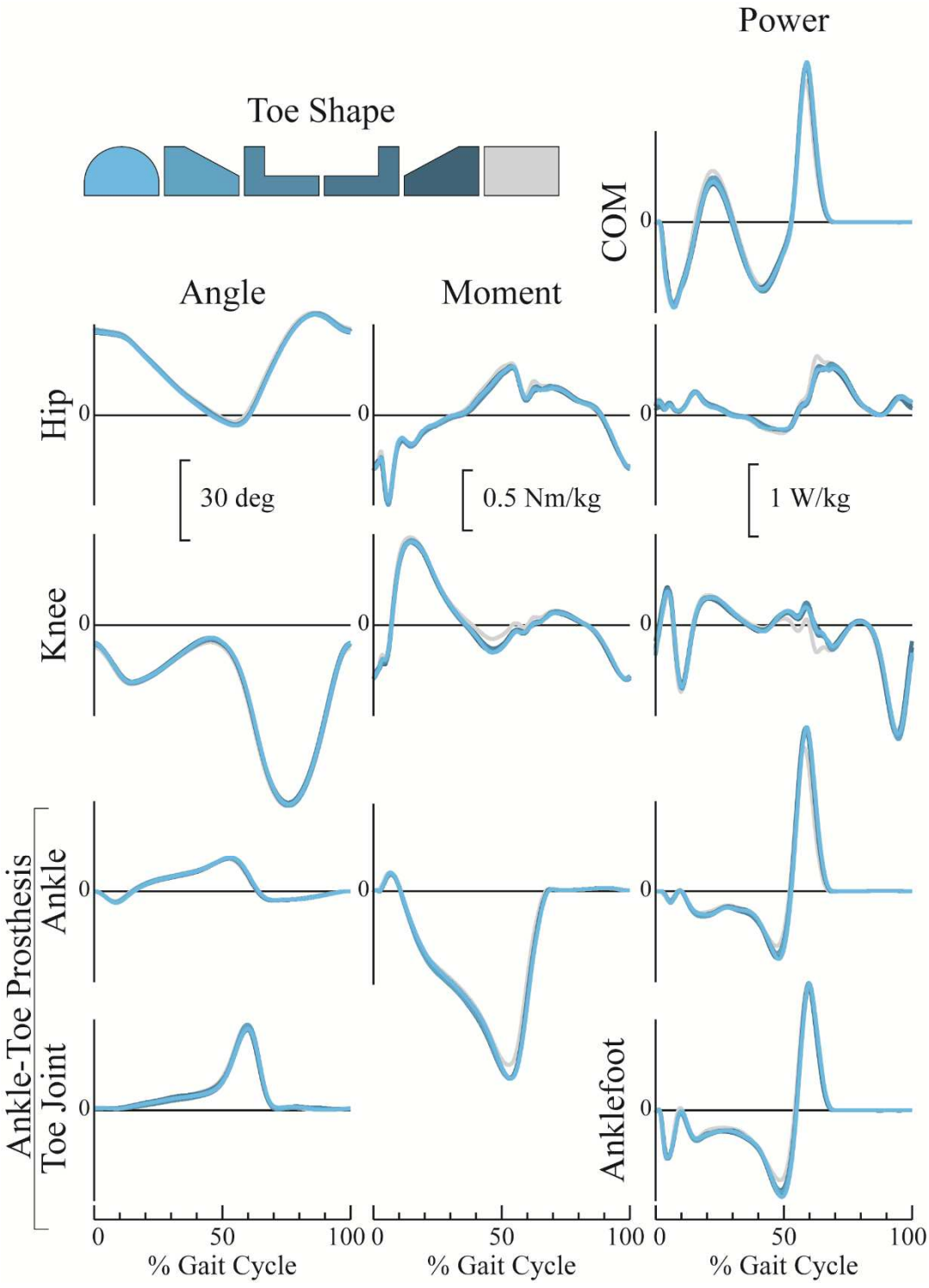


**Figure 5.8 Effects of varying toe joint shape on lower limb kinematics, kinetics and COM power.** Reported time series data is at Ankle Stiffness 3 (AS3, 7.7 N·m/deg) and Toe Joint Stiffness 4 (TJS4, 0.25 N·m/deg), when walking at 1.0 m/s. Curves depict inter-subject means.

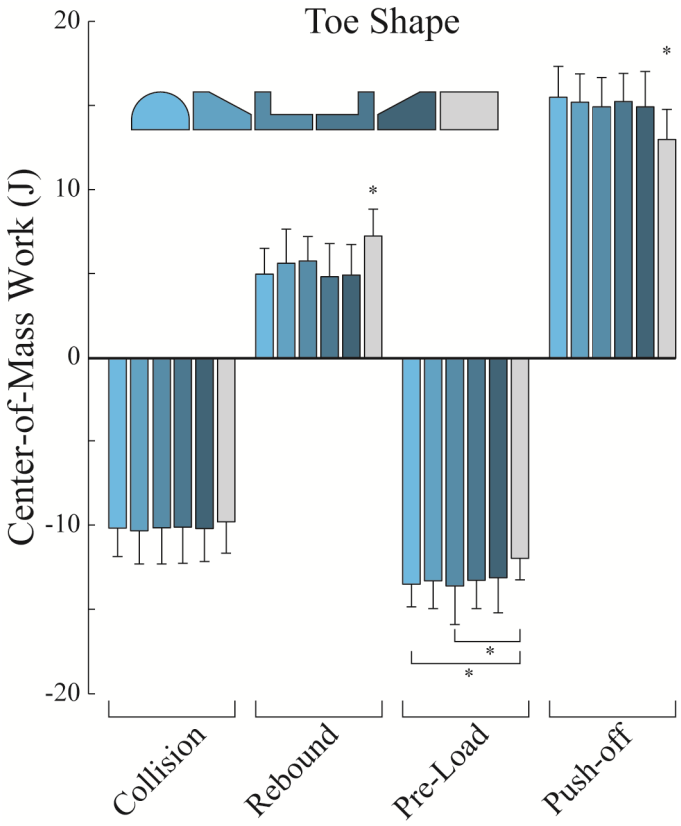


**Figure 5.9 COM work during different phases of gait for different toe shapes tested at a nominal toe joint and ankle stiffness.** Results are from Ankle Stiffness 3 (AS3, 7.7 N·m/deg) and Toe Joint Stiffness 4 (TJS4, 0.25 N·m/deg), when walking at 1.0 m/s. Asterisks during the Rebound and Push-off phase indicate the Square shape was significantly different from all other toe shapes. During Preload, the Square shape was significantly different from the Round and Toe In conditions. All significances levels were evaluated at 0.05. Inter-subject means and standard deviations are shown.

## 5.4 Discussion

We designed an adjustable ankle-toe prosthesis and used it to test individuals walking with a broad range of ankle and toe joint stiffness combinations and toe shapes. This study is the first of its kind to systematically characterize the effects of these toe joint properties on human walking biomechanics. To our surprise, we found that varying toe joint stiffness affected COM Push-off dynamics during walking as much as, or in some cases even more than, varying ankle joint stiffness. In contrast, rather large changes in toe shape appeared to have little effect on forward, level-ground walking dynamics. These findings demonstrate the importance of considering toe joint dynamics, specifically stiffness, in the design of assistive and robotic devices (e.g., prostheses, exoskeletons, humanoid robot feet) and in footwear. Optimizing toe joint stiffness may provide a complementary means of enhancing Push-off or other aspects of locomotor performance (in humans or robots), in conjunction with more conventional approaches such as modifying or augmenting ankle dynamics.

We found that increasing toe joint stiffness led to increased COM Push-off work by the prosthetic limb. The major surprise (as noted above) was that this magnitude of increase in COM Push-off work (across the range of toe joint stiffness values) was comparable to or larger than the change in COM Push-off work due varying ankle joint stiffness (Table 5.1). For the AS3 ankle spring, increasing toe joint stiffness from zero (TJS1) to near-infinite (TJS6) caused COM Push-off work to increase by 48% (Table 5.3). Even if we were to exclude the two extreme toe joint conditions (which could alternatively be described as not having a toe joint at all, but simply having a shorter vs. longer rigid foot), then increasing toe joint stiffness from TJS2 to TJS5 still increased COM Push-off work by 32%. This indicates that these observed Push-off effects were a result of modifying toe joint stiffness, and not simply from having a physically longer rigid

foot, which also affects gait dynamics (Zelik et al. 2014; Adamczyk and Kuo 2013). However, a stiffer toe joint does enable the *effective foot length* (the anterior displacement of the center-of-pressure under the foot expressed as a percentage of total foot length, Hansen, Sam, and Childress 2004) to be longer during gait, by allowing the center-of-pressure to progress more anteriorly beyond the toe joint. This increase in effective foot length is evidenced by increasing ankle moment with increasing toe joint stiffness (Fig. 5.4), resulting in larger magnitudes of elastic energy storage and return at the ankle spring.

**Table 5.1 COM Push-off work for all ankle stiffness (AS) and toe joint stiffness (TJS) conditions.** Mean ± standard deviation (*N*=10) reported in Joules.

| Joint Stiffness (N·m/deg) | AS1 (3.5) | AS2 (6.3) | AS3 (7.7) | AS4 (11.8) | AS5 (15.0) |
|---|---|---|---|---|---|
| TJS1 (0) | 11.0 ± 1.6 | - | 12.0 ± 1.5 | - | 10.7 ± 1.7 |
| TJS2 (0.05) | 8.6 ± 1.4 | - | 10.9 ± 1.5 | - | 10.1 ± 1.2 |
| TJS3 (0.15) | 10.7 ± 1.6 | - | 12.7 ± 1.6 | - | 12.0 ± 1.9 |
| TJS4 (0.25) | 10.8 ± 2.1 | 11.6 ± 2.7 | 13.0 ± 1.8 | 12.6 ± 2.2 | 12.5 ± 2.1 |
| TJS5 (0.61) | 11.0 ± 2.1 | - | 14.4 ± 1.9 | - | 13.3 ± 1.8 |
| TJS6 (~∞) | 12.0 ± 2.4 | - | 17.7 ± 2.7 | - | 16.9 ± 2.7 |

Toe joint stiffness was observed to have a considerable effect on gait biomechanics (Fig. 5.4), as long as the ankle joint was sufficiently stiff (e.g., with AS3 and AS5). We observed relatively little difference in the amount of Push-off work between any of the toe conditions for the softest ankle stiffness (AS1, Table 5.1). Likewise, walking models with a soft ankle spring also demonstrated little difference in the mechanical cost-of-transport with different toe joint stiffness conditions (Yan Huang et al. 2012).

Increases in COM Push-off work with a stiffening toe joint were primarily due to increases in Anklefoot Push-off work. For the AS3 ankle spring, increasing toe joint stiffness from zero (TJS1) to near-infinite (TJS6) led to ~12 J more Anklefoot Push-off work, whereas knee and hip work changes were on the order of ~1-2 J during Push-off. Interestingly, COM

Push-off work only increased by ~6 J over this same parameter range, suggesting that much of the increased Anklefoot work may have gone into changing energy of the segments relative to the COM (Zelik, Takahashi, and Sawicki 2015) and not simply changing the energy state of the COM itself. Such discrepancies between Anklefoot and COM Push-off work have been observed in prior prosthetics studies (e.g., Zelik et al. 2011), and may reflect differences or deficiencies in how elastic energy from the foot is being utilized by or transferred to the prosthesis user during walking. This warrants further investigation in future studies.

In order to understand and optimize locomotor performance, it is beneficial to adopt a holistic view of the entire ankle-foot complex (not simply the ankle, Zelik and Honert 2018). The ankle joint has garnered, and continues to garner, strong research interest for several reasons. The muscle-tendon units about the biological ankle joint are generally considered the main power producers during Push-off in walking (Cappozzo et al. 1976; A. L. Hof, Geelen, and Van den Berg 1983; David A. Winter 1983b). Increases and decreases in ankle Push-off power often result in proportional increases/decreases in COM Push-off power (Zelik and Adamczyk 2016). Theoretical modeling and computational simulations also predict benefits from ankle Push-off dynamics (Neptune, Kautz, and Zajac 2001; Zelik, Huang, et al. 2014; Arthur D. Kuo, Donelan, and Ruina 2005). This research interest has led to the generation of a variety of new ankle-centric prosthetic devices, which have made considerable progress in terms of engineering design, improving certain biomechanical outcomes (Au, Weber, and Herr 2009; Herr and Grabowski 2012; Shultz, Lawson, and Goldfarb 2016; Hitt et al. 2010), and translating new devices into the commercial market. The results from our current study complement and extend this ankle-focused research, by demonstrating that aspects of the foot design (most notably toe joint stiffness, and also foot length) can have a marked effect on gait biomechanics, particularly

during Push-off. Thus foot/toe properties might also be leveraged and optimized to enhance performance of assistive and robotics technologies.

Various walking studies that have increased COM (or ankle) Push-off have shown benefits such as decreased metabolic cost (Caputo and Collins 2014; Jackson and Collins 2015; Herr and Grabowski 2012) and reduced COM Collision (Jackson and Collins 2015; Adamczyk, Roland, and Hahn 2017). For populations, such as persons with amputation, that typically exhibit reduced Push-off from the prosthetic limb (as compared to the intact limb), increasing this Push-off is a common design goal (Quesada, Caputo, and Collins 2016; Herr and Grabowski 2012; Shultz, Lawson, and Goldfarb 2016; Zelik et al. 2011b). In our current study, the largest magnitude of COM Push-off power and work (Fig. 5.4, Table 5.1) was consistently the near-infinite stiffness toe joint (TJS6), which one might initially presume to be the best (biomechanically) based on some prior literature. However, based on subjective feedback from study participants, we found that 9 of the 10 subjects did not prefer the toe joint condition that yielded maximum Push-off (i.e., near-infinite toe joint stiffness in which the joint underwent negligible articulation). The one subject in our study who preferred the near-infinite toe joint stiffness also exhibited a gait pattern with considerably more knee flexion (i.e., a more crouched gait pattern) than the other 9 subjects. The majority of individuals preferred an intermediate stiffness toe joint, in which the joint underwent non-negligible articulation. The reason for this preference, as well as the implications, are not yet clear. These observations suggest an interesting avenue for future gait research: to investigate potential trade-offs between objective biomechanical outcomes (e.g., increasing Push-off) and subjective user preference (similar to prior work on jump landing, Zelik and Kuo 2012). Further investigations collecting metabolic or electromyographic data might provide more insight into potential reasons for this subjective

preference for toe joint articulation.

The way in which toe and ankle joint stiffness interplay with each other to affect gait is exemplified through outcomes such as stride time (Table 5.2), peak Push-off timing (Table 5.3), and Push-off work (Table 5.1). Table 5.2 highlights how increasing toe and ankle stiffness together had an additive effect to mean stride time. Stride time is a clinically-relevant outcome measure used for walking performance assessment of lower limb prosthesis users (e.g., Highsmith et al. 2010). The longest stride time occurred with the stiffest ankle and the stiffest toe joint (AS5-TJS6, Table 5.2), which was 11% longer than the other extreme condition (AS1-TJS1). Table 5.3 highlights how increasing toe and ankle joint stiffness together had an offsetting effect on peak COM Push-off timing. Increasing toe joint stiffness caused later Push-off timing (Fig. 5.4, Table 5.3), whereas increasing ankle stiffness caused earlier Push-off (Fig. 5.6, Table 5.3). When these stiffness values were increased together the COM Push-off timing remained relatively constant (e.g., compare AS1-TJS1 vs. AS5-TSJ6 in Table 5.3). Table 5.1 highlights a slightly more complex, yet still additive interplay between toe and ankle joint stiffness effects. COM Push-off work increased with increasing toe joint stiffness, but was maximal for an intermediate ankle stiffness. Thus, the condition that yielded the largest COM Push-off work was a combination of the stiffest toe joint and the intermediate stiffness ankle (i.e., AS3-TJS6). Of note, the differences in stride time (and thus stride length) between different conditions did not affect the trends reported for COM Push-off work when this work was normalized per meter versus per step.

**Table 5.2 Stride time for all ankle stiffness (AS) and toe joint stiffness (TJS) conditions.** Mean ± standard deviation (N=10) reported in seconds.

| Joint Stiffness (N·m/deg) | AS1 (3.5) | AS2 (6.3) | AS3 (7.7) | AS4 (11.8) | AS5 (15.0) |
|---|---|---|---|---|---|
| TJS1 (0) | 1.18 ± 0.08 | - | 1.19 ± 0.05 | - | 1.20 ± 0.07 |
| TJS2 (0.05) | 1.21 ± 0.07 | - | 1.22 ± 0.08 | - | 1.23 ± 0.09 |
| TJS3 (0.15) | 1.22 ± 0.08 | - | 1.24 ± 0.08 | - | 1.26 ± 0.07 |
| TJS4 (0.25) | 1.22 ± 0.09 | 1.24 ± 0.07 | 1.24 ± 0.08 | 1.26 ± 0.08 | 1.26 ± 0.09 |
| TJS5 (0.61) | 1.22 ± 0.07 | - | 1.26 ± 0.07 | - | 1.26 ± 0.08 |
| TJS6 (~∞) | 1.23 ± 0.08 | - | 1.27 ± 0.09 | - | 1.32 ± 0.09 |

**Table 5.3 Peak COM Push-off timing for all ankle stiffness (AS) and toe joint stiffness (TJS) conditions.** Mean ± standard deviation (N=10) reported in percentage of gait cycle.

| Joint Stiffness (N·m/deg) | AS1 (3.5) | AS2 (6.3) | AS3 (7.7) | AS4 (11.8) | AS5 (15.0) |
|---|---|---|---|---|---|
| TJS1 (0) | 60.0 ± 0.8% | - | 58.4 ± 0.9% | - | 58.2 ± 0.8% |
| TJS2 (0.05) | 60.6 ± 0.8% | - | 58.8 ± 0.9% | - | 58.4 ± 1.0% |
| TJS3 (0.15) | 60.5 ± 0.7% | - | 58.9 ± 1.2% | - | 58.3 ± 1.2% |
| TJS4 (0.25) | 60.3 ± 0.9% | 59.4 ± 0.9% | 58.7 ± 0.8% | 58.8 ± 0.8% | 58.4 ± 0.8% |
| TJS5 (0.61) | 60.7 ± 0.8% | - | 59.0 ± 0.8% | - | 58.5 ± 0.8% |
| TJS6 (~∞) | 62.6 ± 0.8% | - | 60.8 ± 1.5% | - | 60.1 ± 1.1% |

Different toe shapes, including both anatomical and non-anatomical geometries, had little effect on walking biomechanics. These results are consistent with some prior research on partial foot amputation. For instance, one study found that amputation of the hallux (which altered the overall shape of the toes) had minimal effect on ankle Push-off power during level walking (Dillon and Barker 2006), though anecdotally had more effect in sports performance. In our study, the only apparent exception was the Square toe shape, which exhibited more COM Rebound work and slightly less Push-off and Preload work than other toe shapes. However, it is critical to note that the Square toe was not tested at the same time as the other toe shapes (i.e., it was not part of the randomized toe shape parameter sweep, see Table 5.4). Rather the Square toe was tested during the ankle and toe joint stiffness sweep, which occurred separately and earlier in the experimental protocol. Although subjects did perform acclimation training prior to testing, it may be that the Square toe differences were simply due to an ordering effect. We are unable to

confirm or refute this based on the current data set.

Several limitations in experimental protocol should be acknowledged. First, we used a relatively low filter cut-off frequency for motion data (6 Hz) based on the frequency content of gait (Antonsson and Mann 1985). In post-processing we also analyzed data using a higher filtering frequencies (e.g., 15 Hz for both motion and force data) and found it did not affect any of the major trends reported or conclusions draw. Second, there were practical limitations that influenced the protocol and restricted the ankle stiffness values tested. For instance, a zero stiffness ankle would have corresponded to walking on a peg-leg (point foot) with a floppy but useless appendage protruding anteriorly (i.e., the foot plate), which was deemed impractical. We therefore spanned across a limited range of ankle stiffness values, which corresponded roughly to the range of values estimated in commercially-available energy storage and return foot prostheses (Sanderson and Martin 1997; Major et al. 2014; Ferris et al. 2012). In contrast, toe joint stiffness effectively swept from zero to near-infinite, though zero stiffness was achieved by completely removing the toe segment. Third, the joint stiffness conditions tested were not perfectly linear, due to the configuration of the springs within the prosthesis (i.e., cantilevered at the toe joint, and compressed about a rotational ankle joint). Since we swept across a large range of stiffness values, we do not expect any key results or trends to be altered by this limitation. Fourth, due to differences in subject weight, normalized (non-dimensionalized) stiffness ranges were not identical for all subjects. Nonetheless, the normalized stiffness ranges for each subject were still spread across a broad range, including physiological and non-physiological quasi-stiffness values. Fifth, for simplicity, the MTP joints were modeled as a single composite toe axis that was aligned parallel to the ankle joint axis. Future studies are needed to isolate other aspects of the toe, such as the joint axis orientation, number of independent toes, or toe length (all which

were held constant in this present study), and evaluate their effect on forward walking, as well as other tasks. Sixth, leg length was increased by 0.16 m and leg/foot mass was increased by ~1.2 kg due to the simulator boots, similar to prior studies (e.g., Zelik et al. 2011; Caputo and Collins 2014). These changes to anthropometric proportions and mass distribution were consistent for all conditions and therefore are not expected to preclude relative comparisons between conditions tested. In terms of translating these results to clinical populations (e.g., individuals with amputation), it remains to be determined if the trends observed here as a function of varying toe and ankle properties are consistent with trends in such populations. Regardless, the results presented provide new insights about how healthy humans adapt to different toe and ankle properties.

This study brings attention to an aspect of prosthetic and robotic foot design that is often overshadowed by design of the ankle. In prosthetic feet in particular, toe (or forefoot) dynamics are often dictated by the behavior of the cosmesis (rubber shell) and/or footwear. It is unclear to what extent these properties are optimized in most existing commercial prostheses, or whether they are explicitly considered or refined in the design process. The results presented here (e.g., Fig. 5.5) highlight the potential of modifying toe joint dynamics in order to augment locomotor performance, as well as help narrow the potential design space for new prosthetic or robotic feet. Specifically, these findings suggest that integration and optimization of toe joint stiffness can reasonably receive precedence over the identification of an ideal toe shape (at least for forward, level-ground walking, as tested here). Nonetheless, follow-up investigations (e.g., on prosthetic users or specific robots) would be needed to better understand and optimize toe dynamics for a specific patient population, application, implementation or task.

## 5.5 Conclusion

In summary, varying toe joint stiffness had a considerable effect on gait dynamics, specifically on key outcomes such as COM Push-off work. In some cases, varying toe joint stiffness even had a larger effect than varying ankle joint stiffness; which we found surprising given the historical research and design emphasis on ankle dynamics. In contrast, toe shape was observed to have little effect on gait biomechanics. These results suggest the potential to leverage toe joint dynamics to enhance locomotor performance, such as for prosthetic users or walking robots.

## 5.6 Appendix

**Table 5.4 Example protocol.** The experiment was separated into two different sweeps: ankle stiffness (AS#) and toe joint stiffness (TJS#) sweep and toe shape sweep.

| Sweep | Ankle Stiffness Number (Ankle Stiffness [N·m/deg]) | Toe Joint Stiffness Number (Toe Joint Stiffness [N·m/deg]) | Toe Shape |
|---|---|---|---|
| Ankle and Toe Joint Stiffness Sweep | AS1 (3.5) | TJS3 (0.15) | Square |
| | AS1 (3.5) | TJS6 (~Infinite) | Square |
| | AS1 (3.5) | TJS1 (0) | Square |
| | AS1 (3.5) | TJS4 (0.25) | Square |
| | AS1 (3.5) | TJS5 (0.61) | Square |
| | AS1 (3.5) | TJS2 (0.05) | Square |
| | AS3(7.7) | TJS6 (~Infinite) | Square |
| | AS3(7.7) | TJS3 (0.15) | Square |
| | AS3(7.7) | TJS4 (0.25) | Square |
| | AS3(7.7) | TJS1 (0) | Square |
| | AS3(7.7) | TJS5 (0.61) | Square |
| | AS3(7.7) | TJS2 (0.05) | Square |
| | AS2(6.3) | TJS4 (0.25) | Square |
| | AS4(11.8) | TJS4 (0.25) | Square |
| | AS5(15.0) | TJS5 (0.61) | Square |
| | AS5(15.0) | TJS4 (0.25) | Square |
| | AS5(15.0) | TJS2 (0.05) | Square |
| | AS5(15.0) | TJS6 (~Infinite) | Square |
| | AS5(15.0) | TJS3 (0.15) | Square |
| | AS5(15.0) | TJS1 (0) | Square |
| Toe Shape Sweep | AS3(7.7) | TJS4 (0.25) | Round |
| | AS3(7.7) | TJS4 (0.25) | Toe Out |
| | AS3(7.7) | TJS4 (0.25) | Angle Out |
| | AS3(7.7) | TJS4 (0.25) | Angle In |
| | AS3(7.7) | TJS4 (0.25) | Toe In |

## 5.7 Appendix: Limiting Toe Joint Rotation

### 5.7.1 Methods

Ten healthy able-bodied subjects (5 males, 5 females, 23±3 yrs, 76.6±6.4 kg, 1.77±0.06 m) wore a pair of simulator boots and participated in an additional trial to limit the toe joint angle of the adjustable ankle-toe prosthesis. A pair of adjustable ankle-toe prostheses were attach below the simulator boots. All subjects walked at 1.0 m/s on a force-instrumented treadmill (Bertec, Columbus, OH, USA). Forty-six passive-reflective markers were attached to the lower limbs, simulator boots and prostheses of the subjects. The ankle and toe joint stiffness were 7.7 and 0.25 N·m/deg, respectively, and the square toe was used. The angle limit trial occurred after the stiffness and toe shape sweeps.

A toe joint flexion limit was designed and constructed from 6061 Aluminum. The limit was designed with a 10° slope and attaches above the toe joints of the ankle-toe prosthesis. A 3 mm portion of shoe crepe (durometer: 70-75A) padding was attached to the limit on the surface that contacts the toe joint.

We computed joint kinematics and kinetics, and COM power. Marker and force data were low-pass filtered at 6 Hz and 15 Hz respectively with a third order, dual-pass, Butterworth filter. Joint kinematics and kinetics were calculated through Visual3D (C-Motion, Germantown, MD, USA). Data were divided into strides (from foot contact to ipsilateral foot contact), then averaged across strides. Foot contact was defined as when the vertical GRFs increased above 20 N. Cross-over steps (e.g., right foot landing on left belt of instrumented treadmill) were removed from analysis prior to averaging stride-based metrics. COM power was computed from the GRFs via the individual limbs method (Donelan, Kram, and Kuo 2002). COM work was computed during different phases of gait (Collision, Rebound, Preload, and Push-off) by integrating under

the power curve (similar to Zelik, Takahashi, and Sawicki 2015).

For visualization purposes we compared the toe angle limited trial to the trial with the same toe and ankle joint stiffness (AS3, TJS4) and the near infinite toe joint stiffness (AS3, TJS6). Kinematic and kinetic time series data show joint level trends. COM power and work during different phases of gait provide whole-body summary metrics (Zelik et al. 2011; Caputo and Collins 2014; Jackson and Collins 2015). We evaluated differences in the COM work between the three conditions with Kruskal-Wallis tests using post-hoc Wilcoxon Rank-Sum Tests with Holm-Sidak corrections for multiple comparisons. Family-wise significance level was 0.05.

### 5.7.2 Results

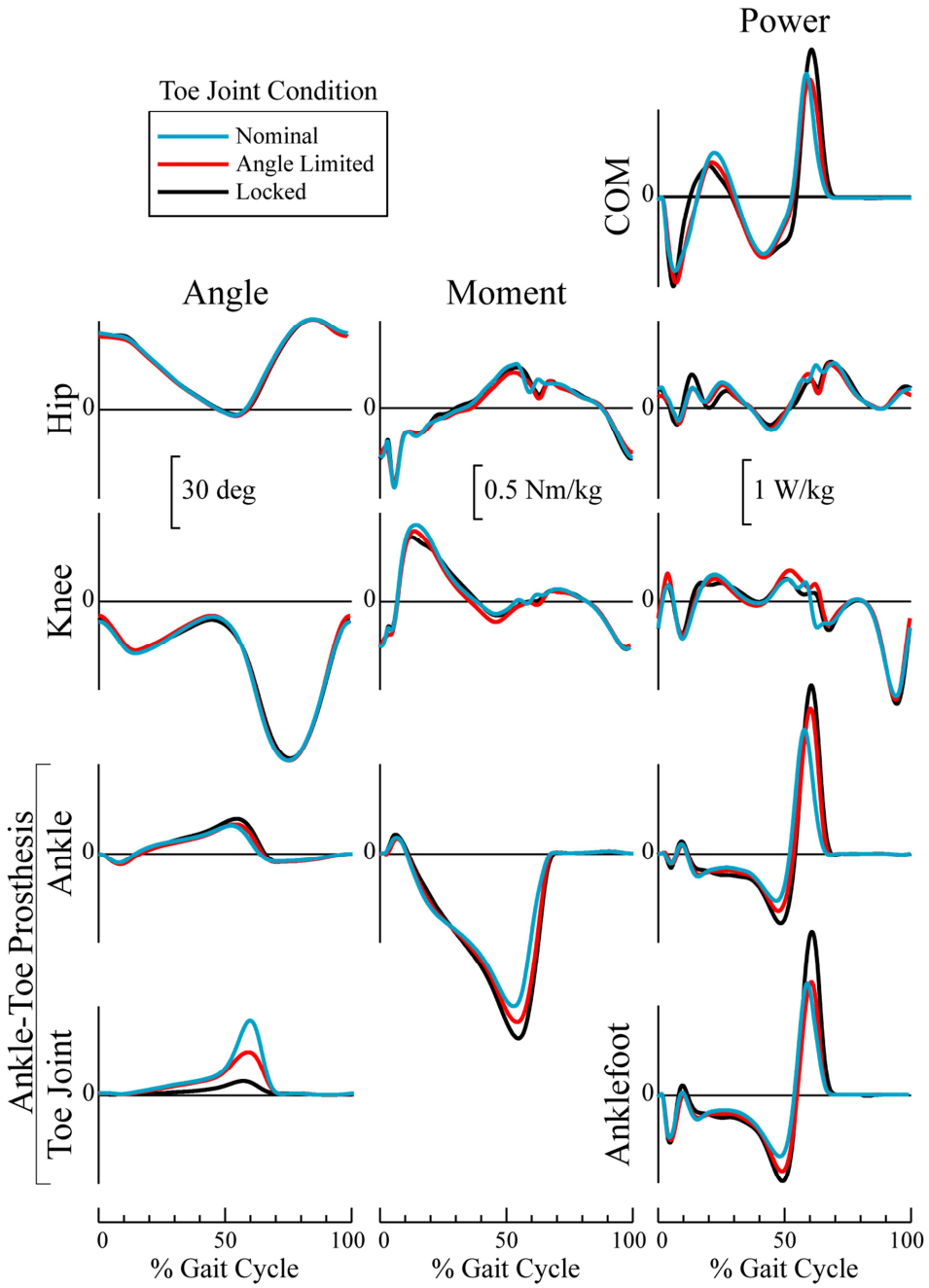


**Figure 5.10. Lower limb kinematics and kinetics for varying amounts toe joint articulation.** Reported time series curves are for walking at 1.0 m/s. The nominal condition is the Ankle Stiffness 3 (AS3, 7.7 N·m/deg) and Toe Joint Stiffness 4 (TJS4, 0.25 N·m/deg). The same ankle and toe joint stiffness conditions were used in the angle limited condition with a hard stop on the toe joint to limit the amount of articulation. The Locked toe joint was the Toe Joint Stiffness 6 (TJS6, ~inf) with the same ankle stiffness as the other two conditions. Curves depict inter-subject means.

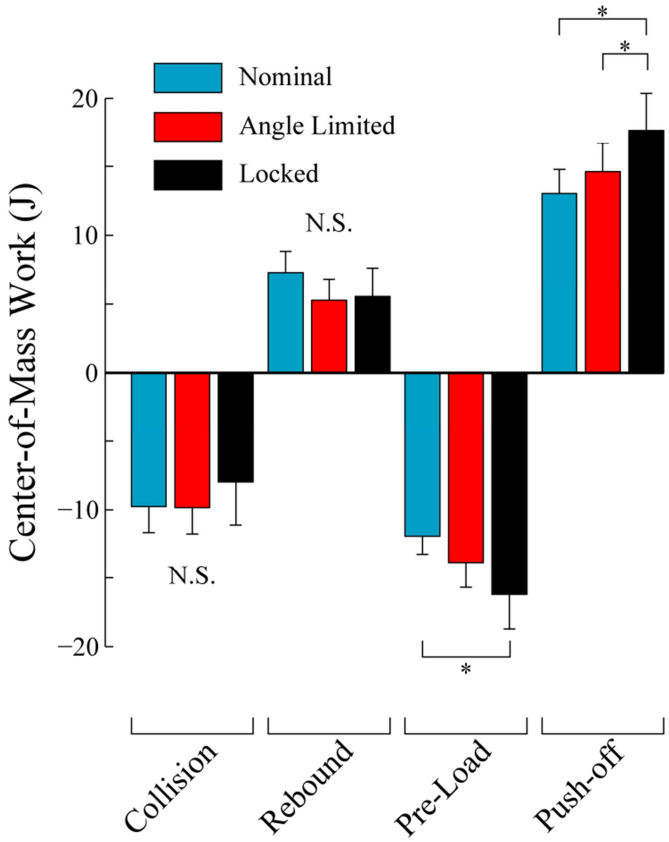


**Figure 5.11. COM work for different phases of gait for varying amounts toe joint articulation.** The nominal condition is the Ankle Stiffness 3 (AS3, 7.7 N·m/deg) and Toe Joint Stiffness 4 (TJS4, 0.25 N·m/deg). The same ankle and toe joint stiffness conditions were used in the angle limited condition with a hard stop on the toe joint to limit the amount of articulation. The Locked toe joint was the Toe Joint Stiffness 6 (TJS6, ~inf) with the same ankle stiffness as the other two conditions. Values depict are inter-subject means and standard deviations. Asterisks indicate significant differences ($p < 0.02$).

# Chapter 6

# Effects of Toe Length, Foot Length and Toe Joint Axis on Bipedal Walking

## 6.1 Introduction

During late stance in human walking, the metatarsophalangeal (MTP) joints of the forefoot undergo extension and flexion (i.e., toe joint articulation). Walking with vs. without this toe joint articulation affects gait mechanics, as evidenced from computational simulations (Kumar et al. 2009; Huang et al. 2010, 2012), bipedal robots (Ahn, Lee, and Go 2003; Buschmann, Lohmeier, and Ulbrich 2009) and foot prostheses (Zhu, Wang, and Wang 2014; Grabowski, Rifkin, and Kram 2010). Furthermore, varying foot and toe parameters can also affect gait mechanics. We recently demonstrated that changes in toe joint stiffness, but not toe shape, substantially altered walking biomechanics, such as push-off dynamics (Honert, Bastas, and Zelik 2018). Further exploration is needed to understand how other foot and toe parameters – namely toe length, toe joint axis angle and foot arch length (i.e., heel-to-toe-joint length) – affect gait.

Simulations that varied foot and toe lengths have found that these parameters can affect walking performance. In such models, increasing foot length improved walking economy (i.e., mechanical cost of transport) by influencing foot-ground collision magnitudes and timing of the energy return from springs acting about the ankle (Zelik et al. 2014; Adamczyk and Kuo 2013). In certain cases, introduction of an articulating toe joint in the foot improved walking economy of these models (i.e., by reducing collision losses); for instance, when foot and toe length proportions were similar to that of human anthropometrics (Huang et al. 2012; Kumar et al.

2009). Similar investigations on foot proportions, which systematically vary the toe and foot length, have not been studied experimentally; perhaps in part due to challenges associated with directly increasing/decreasing these lengths in the human foot.

Previous studies have primarily assessed a toe joint that articulates only in the sagittal plane, including walking simulations (Huang et al. 2012; Zhu, Wang, and Wang 2014), foot prosthesis studies (Zhu, Wang, and Wang 2014; Grabowski, Rifkin, and Kram 2010), and in-shoe orthosis studies that augment toe bending stiffness (Takahashi et al. 2016; Oh and Park 2017; Nigg et al. 1998; Willwacher et al. 2013; McDonald et al. 2016; Roy and Stefanyshyn 2006). However, the biological MTP joints are aligned at an angle relative to the sagittal plane, resulting in additional kinematics and kinetics in the frontal plane (MacWilliams, Cowley, and Nicholson 2003). There remains an open question as to how this toe joint axis angle affects walking biomechanics.

The purpose of this study is to quantify the effects of toe and foot arch lengths, as well as toe joint axis angle, on bipedal walking biomechanics. We accomplish this through the design and testing of an adjustable ankle-toe prosthesis (Honert, Bastas, and Zelik 2018), which enables us to systematically and independently vary each parameter of interest (i.e., toe length, foot arch length, toe joint axis angle). This study serves to fill scientific knowledge gaps, and to provide further insight regarding toe joint function; knowledge which may benefit the design/integration of toe joints into prostheses, exoskeletons and legged robots.

## 6.2 Methods

We utilized a previously developed adjustable ankle-toe prosthesis (Fig. 1) to isolate and examine the effects of toe and foot arch length as well as toe joint axis angle. We tested able-bodied persons walking on a force instrumented-treadmill while wearing a pair of adjustable prostheses attached bilaterally below simulator boots (which fixated their biological ankles). We collected motion and ground reaction force data to compute lower-limb kinematics and kinetics. We examined a wide range of toe and foot arch lengths and also compared walking with a sagittal plane toe joint axis (i.e., parallel to the ankle joint axis) versus walking with toe joint axes that were rotated out of plane.

### 6.2.1 Adjustable Ankle-Toe Prosthesis

In order to systematically assess toe and foot arch length, we used a modified version of the adjustable ankle-toe prosthesis described in (Honert, Bastas, and Zelik 2018, Fig. 1). The prosthesis was modified to accommodate interchangeable foot arch and toe sections, allowing us to respectively vary foot arch and toe lengths (Fig. 1). All foot arch and toe sections were made from 7075 aluminum (63.5 mm wide x 6.4 mm thick). Beneath the aluminum, we adhered shoe crepe (12 mm thick) and Vibram (4 mm thick) to emulate the outsole and tread of a shoe.

To vary the toe joint axis angle, we interchanged the foot arch and toe sections of the adjustable ankle-toe prosthesis. Custom machined foot arch and toe sections allowed for rotation of the toe joint axis (about the vertical axis, see Fig. 1B).

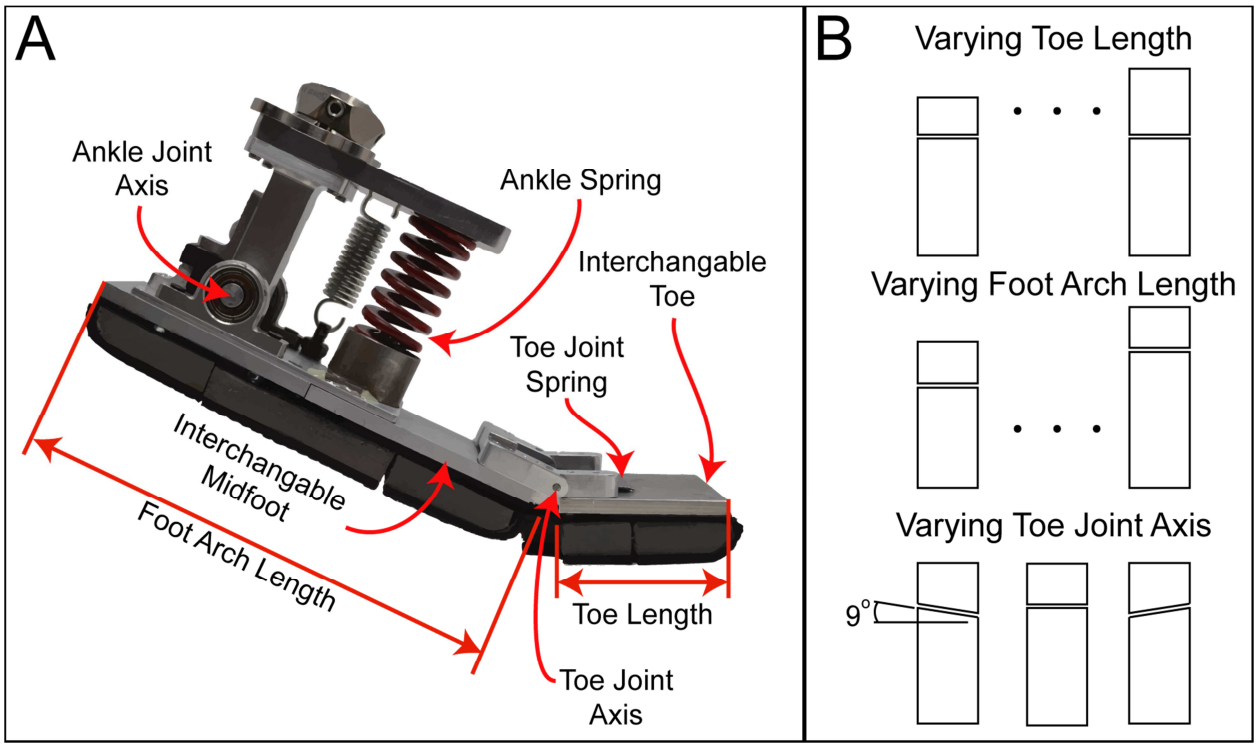


**Figure 6.1. A) Adjustable ankle toe prosthesis and the B) different parameter sweeps performed.** A) The adjustable ankle-toe prosthesis allows for the foot arch and toe sections to be interchanged. B) Five different toe and foot arch lengths were examined in a comprehensive sweep. Different foot arch and toe lengths were accommodated through the interchangeable foot arch and toe sections, respectively. Three different toe joint axis conditions were examined by interchanging both the foot arch and toe sections. The depicted toe joint axis conditions (from left to right) are Angled Out, Neutral and Angled In for the right foot; and are reverse for the left foot. Cartoons depict the foot arch and toe sections of the prosthesis as seen from above.

### 6.2.2 Subject Enrollment

Ten healthy able-bodied subjects (5 male, 5 female, 75.8±5.8 kg, 1.7±0.1 m, 22±3 years) participated in a two-session gait analysis study. All subjects provided written informed consent to the protocol, which was approved by the Institutional Review Board at Vanderbilt University. Subjects wore a pair of adjustable ankle-toe prostheses bilaterally below simulator boots (modified VACOcast, Zelik 2017). We recruited persons without amputation similar to previous studies (Zelik et al. 2011; Caputo and Collins 2014; Adamczyk, Collins, and Kuo 2006; Malcolm et al. 2015), in order to avoid amputation-specific variability (e.g., residual leg length,

amputation type, amputation surgery) and comorbidities (e.g., residual limb pain, osteoarthritic pain, scoliosis). We recruited subjects weighing between 63 and 83 kg in order to test relatively similar mass-normalized prosthetic ankle and toe joint stiffness conditions across all subjects.

### 6.2.3 Session One: Training

The first session lasted approximately one hour in order for each subject to acclimate to walking on the simulator boots and prostheses. Each subject walked over-ground on seven different conditions during this training session: with five random foot arch and toe length combinations and the Angled Out and Angled In toe joint axis conditions (Fig. 1). Subjects were given additional time if they did not appear to be comfortable, as assessed by a trained experimenter.

### 6.2.4 Session Two: Data Collection

Experimental data collection was performed within a week of the first session. Subjects walked at 1.0 m/s on a split-belt, force-instrumented treadmill (Bertec, Columbus, OH, USA) with a pair of ankle-toe prostheses attached bilaterally below the simulator boots. Subjects had 44 passive-reflective markers affixed bilaterally to their lower limbs, simulator boots, and prostheses. Ground reaction forces (GRFs) and marker data (Vicon, Oxford, UK) were collected at 1000 Hz and 200 Hz respectively for 30 seconds per condition. The data collection consisted of 28 conditions: 25 pseudo-randomized toe and foot arch length conditions followed by three randomized toe joint axis conditions. Prior to data collection, the subjects walked for five minutes on the treadmill to re-acclimate to the simulator boots and prostheses. In between each new condition, the subjects walked for at least one minute before data were collected.

### 6.2.5 Toe and Foot Arch Length Sweeps

Twenty-five toe and foot arch length combinations were pseudo-randomized and tested with each subject. The toe length (distance from the toe joint axis to the distal end of the toe, see Fig. 1) was varied from 50 to 90 mm in 10 mm increments. The foot arch length (distance from the heel to toe joint axis, see Fig. 1) was varied from 170 mm to 230 mm in 15 mm increments. These toe and foot arch lengths are typical for persons from 1.6 to 1.9 m tall (Parham, Gordon, and Bensel 1992). The testing order for each foot arch length was randomized. Then within each foot arch length, the testing order for each toe length was randomized. This pseudo-randomization was done to decrease the duration of the experiment as it was time consuming to simultaneously change both the toe and foot arch length for each condition. To determine if there were training effects during the data collection, one condition was tested near the start and then again near the end of each test session. Specifically, the 200-70 condition (i.e., 200 mm foot arch length and 70 mm toe length; this XXX-YY notation is used hereafter for brevity) was tested at the beginning of the experiment (as a part of the toe and foot arch length sweeps), and this same condition was retested near the end of the experiment (as a part of the toe joint axis sweep; Fig. 1). The mass of the ankle-toe prosthesis changed by a small amount: $0.12 \pm 0.04$ kg and $0.11 \pm 0.03$ kg (mean ± standard deviation) with changes in foot arch and toe length, respectively. The ankle and toe joint stiffness were held constant at 7.7 and 0.25 N·m/deg, respectively, for all conditions (an intermediate stiffness for each joint, Hansen et al. 2004; Zhu, Wang, and Wang 2014; Honert, Bastas, and Zelik 2018).

### 6.2.6 Toe Joint Axis Sweep

The toe joint axis of the adjustable ankle-toe prosthesis was randomized between three

different conditions: Angled Out, Angled In and Neutral (see Fig. 1). The Angled Out condition had a 9° laterally rotated toe joint axis in the transverse body plane, relative to the nominal (Neutral) toe joint axis of the prosthesis (Fig. 1B). The Angled In condition was the reverse of the Angled Out condition and the toe joint axis was rotated 9° medially in the transverse body plane (Fig. 1B). Both of these conditions maintained a total foot length of 270 mm with a foot arch length of 200 mm and toe length of 70 mm. The Neutral condition, which aligns the toe joint axis parallel to the ankle joint axis (i.e., the same as the 200-70 condition), was also tested. These three toe joint axis conditions were randomized and performed after the toe and foot arch length sweep. The three toe joint axis conditions varied in mass by less than 0.01 kg. The ankle and toe joint stiffness of the prostheses remained constant, the same as in the toe and foot arch length sweep.

### 6.2.7 Data Analysis

All post-processing was performed using a custom-written MATLAB script (MathWorks, Natick, MA, USA) in combination with Visual3D software (C-Motion, Germantown, MD, USA). Marker and ground reaction force data were filtered at 10 and 15 Hz (Honert and Zelik 2019), respectively, using dual-pass, 3rd order, Butterworth filters. Lower limb kinematics and kinetics were computed using Visual3D and were stride parsed then averaged based on left foot contact. Cross-over steps (i.e., left foot on right treadmill belt) were eliminated prior to averaging. Condition-specific inertial parameters were calculated through computer-aided design software (SolidWorks, Waltham, MA, USA) and implemented in Visual3D. The net power from the prosthesis (including ankle and toe joints) was calculated using previous methods (Takahashi, Kepple, and Stanhope 2012; Zelik and Honert 2018) and termed here Anklefoot

power. Center-of-Mass (COM) power was computed using the individual limbs method (Donelan, Kram, and Kuo 2002). COM work was computed by integrating under the COM power curve during the Collision and Push-off phases of gait (Zelik, Takahashi, and Sawicki 2015). We examined the Push-off phase of walking as this is the period during which the human MTP joints go through their greatest range-of-motion (MacWilliams, Cowley, and Nicholson 2003; Bruening, Cooney, and Buczek 2012) and altering Push-off work has been shown to influence the metabolic cost of walking in some studies (e.g., Caputo and Collins 2014; Malcolm et al. 2015). We also examined the Collision phase of walking as this phase overlaps, on the contralateral limb, with Push-off. Additionally, altering Push-off power and work has often been shown to influence contralateral limb Collision work in some studies (e.g., Adamczyk and Kuo 2013; Adamczyk, Roland, and Hahn 2017; Jackson and Collins 2015).

### 6.2.8 Statistical Analyses

Statistical analyses were performed to determine trends for the foot arch and toe length sweeps and toe joint axis sweep, and to assess potential training effects during the experiment. We examined trends in outcome metrics as a function of increasing foot arch length, toe length and toe joint axis, using a Spearman's rank correlation with a Holm-Sidak post-hoc error correction. The toe lengths, foot arch lengths and outcome metric variables were non-dimensionalized using gravity, subject-specific mass and leg length in order to account for size differences between each subject prior to statistical analyses. Key outcome metrics examined were: stride time, peak toe joint angle, peak ankle angle, peak knee angle (during swing), peak ankle moment, peak ankle power, peak Anklefoot power, peak COM power, ankle Push-off work, hip Push-off work, COM Push-off work and COM Collision work. Additionally, we

evaluated training effects during the experiment by examining the 200-70 condition completed near the beginning vs. end of the data collection. We evaluated differences in the outcome metrics listed above using Wilcoxon Rank-Sum Tests. A family-wise significance level of 0.05 was used for all statistical tests.

## 6.3 Results

### 6.3.1 Toe and Foot Arch Length Sweeps

Increasing the toe length from 50 mm to 90 mm increased: peak knee angle during swing by 14% (9 degrees, Fig. 2), peak ankle power by 10% (0.2 W/kg) and hip Push-off work by 53% (2 J), regardless of foot arch length. All these trends were statistically significant ($p<0.03$, Appendix A). Reported values are the average increases from all five foot arch lengths when increasing the toe length from 50 to 90 mm. With increases in toe length we observed inconsistent trends in the peak ankle moment and peak COM power; there were statistically significant trends with some foot arch lengths, but not others (Appendix A). When increasing toe length we did not observe trends in: stride time, peak toe joint angle, peak ankle angle, peak Anklefoot power, ankle Push-off work, Anklefoot Push-off work (Appendix A), COM Push-off work (Table 1) or COM Collision work (Table 2, $p>0.01$).

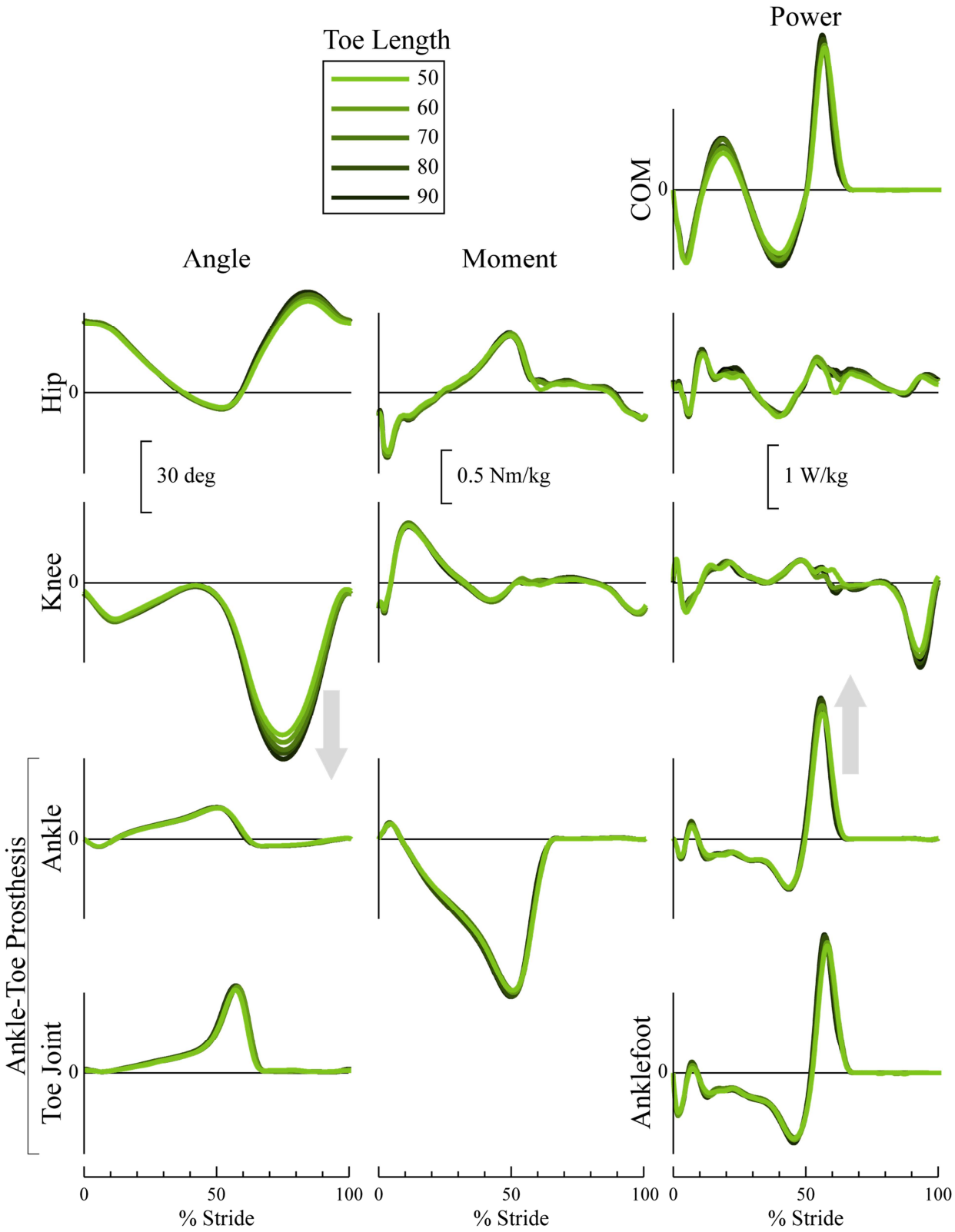


**Figure 6.2. Lower limb kinematics, kinetics and COM power across all toe lengths for a foot arch length of 200 mm.** Presented are inter-subject means (N=10) for walking at 1.0 m/s. Arrows indicate statistically significant trends ($p<0.03$), independent of the toe length.

Increasing the foot arch length from 170 mm to 230 mm led to increased: peak ankle angle by 33% (4 degrees, Fig. 3), peak knee angle during swing by 11% (7 degrees), peak ankle moment magnitude by 34% (0.4 Nm/kg), peak ankle power by 43% (0.8 W/kg), peak Anklefoot power by 64% (1.0 W/kg), peak COM power by 23% (0.5 W/kg), ankle Push-off work by 46% (6 J), Anklefoot Push-off work by 84% (8 J), ankle Push-off work by 46% (6 J) and COM Push-off work by 28% (4 J, Table 1). All these trends were statistically significant ($p<0.003$, see Appendix A and Table 1). Reported values are the average increases from all five toe lengths when increasing the foot arch length from 170 to 230 mm. There was an inconsistent trend in the peak toe joint angle as only the 70 mm toe had a significantly increasing trend with increasing foot arch length ($p=0.005$), whereas the other toe lengths did not exhibit a trend ($p>0.05$, Appendix A). When increasing foot arch length for any of the toe lengths we did not observe trends in: stride time, hip Push-off work or COM Collision work (Appendix A, Table 2, $p>0.08$).

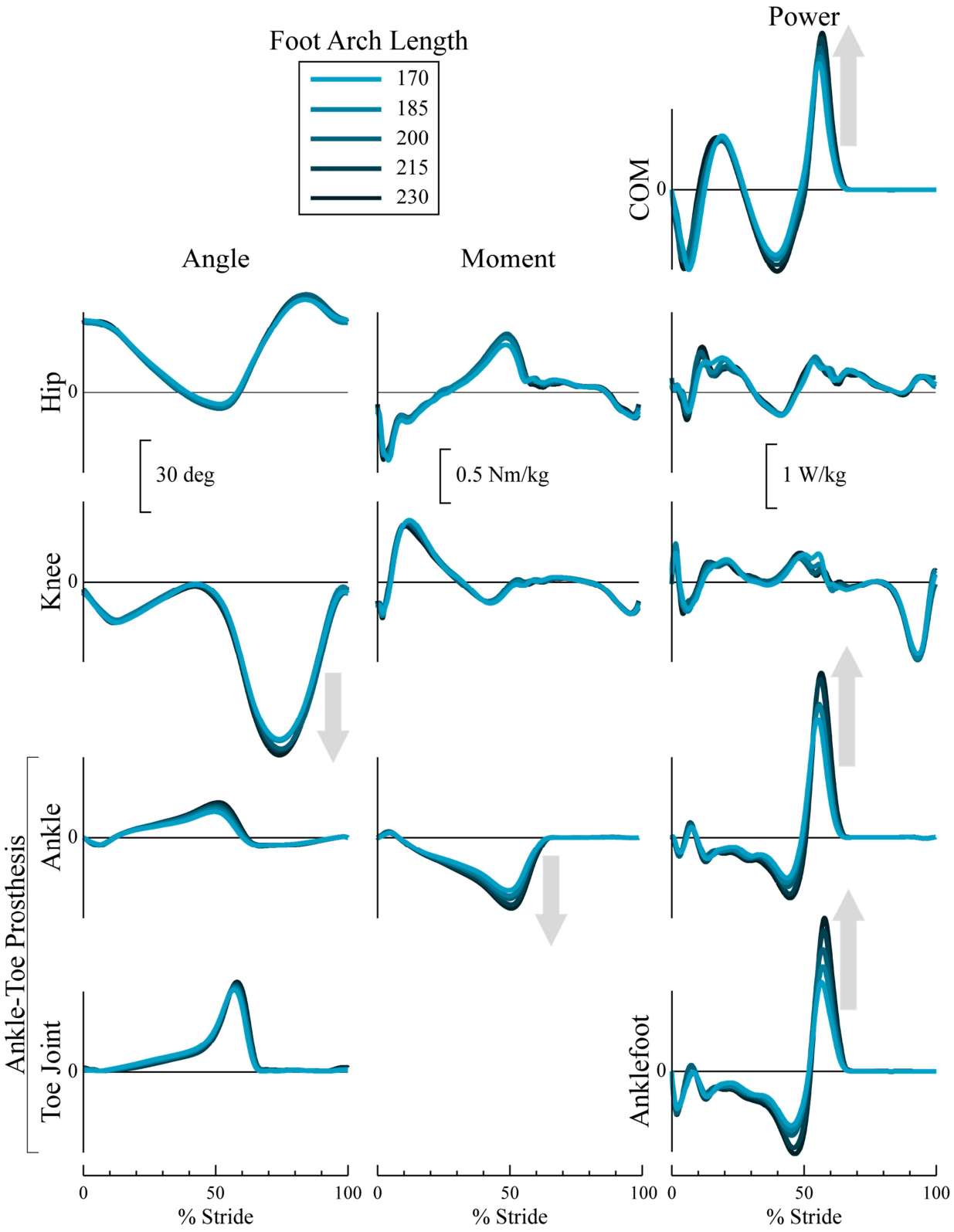


**Figure 6.3. Lower limb kinematics, kinetics and COM power across all foot arch lengths for a toe length of 70 mm.** Presented are inter-subject means (N=10) for walking at 1.0 m/s. Arrows indicate statistically significant trends ($p<0.003$), independent of the foot arch length.

**Table 6.1. COM Push-off work (J) with increasing toe and foot arch length.** *P*-values indicate the significance of the trend in work with increasing foot arch length for each toe length (at the bottom of each column), and with increasing toe length for each foot arch length (at the right of each row). Asterisks indicate trends that are below the family-wise $\alpha = 0.05$. All results shown are the inter-subject mean ± one standard deviation (*N*=10).

| | | Toe Length (mm) | | | | | |
|---|---|---|---|---|---|---|---|
| | | 50 | 60 | 70 | 80 | 90 | *p*-value |
| Foot Arch Length (mm) | 170 | 15.7±2.7 | 15.0±3.0 | 14.5±2.6 | 15.2±2.7 | 15.1±3.1 | 0.6 |
| | 185 | 16.3±2.9 | 15.9±2.6 | 15.5±2.5 | 16.7±2.5 | 16.4±3.0 | 0.3 |
| | 200 | 16.8±2.8 | 16.7±2.2 | 16.4±2.5 | 17.3±2.5 | 17.0±2.7 | 0.3 |
| | 215 | 18.1±3.9 | 17.9±3.2 | 17.6±3.5 | 18.2±3.4 | 18.5±3.5 | 0.2 |
| | 230 | 19.1±3.4 | 19.1±3.6 | 19.1±3.0 | 19.7±3.6 | 19.7±3.2 | 0.4 |
| | *p*-value | 0.003* | 0.0002* | <0.0001* | 0.0001* | <0.0001* | |

**Table 6.2. COM Collision work (J) with increasing toe and foot arch length.** *P*-values indicate the significance of the trend in work with increasing foot arch length for each toe length (at the bottom of each column), and with increasing toe length for each foot arch length (at the right of each row). Asterisks indicate trends that are below the family-wise $\alpha = 0.05$. All results shown are the inter-subject mean ± one standard deviation (*N*=10).

| | | Toe Length (mm) | | | | | |
|---|---|---|---|---|---|---|---|
| | | 50 | 60 | 70 | 80 | 90 | *p*-value |
| Foot Arch Length (mm) | 170 | -9.1±1.9 | -9.3±1.1 | -9.1±1.3 | -8.7±2.0 | -8.6±2.0 | 0.6 |
| | 185 | -7.7±2.1 | -8.4±2.0 | -8.3±2.6 | -8.0±2.3 | -8.2±1.9 | 0.3 |
| | 200 | -7.9±2.4 | -7.4±2.2 | -7.8±2.6 | -7.5±2.6 | -7.1±2.2 | 0.8 |
| | 215 | -7.4±1.7 | -7.8±1.8 | -7.8±1.9 | -8.2±1.8 | -7.8±2.0 | 0.08 |
| | 230 | -7.6±2.1 | -7.6±1.9 | -7.9±2.3 | -7.8±2.6 | -8.7±3.0 | 0.06 |
| | *p*-value | 0.8 | 0.6 | 0.8 | 0.7 | 0.5 | |

### 6.3.2 Toe Joint Axis Sweep

The Angled In, Angled Out, and Neutral toe joint axis conditions did not show any qualitative or quantitative differences in the lower limb kinematics or kinetics (Fig. 4). There were no statistically significant trends when going from the Angled In (-9°) to Neutral (0°) to Angled Out (9°) toe joint axis conditions for any outcome metrics examined ($p>0.40$).

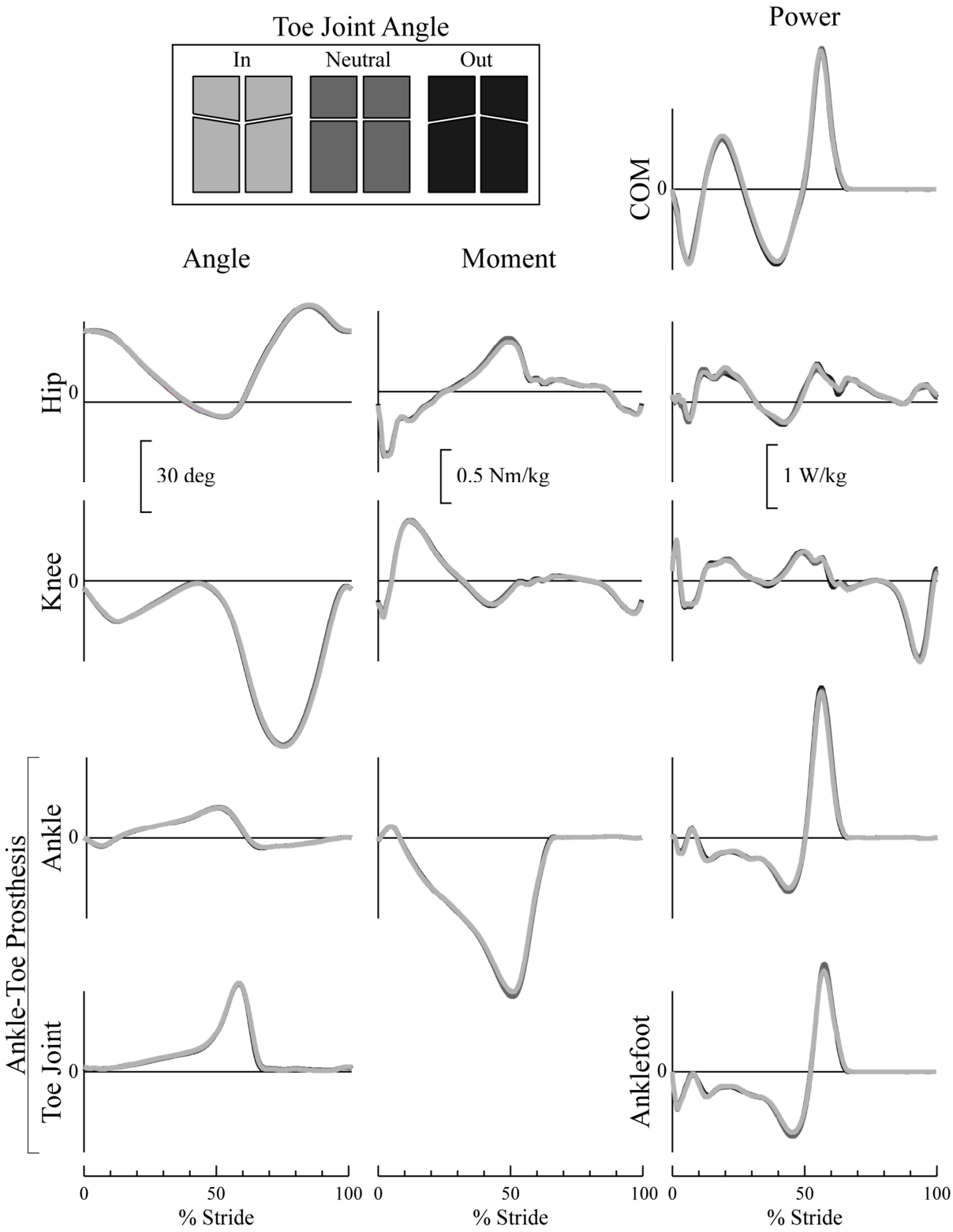


**Figure 6.4. Lower limb kinematics, kinetics and COM power for three different toe joint axis conditions.** All conditions maintained a foot arch and toe length of 200 mm and 70 mm, respectively. Presented are inter-subject means (N=10) for walking at 1.0 m/s.

### 6.3.3 Training Effects during Data Collection

We did not observe statistical differences in 12 out of 13 outcome metrics when comparing the 200-70 condition performed near the beginning of the experiment and the repeated trial performed near the end of the experiment ($p$>0.05, Table B1). There was a single exception: we did observe a statistical difference in the amount of ankle Push-off work between these two trials (15.4 J vs. 18.2 J, $p$ = 0.03); though Anklefoot power was not significantly different (13.6 J vs. 12.2 J, $p$ = 0.1).

## 6.4 Discussion

Here we systematically and independently examined the effects of toe length, foot arch length and toe joint axis angle on human walking biomechanics. We observed that varying foot arch length had greater biomechanical effects than varying toe length over the tested ranges. Additionally, we observed little biomechanical differences in forward, level ground walking with changes in toe joint axis angle.

Increasing foot arch length had a greater effect on lower limb kinetics than increasing toe length. Though we explored a greater length range for the foot arch length (60 mm) than toe length (40 mm), changes in foot arch length had a greater effect even when restricting our comparison to similar length ranges (see Table 1 and Appendix A). For instance, increasing the foot arch length by 30 mm, from 170 mm to 200 mm, increased the COM Push-off work by ~2 J; however, increasing the toe length by 30 mm, from 50 mm to 80 mm, had negligible effects on the COM Push-off work (Table 1).

The effects of increasing the foot arch length we observed here were similar to the effects of increasing overall foot length in walking models. With increases in the foot arch length, the ankle spring stored and returned more elastic energy (Fig. 3) which is consistent with a previous walking simulation that increased overall foot length (Zelik et al. 2014). In this model, increases in foot length also resulted in delayed timing of the trailing limb Push-off work relative to the leading limb Collision work. We observed a similar trend in this study: a longer delay between the initiation of the COM Push-off power with respect to the initiation of the opposite limb COM Collision power with increasing foot arch length ($p$<0.0004, see Fig. 5). This trend was not present with respect to increasing toe length ($p$ = 0.6). Walking models predict that Push-off timing with respect to Collision is sub-optimal (Zelik et al. 2014; Kuo, Donelan, and Ruina 2005;

Ruina, Bertram, and Srinivasan 2005); though experiments have yielded conflicting results (e.g., Malcolm et al. 2015; Galle et al. 2017).

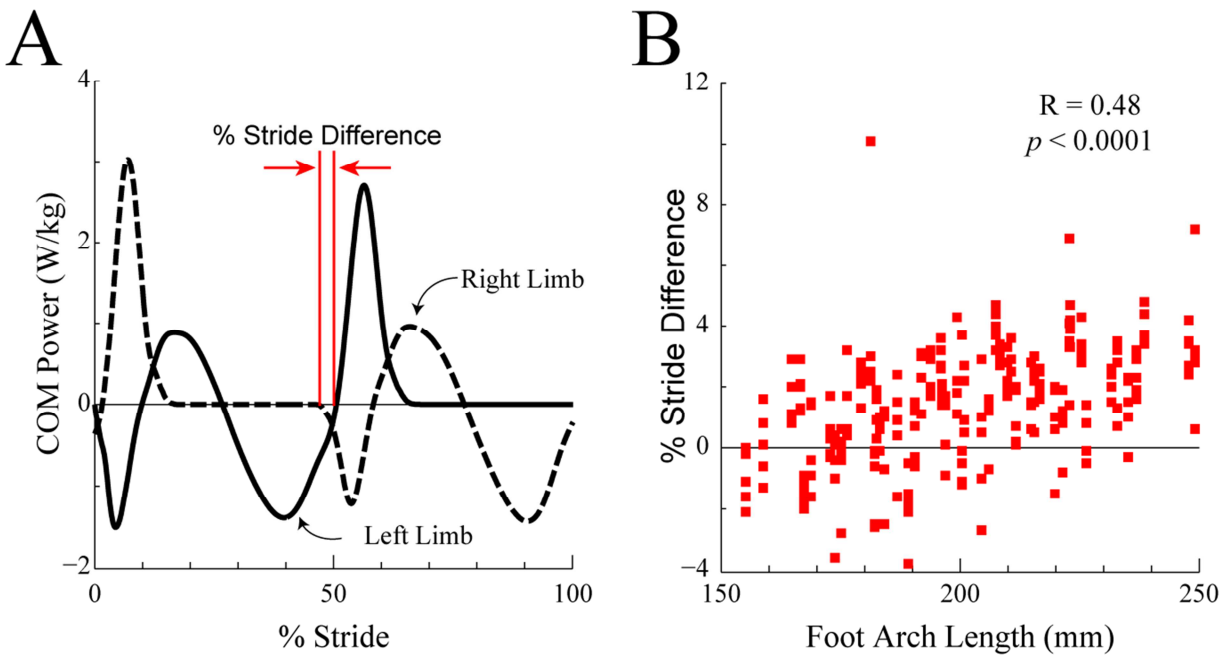


**Figure 6.5. A) COM power for left (solid) and right limb (dotted) and B) the percent stride difference between right limb Collision and left limb Push-off across foot arch lengths for each subject for each trial.** A) Left and right limb COM power is the mean (*N*=10) waveform for the 230 mm foot arch length and 90 mm toe length. B) The negative value in percent stride difference represents left limb COM Push-off initiating prior to right limb COM collision, while positive represents the opposite. The foot arch length was normalized to each subject's leg length and re-dimensionalized based on the mean study leg length. The correlation was computed with a Spearman's rank correlation.

We observed little difference in walking biomechanics with changes in toe joint axis even though we examined up to 18° difference in the axis of rotation of the toe joint (Fig. 4). Prior studies examining the effect of the toe joint have done so through walking simulations (Huang et al. 2012; Zhu, Wang, and Wang 2014) and robots (Kwon and Park 2012; Zhang et al. 2010; Sellaouti et al. 2006), but these applications have primarily examined the effects of a toe joint that rotates in the sagittal plane.

There are several limitations to address with this study. First, we did observe an apparent training effect in one outcome metric, the ankle Push-off work; however, the other 12 outcome metrics tested showed no statistical difference when comparing the 200-70 condition from the

beginning vs. the end of the data collection. As we pseudo-randomized the conditions, we do not expect this trend in a single outcome metric to affect any major conclusions from this study. Additionally, the toe joint of the ankle-toe prosthesis was a single, composite toe joint that approximates the articulation of all five human MTP joints. Further studies are needed to identify the role of individual toes and toe joint axes on human walking biomechanics. Each condition did change the weight of the prosthesis slightly (mean ± s.d. difference between all 28 conditions: 0.23±0.03 kg). This is expected to play a minimal role in results as even greater weight additions to the foot were not shown to greatly affect stance phase kinematics and kinetics of human walking (Browning et al. 2007) and we accounted for the changes in the inertial parameters for the inverse dynamics calculations (see Methods). The use of simulator boots to test the subjects did add 0.16 m in height to the subject's shanks, similar to other simulator boot studies (Zelik et al. 2011; Caputo and Collins 2014; Malcolm et al. 2015; Honert, Bastas, and Zelik 2018). This change in anthropometric lengths is not expected to affect study interpretations as this change was consistent across all subjects and conditions. There remains an open question as to how these observed trends will translate to persons with amputation walking on prostheses with articulating toes. This requires a separate, future experiment on this population to evaluate. Nevertheless, the current results provide insights into the biomechanical contributions of different foot parameters (e.g., which ones affect gait the most) which can help inform prosthetic foot design in these future studies. Finally, this study was only performed at one forward walking speed on level ground. Further studies would be beneficial to explore additional speeds, or other locomotor tasks.

## 6.5 Conclusions

We systematically examined the effects of toe length, foot arch length and toe joint axis on human walking biomechanics. We found that changes in foot arch length had greater effects on walking biomechanics than changes in toe length, while changes in toe joint axis had little effect.

## 6.6 Appendix A: Toe and Foot Arch Length Parameter Sweep Results

**Table 6.3. Peak toe joint angle (deg) with increasing toe and foot arch length.** *P*-values indicate the significance of the trend in angle with increasing foot arch length for each toe length (at the bottom of each column), and with increasing toe length for each foot arch length (at the right of each row). Asterisks indicate trends that are below the family-wise $\alpha = 0.05$. All results shown are the inter-subject mean ± one standard deviation (*N*=10).

| | | Toe Length (mm) | | | | | |
|---|---|---|---|---|---|---|---|
| | | 50 | 60 | 70 | 80 | 90 | *p*-value |
| Foot Arch Length (mm) | 170 | 34.2±1.6 | 34.8±1.7 | 35.2±1.9 | 35.4±1.6 | 36.6±2.1 | 0.02 |
| | 185 | 35.3±2.1 | 36.0±2.4 | 36.6±2.2 | 36.8±1.9 | 37.1±1.8 | 0.3 |
| | 200 | 36.3±3.0 | 37.1±2.6 | 37.4±1.8 | 37.5±3.1 | 37.5±2.2 | 0.5 |
| | 215 | 36.5±4.1 | 37.1±2.7 | 38.0±3.0 | 37.9±2.4 | 38.1±2.4 | 0.2 |
| | 230 | 35.6±2.9 | 36.9±2.9 | 39.1±2.5 | 38.2±2.6 | 38.6±2.3 | 0.01 |
| | *p*-value | 0.3 | 0.3 | 0.005* | 0.05 | 0.1 | |

**Table 6.4. Peak ankle angle (deg) with increasing increasing toe and foot arch length.** *P*-values indicate the significance of the trend in angle with increasing foot arch length for each toe length (at the bottom of each column), and with increasing toe length for each foot arch length (at the right of each row). Asterisks indicate trends that are below the family-wise $\alpha = 0.05$. All results shown are the inter-subject mean ± one standard deviation (*N*=10).

| | | Toe Length (mm) | | | | | |
|---|---|---|---|---|---|---|---|
| | | 50 | 60 | 70 | 80 | 90 | *p*-value |
| Foot Arch Length (mm) | 170 | 11.3±1.2 | 11.4±1.3 | 10.9±1.0 | 11.5±1.2 | 11.3±1.4 | 0.9 |
| | 185 | 12.3±1.1 | 12.3±1.0 | 12.1±1.1 | 12.6±1.1 | 12.6±1.1 | 0.3 |
| | 200 | 13.0±0.9 | 13.1±1.0 | 13.0±0.8 | 13.3±1.2 | 13.3±0.8 | 0.2 |
| | 215 | 14.2±1.0 | 14.3±1.1 | 13.9±1.2 | 14.5±0.9 | 14.6±1.1 | 0.5 |
| | 230 | 14.9±1.1 | 14.9±1.1 | 14.8±1.0 | 15.4±1.2 | 15.2±1.0 | 0.7 |
| | *p*-value | <0.0001* | <0.0001* | <0.0001* | <0.0001* | <0.0001* | |

**Table 6.5. Minimum knee angle (deg) during swing with increasing toe and foot arch length.** *P*-values indicate the significance of the angle in work with increasing foot arch length for each toe length (at the bottom of each column), and with increasing toe length for each foot arch length (at the right of each row). Asterisks indicate trends that are below the family-wise $\alpha = 0.05$. All results shown are the inter-subject mean ± one standard deviation (*N*=10).

| | | Toe Length (mm) | | | | | |
|---|---|---|---|---|---|---|---|
| | | 50 | 60 | 70 | 80 | 90 | *p*-value |
| Foot Arch Length (mm) | 170 | -61.0±4.2 | -64.6±3.0 | -66.6±4.8 | -67.0±3.8 | -69.7±3.7 | <0.0001* |
| | 185 | -62.5±3.0 | -65.3±2.9 | -67.2±3.2 | -69.5±5.6 | -70.7±2.6 | <0.0001* |
| | 200 | -64.4±3.8 | -67.6±3.1 | -70.7±3.0 | -72.1±3.5 | -74.6±4.0 | <0.0001* |
| | 215 | -65.9±3.5 | -69.5±3.1 | -71.6±3.4 | -73.4±2.9 | -75.4±3.4 | <0.0001* |
| | 230 | -67.6±3.6 | -71.8±4.1 | -73.2±3.6 | -75.7±3.8 | -77.7±4.4 | <0.0001* |
| | *p*-value | <0.0001* | <0.0001* | <0.0001* | <0.0001* | <0.0001* | |

**Table 6.6. Peak ankle moment (N*m*kg-1) with increasing toe and foot arch length.** *P*-values indicate the significance of the trend in moment with increasing foot arch length for each toe length (at the bottom of each column), and with increasing toe length for each foot arch length (at the right of each row). Asterisks indicate trends that are below the family-wise $\alpha$ = 0.05. All results shown are the inter-subject mean ± one standard deviation (*N*=10).

| | | Toe Length (mm) | | | | | |
|---|---|---|---|---|---|---|---|
| | | 50 | 60 | 70 | 80 | 90 | *p*-value |
| Foot Arch Length (mm) | 170 | -1.3±0.1 | -1.2±0.1 | -1.2±0.1 | -1.3±0.1 | -1.3±0.1 | 0.03* |
| | 185 | -1.4±0.1 | -1.4±0.1 | -1.4±0.1 | -1.4±0.1 | -1.4±0.1 | 0.01 |
| | 200 | -1.4±0.1 | -1.5±0.1 | -1.4±0.1 | -1.5±0.1 | -1.5±0.1 | 0.01 |
| | 215 | -1.6±0.1 | -1.6±0.1 | -1.6±0.1 | -1.6±0.1 | -1.6±0.1 | 0.02* |
| | 230 | -1.6±0.1 | -1.7±0.1 | -1.7±0.1 | -1.7±0.1 | -1.7±0.1 | 0.02 |
| | *p*-value | <0.0001* | <0.0001* | <0.0001* | <0.0001* | <0.0001* | |

**Table 6.7. Peak ankle power (W*kg-1) with increasing toe and foot arch length.** *P*-values indicate the significance of the trend in power with increasing foot arch length for each toe length (at the bottom of each column), and with increasing toe length for each foot arch length (at the right of each row). Asterisks indicate trends that are below the family-wise $\alpha$ = 0.05. All results shown are the inter-subject mean ± one standard deviation (N=10).

| | | Toe Length (mm) | | | | | |
|---|---|---|---|---|---|---|---|
| | | 50 | 60 | 70 | 80 | 90 | *p*-value |
| Foot Arch Length (mm) | 170 | 1.8±0.2 | 1.9±0.3 | 1.9±0.2 | 2.0±0.3 | 2.0±0.3 | 0.02* |
| | 185 | 2.1±0.3 | 2.2±0.3 | 2.2±0.3 | 2.3±0.3 | 2.3±0.4 | 0.005* |
| | 200 | 2.1±0.2 | 2.2±0.3 | 2.2±0.2 | 2.3±0.3 | 2.3±0.3 | 0.0007* |
| | 215 | 2.4±0.4 | 2.6±0.3 | 2.6±0.4 | 2.7±0.4 | 2.7±0.4 | 0.0006* |
| | 230 | 2.6±0.3 | 2.7±0.3 | 2.7±0.3 | 2.9±0.4 | 2.8±0.4 | 0.03* |
| | *p*-value | <0.0001* | <0.0001* | <0.0001* | <0.0001* | <0.0001* | |

**Table 6.8. Peak Anklefoot power (W*kg-1) with increasing toe and foot arch length.** *P*-values indicate the significance of the trend in work with increasing foot arch length for each toe length (at the bottom of each column), and with increasing toe length for each foot arch length (at the right of each row). Asterisks indicate trends that are below the family-wise $\alpha$ = 0.05. All results shown are the inter-subject mean ± one standard deviation (*N*=10).

| | | Toe Length (mm) | | | | | |
|---|---|---|---|---|---|---|---|
| | | 50 | 60 | 70 | 80 | 90 | *p*-value |
| Foot Arch Length (mm) | 170 | 1.6±0.2 | 1.6±0.2 | 1.5±0.2 | 1.7±0.2 | 1.8±0.3 | 0.06* |
| | 185 | 1.9±0.3 | 1.9±0.2 | 1.8±0.2 | 2.0±0.2 | 2.0±0.2 | 0.02* |
| | 200 | 2.2±0.2 | 2.2±0.3 | 2.1±0.3 | 2.4±0.3 | 2.4±0.3 | 0.01* |
| | 215 | 2.4±0.4 | 2.4±0.3 | 2.3±0.3 | 2.6±0.3 | 2.7±0.3 | 0.01* |
| | 230 | 2.6±0.4 | 2.6±0.4 | 2.6±0.3 | 2.8±0.5 | 2.8±0.4 | 0.09* |
| | *p*-value | <0.0001* | <0.0001* | <0.0001* | <0.0001* | <0.0001* | |

**Table 6.9. Peak COM power (W*kg-1) with increasing toe and foot arch length.** *P*-values indicate the significance of the trend in work with increasing foot arch length for each toe length (at the bottom of each column), and with increasing toe length for each foot arch length (at the right of each row). Asterisks indicate trends that are below the family-wise $\alpha = 0.05$. All results shown are the inter-subject mean ± one standard deviation (*N*=10).

| | | Toe Length (mm) | | | | | |
|---|---|---|---|---|---|---|---|
| | | 50 | 60 | 70 | 80 | 90 | *p*-value |
| Foot Arch Length (mm) | 170 | 2.1±0.2 | 2.1±0.2 | 2.1±0.2 | 2.3±0.2 | 2.3±0.3 | 0.03 |
| | 185 | 2.2±0.2 | 2.3±0.2 | 2.2±0.2 | 2.4±0.2 | 2.4±0.2 | 0.01* |
| | 200 | 2.4±0.2 | 2.4±0.3 | 2.4±0. | 2.6±0.2 | 2.6±0.3 | 0.002* |
| | 215 | 2.5±0.3 | 2.6±0.2 | 2.5±0.3 | 2.7±0.2 | 2.8±0.3 | 0.007* |
| | 230 | 2.6±0.3 | 2.7±0.4 | 2.6±0.3 | 2.8±0.4 | 2.8±0.4 | 0.08 |
| | *p*-value | 5.3e-4* | <0.0001* | <0.0001* | <0.0001* | <0.0001* | |

**Table 6.10. Ankle Push-off work (J) with increasing toe and foot arch length.** *P*-values indicate the significance of the trend in work with increasing foot arch length for each toe length (at the bottom of each column), and with increasing toe length for each foot arch length (at the right of each row). Asterisks indicate trends that are below the family-wise $\alpha = 0.05$. All results shown are the inter-subject mean ± one standard deviation (*N*=10).

| | | Toe Length (mm) | | | | | |
|---|---|---|---|---|---|---|---|
| | | 50 | 60 | 70 | 80 | 90 | *p*-value |
| Foot Arch Length (mm) | 170 | 13.7±2.8 | 13.6±3.0 | 13.2±2.6 | 14.3±3.0 | 14.6±3.2 | 0.9 |
| | 185 | 15.5±2.8 | 15.8±3.1 | 15.5±2.5 | 16.8±2.7 | 16.7±2.8 | 0.03 |
| | 200 | 15.2±2.1 | 15.8±1.9 | 15.4±1.9 | 16.5±2.2 | 16.2±2.3 | 0.03 |
| | 215 | 18.1±3.5 | 18.8±3.0 | 18.6±3.4 | 19.7±3.0 | 19.5±3.3 | 0.02 |
| | 230 | 19.4±2.9 | 19.8±3.4 | 19.9±3.1 | 21.1±3.7 | 20.7±2.7 | 0.06 |
| | *p*-value | <0.0001* | <0.0001* | <0.0001* | <0.0001* | <0.0001* | |

**Table 6.11. Anklefoot Push-off work (J) with increasing toe and foot arch length.** *P*-values indicate the significance of the trend in work with increasing foot arch length for each toe length (at the bottom of each column), and with increasing toe length for each foot arch length (at the right of each row). Asterisks indicate trends that are below the family-wise $\alpha = 0.05$. All results shown are the inter-subject mean ± one standard deviation (*N*=10).

| | | Toe Length (mm) | | | | | |
|---|---|---|---|---|---|---|---|
| | | 50 | 60 | 70 | 80 | 90 | *p*-value |
| Foot Arch Length (mm) | 170 | 9.4±2.4 | 9.2±2.3 | 8.4±2.6 | 9.7±2.0 | 10.1±2.7 | 0.2 |
| | 185 | 11.0±2.6 | 10.8±2.0 | 10.8±19 | 12.0±2.1 | 11.6±1.9 | 0.06 |
| | 200 | 13.6±2.0 | 14.0±2.4 | 13.6±2.0 | 14.8±2.8 | 14.8±2.4 | 0.07 |
| | 215 | 15.3±2.9 | 15.5±2.8 | 15.1±3.4 | 15.7±2.8 | 16.4±3.5 | 0.08 |
| | 230 | 16.9±3.5 | 16.3±3.5 | 16.6±3.5 | 18.2±4.2 | 17.7±2.8 | 0.1 |
| | *p*-value | <0.0001* | <0.0001* | <0.0001* | <0.0001* | <0.0001* | |

**Table 6.12. Hip Push-off work (J) with increasing toe and foot arch length.** *P*-values indicate the significance of the trend in work with increasing foot arch length for each toe length (at the bottom of each column), and with increasing toe length for each foot arch length (at the right of each row). Asterisks indicate trends that are below the family-wise $\alpha = 0.05$. All results shown are the inter-subject mean ± one standard deviation (*N*=10).

| | | Toe Length (mm) | | | | | |
|---|---|---|---|---|---|---|---|
| | | 50 | 60 | 70 | 80 | 90 | *p*-value |
| Foot Arch Length (mm) | 170 | 4.6±1.5 | 5.2±1.6 | 5.2±1.8 | 6.0±1.4 | 7.1±1.5 | 3.0e-4* |
| | 185 | 4.2±1.4 | 5.1±1.4 | 5.9±1.6 | 6.1±1.6 | 6.6±1.6 | <0.0001* |
| | 200 | 3.8±1.2 | 5.5±1.4 | 5.4±1.3 | 5.5±1.4 | 5.8±1.3 | 0.0013* |
| | 215 | 4.2±1.0 | 5.1±0.9 | 5.7±1.2 | 5.5±1.3 | 6.6±1.2 | <0.0001* |
| | 230 | 4.0±1.2 | 4.8±1.2 | 5.3±1.2 | 5.6±1.2 | 5.8±1.1 | 0.0004* |
| | *p*-value | 0.9 | 0.3 | 0.3 | 1 | 0.4 | |

**Table 6.13. Stride time (sec) with increasing toe and foot arch length.** *P*-values indicate the significance of the trend in work with increasing foot arch length for each toe length (at the bottom of each column), and with increasing toe length for each foot arch length (at the right of each row). Asterisks indicate trends that are below the family-wise $\alpha = 0.05$. All results shown are the inter-subject mean ± one standard deviation (*N*=10).

| | | Toe Length (mm) | | | | | |
|---|---|---|---|---|---|---|---|
| | | 50 | 60 | 70 | 80 | 90 | *p*-value |
| Foot Arch Length (mm) | 170 | 1.3±0.1 | 1.3±0.1 | 1.3±0.1 | 1.3±0.1 | 1.3±0.1 | 0.8 |
| | 185 | 1.3±0.1 | 1.3±0.1 | 1.3±0.1 | 1.3±0.1 | 1.3±0.1 | 0.6 |
| | 200 | 1.3±0.1 | 1.3±0.1 | 1.3±0.1 | 1.3±0.1 | 1.3±0.1 | 0.5 |
| | 215 | 1.3±0.1 | 1.3±0.1 | 1.3±0.1 | 1.3±0.1 | 1.4±0.1 | 0.3 |
| | 230 | 1.3±0.1 | 1.3±0.1 | 1.4±0.1 | 1.4±0.1 | 1.4±0.1 | 0.2 |
| | *p*-value | 0.7 | 0.6 | 0.1 | 0.2 | 0.09 | |

## 6.7 Appendix B: Acclimation Outcome Metrics

**Table 6.14. All outcome metrics for the foot arch length 200 mm and toe length 70 mm conditions near the start and near the end of the experimental data collection.** The condition near the start of the experimental data collection was a part of the toe and foot arch length sweep while the condition near the end was a part of the toe joint axis sweep. Asterisk indicates significant difference between the two conditions. All results shown are the inter-subject mean ± one standard deviation ($N$=10).

| Outcome Metric | Near Start | Near End | $p$-value |
|---|---|---|---|
| Stride Time | 1.3±0.1 s | 1.3±0.1 s | 0.6 |
| Peak Toe Joint Angle | 37.4±1.9° | 37.9±2.3° | 0.8 |
| Peak Ankle Angle | 13.0±0.8° | 13.2±0.9° | 0.7 |
| Min Knee Angle | -70.7±3.0° | -69.0±3.1° | 0.2 |
| Peak Ankle Moment | -1.4±0.1 Nm/kg | -1.5±0.1 Nm/kg | 0.2 |
| Peak Ankle Power | 2.2±0.2 W/kg | 2.5±0.3 W/kg | 0.05 |
| Peak Anklefoot Power | 2.1±0.3 W/kg | 2.0±0.3 W/kg | 0.3 |
| Peak COM Power | 2.4±0.2 W/kg | 2.4±0.2 W/kg | 0.9 |
| Ankle Push-off Work | 15.4±1.9 J | 18.2±2.9 J | 0.03* |
| Anklefoot Push-off Work | 13.6±2.0 J | 12.2±2.6 J | 0.1 |
| Hip Push-off Work | 5.4±1.3 J | 5.6±1.6 J | 0.7 |
| COM Push-off Work | 16.4±2.5 J | 17.0±2.7 J | 0.6 |
| COM Collision Work | -7.8±2.6 J | -8.3±2.0 J | 0.7 |

# Chapter 7

## Conclusions and Future Work

This dissertation has provided several scientific contributions pertaining to the role of the foot during walking. Expanding upon the presented research on the role of the toe joint could provide increased scientific understanding of the toes during human walking and could demonstrate further benefit for prosthetic foot users. The following sections outline further directions for examining toe properties and implementing a toe joint into a prosthesis for persons with lower limb amputation.

## 7.1 Future Work: The Effects of a Toe Joint during Uneven Terrain Walking

The research presented here only quantified the effects of different toe properties for level ground, forward walking. Further investigations are needed to examine how the toe joint can affect walking biomechanics during slope or uneven terrain walking. These studies could expand our basic scientific knowledge of the function of the toe joint and could demonstrate further benefits for persons with amputation. These investigation can be performed with a passive ankle (as done before in Chapters 5 and 6) or with the robotic ankle prosthesis developed at Vanderbilt University, as the foot of the ankle-toe prosthesis was designed to attach to this prosthesis.

## 7.2 Future Work: Carbon Fiber Foot Prosthesis with Toe Joint

The work presented here on the biomechanical effects of different toe parameters on human walking can be used to create a foot prosthesis with a toe joint for persons with amputation. A toe joint should be integrated into a commonly prescribed carbon-fiber prosthesis in order to reduce the amount of acclimation time for the user. Toe parameters that provided significant effects for able-bodied users, such as joint stiffness and length, will be also examined with persons with lower limb amputation.

## 7.3 Conclusions

This dissertation will provide five major contributions to the field of biomechanics. Chapter 2 developed a new musculoskeletal model that examines both mono- and multi- articular muscle contributions that are not captured by common inverse dynamics estimates. Chapter 3 provides a new framework for quantifying ankle, foot, and combined anklefoot power during walking. Chapter 4 expanded upon prior whole-body human locomotion research and evaluated the soft tissue absorption performed by the foot versus the rest of the body during sloped and level ground walking. Chapter 5 was first study to systematically evaluate the effects of toe joint stiffness and toe shape to human walking. Chapter 5 was the first study to systematically evaluate the biomechanical role of toe length, foot arch length and toe joint axis to human walking. Chapters 5 and 6 may provide a complementary means of enhancing locomotor performance for persons with amputation, in conjunction with the more conventional approach of augmenting ankle dynamics. These biological and prosthetic based studies provide dual understanding of the foot and its function during walking which may enhance locomotor performance for prosthetic users.

# REFERENCES


Adamczyk, Peter G., Steven H. Collins, and Arthur D. Kuo. 2006. "The Advantages of a Rolling Foot in Human Walking." *Journal of Experimental Biology* 209 (20): 3953–63. https://doi.org/10.1242/jeb.02455.

Adamczyk, Peter G., and Arthur D. Kuo. 2013. "Mechanical and Energetic Consequences of Rolling Foot Shape in Human Walking." *Journal of Experimental Biology* 216 (14): 2722–31. https://doi.org/10.1242/jeb.082347.

Adamczyk, Peter G., Michelle Roland, and Michael E. Hahn. 2017. "Sensitivity of Biomechanical Outcomes to Independent Variations of Hindfoot and Forefoot Stiffness in Foot Prostheses." *Human Movement Science* 54 (Supplement C): 154–71. https://doi.org/10.1016/j.humov.2017.04.005.

Aerts, P., and D. De Clercq. 1993. "Deformation Characteristics of the Heel Region of the Shod Foot during a Simulated Heel Strike: The Effect of Varying Midsole Hardness." *Journal of Sports Sciences* 11 (5): 449–61. https://doi.org/10.1080/02640419308730011.

Aerts, P., R. F Ker, D. De Clercq, D. W. Ilsley, and R. McN. Alexander. 1995. "The Mechanical Properties of the Human Heel Pad: A Paradox Resolved." *Journal of Biomechanics* 28 (11): 1299–1308. https://doi.org/10.1016/0021-9290(95)00009-7.

Ahn, Cheol Ki, Min Cheol Lee, and Seok Jo Go. 2003. "Development of a Biped Robot with Toes to Improve Gait Pattern." In *Proceedings 2003 IEEE/ASME International Conference on Advanced Intelligent Mechatronics (AIM 2003)*, 2:729–34 vol.2. https://doi.org/10.1109/AIM.2003.1225433.

Aleshinsky, Sergei Yu. 1986. "An Energy 'Sources' and 'Fractions' Approach to the Mechanical Energy Expenditure Problem—II. Movement of the Multi-Link Chain Model." *Journal of Biomechanics* 19 (4): 295–300. https://doi.org/10.1016/0021-9290(86)90004-7.

Antonsson, E. K., and R. W. Mann. 1985. "The Frequency Content of Gait." *Journal of Biomechanics* 18 (1): 39–47.

Aper, Rhonda L. MS, Charles L. Saltzman, and Thomas D. Brown. 1996. "The Effect of Hallux Sesamoid Excision on the Flexor Hallucis Longus Moment Arm." *Clinical Orthopaedics & Related Research* 325 (April): 209–17.

Arch, Elisa S., and Bretta L. Fylstra. 2016. "Combined Ankle–Foot Energetics Are Conserved When Distal Foot Energy Absorption Is Minimized." *Journal of Applied Biomechanics* 32 (6): 571–77. https://doi.org/10.1123/jab.2016-0108.

Ashby, Blake M, Nathaniel Vlietstra, Lauren J Hickox, and Gordon J Alderink. 2015. "METHODS FOR FULL BODY INVERSE DYNAMICS ANALYSIS OF STANDING LONG JUMP." In *39th Annual Meeting of the American Society of Biomechanics*, 84–85. Columbus, OH, USA.

Au, S.K., J. Weber, and H. Herr. 2009. "Powered Ankle–Foot Prosthesis Improves Walking Metabolic Economy." *IEEE Transactions on Robotics* 25 (1): 51–66. https://doi.org/10.1109/TRO.2008.2008747.

Baker, Richard W. 2013. *Measuring Walking: A Handbook of Clinical Gait Analysis*. Wiley.

Bartlett, H. L., B. E. Lawson, and M. Goldfarb. 2017. "Design of a Power-Asymmetric Actuator for a Transtibial Prosthesis." In *2017 International Conference on*

*Rehabilitation Robotics (ICORR)*, 1531–36. https://doi.org/10.1109/ICORR.2017.8009465.
Bennett, M B, and R F Ker. 1990. “The Mechanical Properties of the Human Subcalcaneal Fat Pad in Compression.” *Journal of Anatomy* 171 (August): 131–38.
Bezodis, Neil E., Aki I. T. Salo, and Grant Trewartha. 2013. “Excessive Fluctuations in Knee Joint Moments during Early Stance in Sprinting Are Caused by Digital Filtering Procedures.” *Gait & Posture* 38 (4): 653–57. https://doi.org/10.1016/j.gaitpost.2013.02.015.
Biewener, Andrew A., Claire T. Farley, Thomas J. Roberts, and Marco Temaner. 2004. “Muscle Mechanical Advantage of Human Walking and Running: Implications for Energy Cost.” *Journal of Applied Physiology* 97 (6): 2266–74. https://doi.org/10.1152/japplphysiol.00003.2004.
Bogey, R.A., J. Perry, and A.J. Gitter. 2005. “An EMG-to-Force Processing Approach for Determining Ankle Muscle Forces during Normal Human Gait.” *IEEE Transactions on Neural Systems and Rehabilitation Engineering* 13 (3): 302–10. https://doi.org/10.1109/TNSRE.2005.851768.
Bojsen-Møller, Finn, and Larry Lamoreux. 1979. “Significance of Free Dorsiflexion of the Toes in Walking.” *Acta Orthopaedica Scandinavica* 50 (4): 471–79. https://doi.org/10.3109/17453677908989792.
Browning, Raymond C., Jesse R. Modica, Rodger Kram, and Ambarish Goswami. 2007. “The Effects of Adding Mass to the Legs on the Energetics and Biomechanics of Walking:” *Medicine & Science in Sports & Exercise* 39 (3): 515–25. https://doi.org/10.1249/mss.0b013e31802b3562.
Bruening, Dustin A., Kevin M. Cooney, and Frank L. Buczek. 2012a. “Analysis of a Kinetic Multi-Segment Foot Model. Part I: Model Repeatability and Kinematic Validity.” *Gait & Posture* 35 (4): 529–34. https://doi.org/10.1016/j.gaitpost.2011.10.363.
———. 2012b. “Analysis of a Kinetic Multi-Segment Foot Model Part II: Kinetics and Clinical Implications.” *Gait & Posture* 35 (4): 535–40. https://doi.org/10.1016/j.gaitpost.2011.11.012.
Buchanan, Thomas S., David G. Lloyd, Kurt Manal, and Thor F. Besier. 2004. “Neuromusculoskeletal Modeling: Estimation of Muscle Forces and Joint Moments and Movements From Measurements of Neural Command.” *Journal of Applied Biomechanics* 20 (4): 367–95.
Buczek, Frank L., Thomas M. Kepple, Karen Lohmann Siegel, and Steven J. Stanhope. 1994. “Translational and Rotational Joint Power Terms in a Six Degree-of-Freedom Model of the Normal Ankle Complex.” *Journal of Biomechanics* 27 (12): 1447–57. https://doi.org/10.1016/0021-9290(94)90194-5.
Buschmann, Thomas, Sebastian Lohmeier, and Heinz Ulbrich. 2009. “Humanoid Robot Lola: Design and Walking Control.” *Journal of Physiology-Paris*, Neurorobotics, 103 (3–5): 141–48. https://doi.org/10.1016/j.jphysparis.2009.07.008.
Callaghan, Jack P., Aftab E. Patla, and Stuart M. McGill. 1999. “Low Back Three-Dimensional Joint Forces, Kinematics, and Kinetics during Walking.” *Clinical Biomechanics* 14 (3): 203–16. https://doi.org/10.1016/S0268-0033(98)00069-2.
Cappozzo, A., F. Figura, M. Marchetti, and A. Pedotti. 1976. “The Interplay of Muscular and External Forces in Human Ambulation.” *Journal of Biomechanics* 9 (1): 35–43. https://doi.org/10.1016/0021-9290(76)90137-8.

Caputo, Joshua M., and Steven H. Collins. 2014. “Prosthetic Ankle Push-off Work Reduces Metabolic Rate but Not Collision Work in Non-Amputee Walking.” *Scientific Reports* 4 (December): 7213. https://doi.org/10.1038/srep07213.

Carrier, David R., Norman C. Heglund, and Kathleen D. Earls. 1994. “Variable Gearing during Locomotion in the Human Musculoskeletal System.” *SCIENCE-NEW YORK THEN WASHINGTON-*, 651–651.

Cazzola, D. 2009. “INVESTIGATING THE METABOLIC PROFILE OF RUN-UP RACES AND THE MECHANICS OF WOBBLING VISCERAL MASS IN VERTICAL JUMPS.” Milan, Italy: UNIVERSITÁ DEGLI STUDI DI MILANO. https://air.unimi.it/handle/2434/150073#.WtYVxC7wbIU.

Cimolin, Veronica, Manuela Galli, Giorgio Albertini, Marcello Crivellini, Jacqueline Romkes, and Reinald Brunner. 2012. “Quantitative Analysis of Upper Limbs during Gait: A Marker Set Protocol.” *Journal of Applied Biomaterials & Functional Materials* 10 (1): 49–55. https://doi.org/10.5301/JABFM.2012.9277.

Collins, S. H, and A. D Kuo. 2010. “Recycling Energy to Restore Impaired Ankle Function during Human Walking.” *PLoS One* 5 (2): e9307.

Crimin, Anthony, Anthony McGarry, Elena Jane Harris, and Stephan Emanuel Solomonidis. 2014. “The Effect That Energy Storage and Return Feet Have on the Propulsion of the Body: A Pilot Study.” *Proceedings of the Institution of Mechanical Engineers, Part H: Journal of Engineering in Medicine* 228 (9): 908–15. https://doi.org/10.1177/0954411914549392.

Danforth, C. H. 1924. “The Heredity of Unilateral Variations in Man.” *Genetics* 9 (3): 199–211.

De Asha, Alan R., Ramesh Munjal, Jai Kulkarni, and John G. Buckley. 2013. “Walking Speed Related Joint Kinetic Alterations in Trans-Tibial Amputees: Impact of Hydraulic 'ankle’ Damping.” *Journal of NeuroEngineering and Rehabilitation* 10 (October): 107. https://doi.org/10.1186/1743-0003-10-107.

Dieën, J. H. van, C. E. a. M. Thissen, A. J. G. M. van de Ven, and H. M. Toussaint. 1991. “The Electro-Mechanical Delay of the Erector Spinae Muscle: Influence of Rate of Force Development, Fatigue and Electrode Location.” *European Journal of Applied Physiology and Occupational Physiology* 63 (3–4): 216–22. https://doi.org/10.1007/BF00233851.

Dillon, Michael P., and Timothy M. Barker. 2006. “Preservation of Residual Foot Length in Partial Foot Amputation: A Biomechanical Analysis.” *Foot & Ankle International* 27 (2): 110–16. https://doi.org/10.1177/107110070602700207.

Dixon, Philippe C., Harald Böhm, and Leonhard Döderlein. 2012. “Ankle and Midfoot Kinetics during Normal Gait: A Multi-Segment Approach.” *Journal of Biomechanics* 45 (6): 1011–16. https://doi.org/10.1016/j.jbiomech.2012.01.001.

Donelan, J. Maxwell, Rodger Kram, and Arthur D. Kuo. 2002. “Simultaneous Positive and Negative External Mechanical Work in Human Walking.” *Journal of Biomechanics* 35 (1): 117–24. https://doi.org/10.1016/S0021-9290(01)00169-5.

Duncan, Jeffrey A., David L. Kowalk, and Christopher L. Vaughan. 1997. “Six Degree of Freedom Joint Power in Stair Climbing.” *Gait & Posture* 5 (3): 204–10. https://doi.org/10.1016/S0966-6362(96)01086-7.

Ebrahimi, Anahid. 2018. “The Development and Application of a Framework for Exploring the Energetics of Gait Strategy Adaptations.” University of Delaware.

Ebrahimi, Anahid, John D. Collins, Thomas M. Kepple, Kota Z. Takahashi, Jill S.

Higginson, and Steven J. Stanhope. 2017. “A Mathematical Analysis to Address the 6 Degree-of-Freedom Segmental Power Imbalance.” *Journal of Biomechanics*, November. https://doi.org/10.1016/j.jbiomech.2017.10.034.

Ebrahimi, Anahid, Saryn R. Goldberg, Jason M. Wilken, and Steven J. Stanhope. 2017. “Constituent Lower Extremity Work (CLEW) Approach: A Novel Tool to Visualize Joint and Segment Work.” *Gait & Posture* 56 (July): 49–53. https://doi.org/10.1016/j.gaitpost.2017.04.024.

Egleston, Brian L., Suzanne M. Miller, and Neal J. Meropol. 2011. “The Impact of Misclassification Due to Survey Response Fatigue on Estimation and Identifiability of Treatment Effects.” *Statistics in Medicine* 30 (30): 3560–72. https://doi.org/10.1002/sim.4377.

Ehrig, Rainald M., William R. Taylor, Georg N. Duda, and Markus O. Heller. 2006. “A Survey of Formal Methods for Determining the Centre of Rotation of Ball Joints.” *Journal of Biomechanics* 39 (15): 2798–2809. https://doi.org/10.1016/j.jbiomech.2005.10.002.

Elftman, Herbert. 1939. “Forces and Energy Changes in the Leg during Walking.” *American Journal of Physiology–Legacy Content* 125 (2): 339–356.

Farris, Dominic James, and Gregory S. Sawicki. 2012a. “The Mechanics and Energetics of Human Walking and Running: A Joint Level Perspective.” *Journal of The Royal Society Interface* 9 (66): 110–18. https://doi.org/10.1098/rsif.2011.0182.

———. 2012b. “Human Medial Gastrocnemius Force–Velocity Behavior Shifts with Locomotion Speed and Gait.” *Proceedings of the National Academy of Sciences* 109 (3): 977–82. https://doi.org/10.1073/pnas.1107972109.

Ferris, Abbie E., Jennifer M. Aldridge, Christopher A. Rábago, and Jason M. Wilken. 2012. “Evaluation of a Powered Ankle-Foot Prosthetic System During Walking.” *Archives of Physical Medicine and Rehabilitation* 93 (11): 1911–18. https://doi.org/10.1016/j.apmr.2012.06.009.

Fessler, Daniel M. T., Kevin J. Haley, and Roshni D. Lal. 2005. “Sexual Dimorphism in Foot Length Proportionate to Stature.” *Annals of Human Biology* 32 (1): 44–59. https://doi.org/10.1080/03014460400027581.

Franz, Jason R., Nicholas E. Lyddon, and Rodger Kram. 2012. “Mechanical Work Performed by the Individual Legs during Uphill and Downhill Walking.” *Journal of Biomechanics* 45 (2): 257–62. https://doi.org/10.1016/j.jbiomech.2011.10.034.

Fu, Xiao-Yu, Karl E. Zelik, Wayne J. Board, Raymond C. Browning, and Arthur D. Kuo. 2015. “Soft Tissue Deformations Contribute to the Mechanics of Walking in Obese Adults.” *Medicine and Science in Sports and Exercise* 47 (7): 1435–43. https://doi.org/10.1249/MSS.0000000000000554.

Fukunaga, Tetsuo, Yasuo Kawakami, Keitaro Kubo, and Hiroaki Kanehisa. 2002. “Muscle and Tendon Interaction during Human Movements.” *Exercise and Sport Sciences Reviews* 30 (3): 106–10.

Gailey, R. S., M. S. Nash, T. A. Atchley, R. M. Zilmer, G. R. Moline-Little, N. Morris-Cresswell, and L. I. Siebert. 1997. “The Effects of Prosthesis Mass on Metabolic Cost of Ambulation in Non-Vascular Trans-Tibial Amputees.” *Prosthetics and Orthotics International* 21 (1): 9–16. https://doi.org/10.3109/03093649709164525.

Galle, Samuel, Philippe Malcolm, Steven Hartley Collins, and Dirk De Clercq. 2017. “Reducing the Metabolic Cost of Walking with an Ankle Exoskeleton: Interaction between Actuation Timing and Power.” *Journal of NeuroEngineering and*

*Rehabilitation* 14 (1): 35. https://doi.org/10.1186/s12984-017-0235-0.
Grabowski, Alena M., Jerome Rifkin, and Rodger Kram. 2010. "K3 Promoter$^{TM}$ Prosthetic Foot Reduces the Metabolic Cost of Walking for Unilateral Transtibial Amputees:" *JPO Journal of Prosthetics and Orthotics* 22 (2): 113–20. https://doi.org/10.1097/JPO.0b013e3181cca79c.
Hamner, Samuel R., Ajay Seth, and Scott L. Delp. 2010. "Muscle Contributions to Propulsion and Support during Running." *Journal of Biomechanics* 43 (14): 2709–16. https://doi.org/10.1016/j.jbiomech.2010.06.025.
Hansen, Andrew H., Dudley S. Childress, Steve C. Miff, Steven A. Gard, and Kent P. Mesplay. 2004. "The Human Ankle during Walking: Implications for Design of Biomimetic Ankle Prostheses." *Journal of Biomechanics* 37 (10): 1467–74. https://doi.org/10.1016/j.jbiomech.2004.01.017.
Hansen, Andrew H., Michel Sam, and Dudley S. Childress. 2004. "The Effective Foot Length Ratio: A Potential Tool for Characterization and Evaluation of Prosthetic Feet." *JPO: Journal of Prosthetics and Orthotics* 16 (2): 41.
Hefti, Fritz. 2007. *Pediatric Orthopedics in Practice*. Springer Science & Business Media.
Hermens, Hermie, Bart Freriks, Roberto Merletti, Dick Stegeman, Joleen Blok, and G. Rau. 1999. "European Recommendations for Surface Electromyography." *Roessing Research and Development, Enschede*.
Herr, Hugh M, and Alena M Grabowski. 2012. "Bionic Ankle–Foot Prosthesis Normalizes Walking Gait for Persons with Leg Amputation." *Proceedings of the Royal Society B: Biological Sciences* 279 (1728): 457–64. https://doi.org/10.1098/rspb.2011.1194.
Highsmith, M. Jason, Brian W. Schulz, Stephanie Hart-Hughes, Gail A. Latlief, and Sam L. Phillips. 2010. "Differences in the Spatiotemporal Parameters of Transtibial and Transfemoral Amputee Gait." *JPO: Journal of Prosthetics and Orthotics* 22 (1): 26–30. https://doi.org/10.1097/JPO.0b013e3181cc0e34.
Hirasaki, Eishi, Steven T. Moore, T. Raphan, and Bernard Cohen. 1999. "Effects of Walking Velocity on Vertical Head and Body Movements during Locomotion." *Experimental Brain Research* 127 (2): 117–30. https://doi.org/10.1007/s002210050781.
Hitt, Joseph K., Thomas G. Sugar, Matthew Holgate, and Ryan Bellman. 2010. "An Active Foot-Ankle Prosthesis With Biomechanical Energy Regeneration." *Journal of Medical Devices* 4 (1): 011003-011003–9. https://doi.org/10.1115/1.4001139.
Hof, A. L. 1984. "EMG and Muscle Force: An Introduction." *Human Movement Science* 3 (1–2): 119–53. https://doi.org/10.1016/0167-9457(84)90008-3.
Hof, A. L., B. A. Geelen, and Jw. Van den Berg. 1983. "Calf Muscle Moment, Work and Efficiency in Level Walking; Role of Series Elasticity." *Journal of Biomechanics* 16 (7): 523–37. https://doi.org/10.1016/0021-9290(83)90067-2.
Hof, At L., Jelle Nauta, Erik R. van der Knaap, Michiel A. A. Schallig, and D. Peter Struwe. 1993. "Calf Muscle Work and Segment Energy Changes in Human Treadmill Walking." *Journal of Electromyography and Kinesiology* 2 (4): 203–16. https://doi.org/10.1016/1050-6411(92)90024-D.
Honert, Eric C, Gerasimos Bastas, and Karl E Zelik. 2018. "Effect of Toe Joint Stiffness and Toe Shape on Walking Biomechanics." *Bioinspiration & Biomimetics* 13 (6): 066007. https://doi.org/10.1088/1748-3190/aadf46.
Honert, Eric C., and Karl E. Zelik. 2016. "Inferring Muscle-Tendon Unit Power from Ankle Joint Power during the Push-Off Phase of Human Walking: Insights from a

Multiarticular EMG-Driven Model." *PLOS ONE* 11 (10): e0163169. https://doi.org/10.1371/journal.pone.0163169.
———. 2019. "Foot and Shoe Responsible for Majority of Soft Tissue Work in Early Stance of Walking." *Human Movement Science* 64 (April): 191–202. https://doi.org/10.1016/j.humov.2019.01.008.
Hsu, Tsz-Ching, Chung-Li Wang, Wen-Chung Tsai, Jung-Kun Kuo, and Fuk-Tan Tang. 1998. "Comparison of the Mechanical Properties of the Heel Pad between Young and Elderly Adults." *Archives of Physical Medicine and Rehabilitation* 79 (9): 1101–4. https://doi.org/10.1016/S0003-9993(98)90178-2.
Huang, Y., B. Chen, Q. Wang, and L. Wang. 2010. "Adding Segmented Feet to Passive Dynamic Walkers." In *2010 IEEE/ASME International Conference on Advanced Intelligent Mechatronics*, 652–57. https://doi.org/10.1109/AIM.2010.5695776.
Huang, Yan, Qi-Ning Wang, Yue Gao, and Guang-Ming Xie. 2012. "Modeling and Analysis of Passive Dynamic Bipedal Walking with Segmented Feet and Compliant Joints." *Acta Mechanica Sinica* 28 (5): 1457–65. https://doi.org/10.1007/s10409-012-0079-6.
Ingen Schenau, G J van, M F Bobbert, and R H Rozendal. 1987. "The Unique Action of Bi-Articular Muscles in Complex Movements." *Journal of Anatomy* 155 (December): 1–5.
Inman, Verne Thompson, Henry James Ralston, and Frank Todd. 1981. *Human Walking*. Williams & Wilkins.
Ishikawa, Masaki, Paavo V Komi, Michael J Grey, Vesa Lepola, and Gert-Peter Bruggemann. 2005. "Muscle-Tendon Interaction and Elastic Energy Usage in Human Walking." *Journal of Applied Physiology* 99 (2): 603–8. https://doi.org/10.1152/japplphysiol.00189.2005.
Jackson, Rachel W., and Steven H. Collins. 2015. "An Experimental Comparison of the Relative Benefits of Work and Torque Assistance in Ankle Exoskeletons." *Journal of Applied Physiology* 119 (5): 541–57. https://doi.org/10.1152/japplphysiol.01133.2014.
Kelly, Luke A., Andrew G. Cresswell, and Dominic J. Farris. 2018. "The Energetic Behaviour of the Human Foot across a Range of Running Speeds." *Scientific Reports* 8 (July). https://doi.org/10.1038/s41598-018-28946-1.
Kelly, Luke A., Andrew G. Cresswell, Sebastien Racinais, Rodney Whiteley, and Glen Lichtwark. 2014. "Intrinsic Foot Muscles Have the Capacity to Control Deformation of the Longitudinal Arch." *Journal of The Royal Society Interface* 11 (93): 20131188. https://doi.org/10.1098/rsif.2013.1188.
Kelly, Luke A., Glen Lichtwark, and Andrew G. Cresswell. 2015. "Active Regulation of Longitudinal Arch Compression and Recoil during Walking and Running." *Journal of The Royal Society Interface* 12 (102): 20141076. https://doi.org/10.1098/rsif.2014.1076.
Ker, R. F., M. B. Bennett, R. McN Alexander, and R. C. Kester. 1989. "Foot Strike and the Properties of the Human Heel Pad." *Proceedings of the Institution of Mechanical Engineers, Part H: Journal of Engineering in Medicine* 203 (4): 191–96. https://doi.org/10.1243/PIME_PROC_1989_203_038_01.
Ker, R. F., M. B. Bennett, S. R. Bibby, R. C. Kester, and R. M. Alexander. 1987. "The Spring in the Arch of the Human Foot." *Nature* 325: 147–49.
Killian Bouillard, Antoine Nordez, and François Hug. 2011. "Estimation of Individual

Muscle Force Using Elastography." *PLoS ONE* 6 (12): e29261. https://doi.org/10.1371/journal.pone.0029261.
Kirane, Y. M., J. D. Michelson, and N. A. Sharkey. 2008. "Evidence of Isometric Function of the Flexor Hallucis Longus Muscle in Normal Gait." *Journal of Biomechanics* 41 (9): 1919–28. https://doi.org/10.1016/j.jbiomech.2008.03.040.
Klute, Glenn K., Jocelyn S. Berge, and Ava D. Segal. 2004. "Heel-Region Properties of Prosthetic Feet and Shoes." *Journal of Rehabilitation Research and Development; Washington* 41 (4): 535–46.
Krishnaswamy, Pavitra, Emery N. Brown, and Hugh M. Herr. 2011. "Human Leg Model Predicts Ankle Muscle-Tendon Morphology, State, Roles and Energetics in Walking." *PLoS Comput Biol* 7 (3): e1001107. https://doi.org/10.1371/journal.pcbi.1001107.
Kristianslund, Eirik, Tron Krosshaug, and Antonie J. van den Bogert. 2012. "Effect of Low Pass Filtering on Joint Moments from Inverse Dynamics: Implications for Injury Prevention." *Journal of Biomechanics* 45 (4): 666–71. https://doi.org/10.1016/j.jbiomech.2011.12.011.
Kruk, E. van der, F. C. T. van der Helm, H. E. J. Veeger, and A. L. Schwab. 2018. "Power in Sports: A Literature Review on the Application, Assumptions, and Terminology of Mechanical Power in Sport Research." *Journal of Biomechanics* 79 (October): 1–14. https://doi.org/10.1016/j.jbiomech.2018.08.031.
Kumar, R. Prasanth, Jungwon Yoon, Christiand, and Gabsoon Kim. 2009. "The Simplest Passive Dynamic Walking Model with Toed Feet: A Parametric Study." *Robotica* 27 (05): 701. https://doi.org/10.1017/S0263574708005079.
Kuo, A. D. 2002. "Energetics of Actively Powered Locomotion Using the Simplest Walking Model." *Journal of Biomechanical Engineering* 124: 113.
Kuo, A. D, J. M Donelan, and A. Ruina. 2005. "Energetic Consequences of Walking like an Inverted Pendulum: Step-to-Step Transitions." *Exercise and Sport Sciences Reviews* 33 (2): 88.
Kuo, Arthur D., and J. Maxwell Donelan. 2010. "Dynamic Principles of Gait and Their Clinical Implications." *Physical Therapy* 90 (2): 157–74. https://doi.org/10.2522/ptj.20090125.
Kuo, Arthur D., J. Maxwell Donelan, and Andy Ruina. 2005. "Energetic Consequences of Walking like an Inverted Pendulum: Step-to-Step Transitions." *Exercise and Sport Sciences Reviews* 33 (2): 88–97.
Kwon, SangJoo, and Jinhee Park. 2012. "Kinesiology-Based Robot Foot Design for Human-Like Walking." *International Journal of Advanced Robotic Systems* 9 (6): 259. https://doi.org/10.5772/54763.
La Scaleia, Valentina, Yuri P. Ivanenko, Karl E. Zelik, and Francesco Lacquaniti. 2014. "Spinal Motor Outputs during Step-to-Step Transitions of Diverse Human Gaits." *Frontiers in Human Neuroscience* 8 (May). https://doi.org/10.3389/fnhum.2014.00305.
Latash, Mark L., and Vladimir M. Zatsiorsky. 1993. "Joint Stiffness: Myth or Reality?" *Human Movement Science* 12 (6): 653–92. https://doi.org/10.1016/0167-9457(93)90010-M.
Leardini, A., M. G. Benedetti, L. Berti, D. Bettinelli, R. Nativo, and S. Giannini. 2007. "Rear-Foot, Mid-Foot and Fore-Foot Motion during the Stance Phase of Gait." *Gait & Posture* 25 (3): 453–62. https://doi.org/10.1016/j.gaitpost.2006.05.017.

Levine, David, Jim Richards, and Michael W. Whittle. 2012. *Whittle's Gait Analysis*. Elsevier Health Sciences.

Lichtwark, G. A., and A. M. Wilson. 2006. "Interactions between the Human Gastrocnemius Muscle and the Achilles Tendon during Incline, Level and Decline Locomotion." *Journal of Experimental Biology* 209 (21): 4379–88. https://doi.org/10.1242/jeb.02434.

Lipfert, Susanne W, Michael Günther, Daniel Renjewski, and Andre Seyfarth. 2014. "Impulsive Ankle Push-off Powers Leg Swing in Human Walking." *The Journal of Experimental Biology* 217 (Pt 8): 1218–28. https://doi.org/10.1242/jeb.097345.

Lloyd, David G, and Thor F Besier. 2003. "An EMG-Driven Musculoskeletal Model to Estimate Muscle Forces and Knee Joint Moments in Vivo." *Journal of Biomechanics* 36 (6): 765–76. https://doi.org/10.1016/S0021-9290(03)00010-1.

MacWilliams, Bruce A., Matthew Cowley, and Diane E. Nicholson. 2003. "Foot Kinematics and Kinetics during Adolescent Gait." *Gait & Posture* 17 (3): 214–24. https://doi.org/10.1016/S0966-6362(02)00103-0.

Mager, Fabian, Jim Richards, Malika Hennies, Eugen Dötzel, Ambreen Chohan, Alex Mbuli, and Felix Capanni. 2018. "Determination of Ankle and Metatarsophalangeal Stiffness During Walking and Jogging." *Journal of Applied Biomechanics*, May, 1–20. https://doi.org/10.1123/jab.2017-0265.

Major, Matthew J., Martin Twiste, Laurence P. J. Kenney, and David Howard. 2014. "The Effects of Prosthetic Ankle Stiffness on Ankle and Knee Kinematics, Prosthetic Limb Loading, and Net Metabolic Cost of Trans-Tibial Amputee Gait." *Clinical Biomechanics* 29 (1): 98–104. https://doi.org/10.1016/j.clinbiomech.2013.10.012.

Malcolm, Philippe, Roberto E Quesada, Joshua M Caputo, and Steven H Collins. 2015. "The Influence of Push-off Timing in a Robotic Ankle-Foot Prosthesis on the Energetics and Mechanics of Walking." *Journal of NeuroEngineering and Rehabilitation* 12 (1). https://doi.org/10.1186/s12984-015-0014-8.

Mann, R. A., and J. Hagy. 1980. "Biomechanics of Walking, Running, and Sprinting." *The American Journal of Sports Medicine* 8 (5): 345–50. https://doi.org/10.1177/036354658000800510.

Martínez, A., B. Lawson, and M. Goldfarb. 2018. "A Controller for Guiding Leg Movement During Overground Walking With a Lower Limb Exoskeleton." *IEEE Transactions on Robotics* 34 (1): 183–93. https://doi.org/10.1109/TRO.2017.2768035.

McCaw, Steven T., Jacob K. Gardner, Lindsay N. Stafford, and Michael R. Torry. 2013. "Filtering Ground Reaction Force Data Affects the Calculation and Interpretation of Joint Kinetics and Energetics During Drop Landings." *Journal of Applied Biomechanics* 29 (6): 804–9. https://doi.org/10.1123/jab.29.6.804.

McCullough, Matthew B. A., Stacie I. Ringleb, Kenichiro Arai, Harold B. Kitaoka, and Kenton R. Kaufman. 2011. "Moment Arms of the Ankle Throughout the Range of Motion in Three Planes." *Foot & Ankle International* 32 (3): 300–306. https://doi.org/10.3113/FAI.2011.0300.

McDonald, Kirsty A., Sarah M. Stearne, Jacqueline A. Alderson, Ian North, Neville J. Pires, and Jonas Rubenson. 2016. "The Role of Arch Compression and Metatarsophalangeal Joint Dynamics in Modulating Plantar Fascia Strain in Running." *PLOS ONE* 11 (4): e0152602. https://doi.org/10.1371/journal.pone.0152602.

Meinders, M, A Gitter, and J M Czerniecki. 1998. “The Role of Ankle Plantar Flexor Muscle Work during Walking.” *Scandinavian Journal of Rehabilitation Medicine* 30 (1): 39–46.

Minetti, Alberto E., and Giancesare Belli. 1994. “A Model for the Estimation of Visceral Mass Displacement in Periodic Movements.” *Journal of Biomechanics* 27 (1): 97–101. https://doi.org/10.1016/0021-9290(94)90036-1.

Morgenroth, David C., Ava D. Segal, Karl E. Zelik, Joseph M. Czerniecki, Glenn K. Klute, Peter G. Adamczyk, Michael S. Orendurff, Michael E. Hahn, Steven H. Collins, and Art D. Kuo. 2011. “The Effect of Prosthetic Foot Push-off on Mechanical Loading Associated with Knee Osteoarthritis in Lower Extremity Amputees.” *Gait & Posture* 34(4): 502–7. https://doi.org/16/j.gaitpost.2011.07.001.

Murley, George S., Andrew K. Buldt, Philip J. Trump, and James B. Wickham. 2009. “Tibialis Posterior EMG Activity during Barefoot Walking in People with Neutral Foot Posture.” *Journal of Electromyography and Kinesiology* 19 (2): e69–77. https://doi.org/10.1016/j.jelekin.2007.10.002.

Neptune, R. R., S. A. Kautz, and F. E. Zajac. 2001. “Contributions of the Individual Ankle Plantar Flexors to Support, Forward Progression and Swing Initiation during Walking.” *Journal of Biomechanics* 34 (11): 1387–1398.

Nigg, Benno M., Asra Khan, Veronica Fisher, and Darren Stefanyshyn. 1998. “Effect of Shoe Insert Construction on Foot and Leg Movement.” *Medicine & Science in Sports & Exercise* 30 (4): 550–55.

Oh, Keonyoung, and Sukyung Park. 2017. “The Bending Stiffness of Shoes Is Beneficial to Running Energetics If It Does Not Disturb the Natural MTP Joint Flexion.” *Journal of Biomechanics* 0 (0). https://doi.org/10.1016/j.jbiomech.2017.01.014.

Ozden, Hilmi, Yasemin Balci, Canan Demirüstü, Akin Turgut, and Mehmet Ertugrul. 2005. “Stature and Sex Estimate Using Foot and Shoe Dimensions.” *Forensic Science International*, Sex and Body Size, 147 (2): 181–84. https://doi.org/10.1016/j.forsciint.2004.09.072.

Pain, Matthew T.G., and John H. Challis. 2002. “Soft Tissue Motion during Impacts: Their Potential Contributions to Energy Dissipation.” *Journal of Applied Biomechanics* 18 (3): 231–42. https://doi.org/10.1123/jab.18.3.231.

Parham, Kenneth R., Claire C. Gordon, and Carolyn K. Bensel. 1992. “Anthropometry of the Foot and Lower Leg of US Army Soldiers: Fort Jackson, SC--1985.” NATICK/TR-92/028. ARMY NATICK RESEARCH DEVELOPMENT AND ENGINEERING CENTER MA.

Perry, Jacquelin. 1992. *Gait Analysis: Normal and Pathological Function*. Delmar Learning. http://www.amazon.ca/exec/obidos/redirect?tag=citeulike09-20&path=ASIN/1556421923.

Perry, Jacquelin, and Judith M. Burnfield. 2010. *Gait Analysis: Normal and Pathological Function*. 2nd ed. Vol. 9. SLACK Incorporated.

Potvin, J. R., and S. H. M Brown. 2004. “Less Is More: High Pass Filtering, to Remove up to 99% of the Surface EMG Signal Power, Improves EMG-Based Biceps Brachii Muscle Force Estimates.” *Journal of Electromyography and Kinesiology* 14 (3): 389–99. https://doi.org/10.1016/j.jelekin.2003.10.005.

Prince, F., David A. Winter, G. Sjonnesen, and R. K. Wheeldon. 1994. “A New Technique for the Calculation of the Energy Stored, Dissipated, and Recovered in Different Ankle-Foot Prostheses.” *Rehabilitation Engineering, IEEE Transactions On* 2 (4):

247–255.
Quesada, Roberto E., Joshua M. Caputo, and Steven H. Collins. 2016. “Increasing Ankle Push-off Work with a Powered Prosthesis Does Not Necessarily Reduce Metabolic Rate for Transtibial Amputees.” *Journal of Biomechanics* 49 (14): 3452–59. https://doi.org/10.1016/j.jbiomech.2016.09.015.
Ranchos Los Amigos National Rehabilitation Center. 2001. *Observational Gait Analysis*. Revised edition. Downey, CA: Los Amigos Research &.
Reinschmidt, C, A. J van den Bogert, A Lundberg, B. M Nigg, N Murphy, A Stacoff, and A Stano. 1997. “Tibiofemoral and Tibiocalcaneal Motion during Walking: External vs. Skeletal Markers.” *Gait & Posture* 6 (2): 98–109. https://doi.org/10.1016/S0966-6362(97)01110-7.
Ren, Lei, Richard K. Jones, and David Howard. 2008. “Whole Body Inverse Dynamics over a Complete Gait Cycle Based Only on Measured Kinematics.” *Journal of Biomechanics* 41 (12): 2750–59. https://doi.org/10.1016/j.jbiomech.2008.06.001.
Riddick, R. C., and A. D. Kuo. 2016. “Soft Tissues Store and Return Mechanical Energy in Human Running.” *Journal of Biomechanics* 49 (3): 436–41. https://doi.org/10.1016/j.jbiomech.2016.01.001.
Ringleb, S. I., S. J. Kavros, B. R. Kotajarvi, D. K. Hansen, H. B. Kitaoka, and K. R. Kaufman. 2007. “Changes in Gait Associated with Acute Stage II Posterior Tibial Tendon Dysfunction.” *Gait & Posture* 25 (4): 555–64. https://doi.org/10.1016/j.gaitpost.2006.06.008.
Robertson, D. Gordon E., Graham E. Caldwell, Joseph Hamill, Gary Kamen, and Whittlesey. 2013. *Research Methods In Biomechanics 2nd Edition*. Human Kinetics.
Robertson, Gordon, Graham Caldwell, Joseph Hamill, Gary Kamen, and Saunders Whittlesey. 2013. *Research Methods in Biomechanics*. 2nd ed. Human Kinetics.
Roewer, Benjamin D., Kevin R. Ford, Gregory D. Myer, and Timothy E. Hewett. 2014. “The ‘Impact’ of Force Filtering Cut-off Frequency on the Peak Knee Abduction Moment during Landing: Artefact or ‘Artifiction’?” *Br J Sports Med* 48 (6): 464–68. https://doi.org/10.1136/bjsports-2012-091398.
Rolian, Campbell, Daniel E. Lieberman, Joseph Hamill, John W. Scott, and William Werbel. 2009. “Walking, Running and the Evolution of Short Toes in Humans.” *Journal of Experimental Biology* 212 (5): 713–21. https://doi.org/10.1242/jeb.019885.
Rouse, Elliott J., Levi J. Hargrove, Eric J. Perreault, Michael A. Peshkin, and Todd A. Kuiken. 2013. “Development of a Mechatronic Platform and Validation of Methods for Estimating Ankle Stiffness during the Stance Phase of Walking.” *Journal of Biomechanical Engineering* 135 (8): 081009.
Roy, Jean-Pierre R., and Darren J. Stefanyshyn. 2006. “Shoe Midsole Longitudinal Bending Stiffness and Running Economy, Joint Energy, and EMG.” *Medicine & Science in Sports & Exercise* 38 (3): 562–69. https://doi.org/10.1249/01.mss.0000193562.22001.e8.
Sanderson, David J, and Philip E Martin. 1997. “Lower Extremity Kinematic and Kinetic Adaptations in Unilateral Below-Knee Amputees during Walking.” *Gait & Posture* 6 (2): 126–36. https://doi.org/10.1016/S0966-6362(97)01112-0.
Sartori, Massimo, Monica Reggiani, Dario Farina, and David G. Lloyd. 2012. “EMG-Driven Forward-Dynamic Estimation of Muscle Force and Joint Moment about

Multiple Degrees of Freedom in the Human Lower Extremity." *PLoS ONE* 7 (12): e52618. https://doi.org/10.1371/journal.pone.0052618.
Sawers, Andrew, and Michael E. Hahn. 2011. "Trajectory of the Center of Rotation in Non-Articulated Energy Storage and Return Prosthetic Feet." *Journal of Biomechanics* 44 (9): 1673–77. https://doi.org/10.1016/j.jbiomech.2011.03.028.
Schmitt, Syn, and Michael Günther. 2011. "Human Leg Impact: Energy Dissipation of Wobbling Masses." *Archive of Applied Mechanics* 81 (7): 887–97. https://doi.org/10.1007/s00419-010-0458-z.
Scott, Stephen H., and David A. Winter. 1993. "Biomechanical Model of the Human Foot: Kinematics and Kinetics during the Stance Phase of Walking." *Journal of Biomechanics* 26 (9): 1091–1104. https://doi.org/10.1016/S0021-9290(05)80008-9.
Segal, Ava D., Kyle H. Yeates, Richard R. Neptune, and Glenn K. Klute. 2018. "Foot and Ankle Joint Biomechanical Adaptations to an Unpredictable Coronally Uneven Surface." *Journal of Biomechanical Engineering* 140 (3): 031004. https://doi.org/10.1115/1.4037563.
Segal, Ava D., Karl E. Zelik, Glenn K. Klute, David C. Morgenroth, Michael E. Hahn, Michael S. Orendurff, Peter G. Adamczyk, Steven H. Collins, Arthur D. Kuo, and Joseph M. Czerniecki. 2012. "The Effects of a Controlled Energy Storage and Return Prototype Prosthetic Foot on Transtibial Amputee Ambulation." *Human Movement Science*. https://doi.org/10.1016/j.humov.2011.08.005.
Sellaouti, R., O. Stasse, S. Kajita, K. Yokoi, and A. Kheddar. 2006. "Faster and Smoother Walking of Humanoid HRP-2 with Passive Toe Joints." In *2006 IEEE/RSJ International Conference on Intelligent Robots and Systems*, 4909–14. https://doi.org/10.1109/IROS.2006.282449.
Shorten, Martyn R. 1993. "The Energetics of Running and Running Shoes." *Journal of Biomechanics* 26 (January): 41–51. https://doi.org/10.1016/0021-9290(93)90078-S.
Shultz, A. H., B. E. Lawson, and M. Goldfarb. 2016. "Variable Cadence Walking and Ground Adaptive Standing With a Powered Ankle Prosthesis." *IEEE Transactions on Neural Systems and Rehabilitation Engineering* 24 (4): 495–505. https://doi.org/10.1109/TNSRE.2015.2428196.
Siegel, Karen Lohmann, Thomas M. Kepple, and Graham E. Caldwell. 1996. "Improved Agreement of Foot Segmental Power and Rate of Energy Change during Gait: Inclusion of Distal Power Terms and Use of Three-Dimensional Models." *Journal of Biomechanics* 29 (6): 823–27. https://doi.org/10.1016/0021-9290(96)83336-7.
Sloot, L. H., M. M. van der Krogt, and J. Harlaar. 2014. "Energy Exchange between Subject and Belt during Treadmill Walking." *Journal of Biomechanics* 47 (6): 1510–13. https://doi.org/10.1016/j.jbiomech.2014.02.001.
Stearne, Sarah M., Kirsty A. McDonald, Jacqueline A. Alderson, Ian North, Charles E. Oxnard, and Jonas Rubenson. 2016. "The Foot's Arch and the Energetics of Human Locomotion." *Scientific Reports* 6 (January): srep19403. https://doi.org/10.1038/srep19403.
Stebbins, J., M. Harrington, N. Thompson, A. Zavatsky, and T. Theologis. 2006. "Repeatability of a Model for Measuring Multi-Segment Foot Kinematics in Children." *Gait & Posture* 23 (4): 401–10. https://doi.org/10.1016/j.gaitpost.2005.03.002.
Stefanyshyn, Darren J., and Benno M. Nigg. 1997. "Mechanical Energy Contribution of the Metatarsophalangeal Joint to Running and Sprinting." *Journal of Biomechanics*

30 (11): 1081–85. https://doi.org/10.1016/S0021-9290(97)00081-X.
Stokes, I A, W C Hutton, and J R Stott. 1979. “Forces Acting on the Metatarsals during Normal Walking.” *Journal of Anatomy* 129 (Pt 3): 579–90.
Takahashi, Kota Z., Michael T. Gross, Herman van Werkhoven, Stephen J. Piazza, and Gregory S. Sawicki. 2016. “Adding Stiffness to the Foot Modulates Soleus Force-Velocity Behaviour during Human Walking.” *Scientific Reports* 6 (July). https://doi.org/10.1038/srep29870.
Takahashi, Kota Z., John R. Horne, and Steven J. Stanhope. 2014. “Comparison of Mechanical Energy Profiles of Passive and Active Below-Knee Prostheses: A Case Study.” *Prosthetics and Orthotics International*, January, 0309364613513298. https://doi.org/10.1177/0309364613513298.
Takahashi, Kota Z., Thomas M. Kepple, and Steven J. Stanhope. 2012. “A Unified Deformable (UD) Segment Model for Quantifying Total Power of Anatomical and Prosthetic below-Knee Structures during Stance in Gait.” *Journal of Biomechanics* 45 (15): 2662–67. https://doi.org/10.1016/j.jbiomech.2012.08.017.
Takahashi, Kota Z., and Steven J. Stanhope. 2013. “Mechanical Energy Profiles of the Combined Ankle–Foot System in Normal Gait: Insights for Prosthetic Designs.” *Gait & Posture*. https://doi.org/10.1016/j.gaitpost.2013.04.002.
Takahashi, Kota Z., Kate Worster, and Dustin A. Bruening. 2017. “Energy Neutral: The Human Foot and Ankle Subsections Combine to Produce near Zero Net Mechanical Work during Walking.” *Scientific Reports* 7 (1): 15404. https://doi.org/10.1038/s41598-017-15218-7.
Taylor, W. R., E. I. Kornaropoulos, G. N. Duda, S. Kratzenstein, R. M. Ehrig, A. Arampatzis, and M. O. Heller. 2010. “Repeatability and Reproducibility of OSSCA, a Functional Approach for Assessing the Kinematics of the Lower Limb.” *Gait & Posture* 32 (2): 231–36. https://doi.org/10.1016/j.gaitpost.2010.05.005.
Thelen, Darryl G., and Frank C. Anderson. 2006. “Using Computed Muscle Control to Generate Forward Dynamic Simulations of Human Walking from Experimental Data.” *Journal of Biomechanics* 39 (6): 1107–15. https://doi.org/10.1016/j.jbiomech.2005.02.010.
Venkadesan, Madhusudhan, Marcelo A. Dias, Dhiraj K. Singh, Mahesh M. Bandi, and Shreyas Mandre. 2017. “Stiffness of the Human Foot and Evolution of the Transverse Arch.” *ArXiv:1705.10371 [Physics, q-Bio]*, May. http://arxiv.org/abs/1705.10371.
Viitasalo, Jukka T., and Paavo V. Komi. 1981. “Interrelationships between Electromyographic, Mechanical, Muscle Structure and Reflex Time Measurements in Man.” *Acta Physiologica Scandinavica* 111 (1): 97–103. https://doi.org/10.1111/j.1748-1716.1981.tb06710.x.
Virgin, W. J. 1951. “Experimental Investigations into the Physical Properties of the Intervertebral Disc.” *The Journal of Bone and Joint Surgery. British Volume* 33-B (4): 607–11. https://doi.org/10.1302/0301-620X.33B4.607.
Wager, Justin C., and John H. Challis. 2016. “Elastic Energy within the Human Plantar Aponeurosis Contributes to Arch Shortening during the Push-off Phase of Running.” *Journal of Biomechanics* 49 (5): 704–9. https://doi.org/10.1016/j.jbiomech.2016.02.023.
Ward, Samuel R., Carolyn M. Eng, Laura H. Smallwood, and Richard L. Lieber. 2008. “Are Current Measurements of Lower Extremity Muscle Architecture Accurate?”

*Clinical Orthopaedics and Related Research* 467 (4): 1074–82. https://doi.org/10.1007/s11999-008-0594-8.
Westblad, Pär, Takeshi Hashimoto, Ian Winson, Arne Lundberg, and Anton Arndt. 2002. "Differences in Ankle-Joint Complex Motion During the Stance Phase of Walking as Measured by Superficial and Bone-Anchored Markers." *Foot & Ankle International* 23 (9): 856–63. https://doi.org/10.1177/107110070202300914.
Wezenberg, Daphne, Andrea G. Cutti, Antonino Bruno, and Han Houdijk. 2014. "Differentiation between Solid-Ankle Cushioned Heel and Energy Storage and Return Prosthetic Foot Based on Step-to-Step Transition Cost." *Journal of Rehabilitation Research and Development* 51 (10): 1579–90. https://doi.org/10.1682/JRRD.2014.03.0081.
Whittle, Michael W. 1999. "Generation and Attenuation of Transient Impulsive Forces beneath the Foot: A Review." *Gait & Posture* 10 (3): 264–75. https://doi.org/10.1016/S0966-6362(99)00041-7.
———. 2014. *Gait Analysis: An Introduction*. Butterworth-Heinemann.
Willwacher, Steffen, Manuel König, Wolfgang Potthast, and Gert-Peter Brüggemann. 2013. "Does Specific Footwear Facilitate Energy Storage and Return at the Metatarsophalangeal Joint in Running?" *Journal of Applied Biomechanics* 29 (5): 583–592.
Winter, D. A. 1979. "A New Definition of Mechanical Work Done in Human Movement." *Journal of Applied Physiology* 46 (1): 79–83. https://doi.org/10.1152/jappl.1979.46.1.79.
Winter, DA. 2009. *Biomechanics and Motor Control of Human Movement*. Wiley.
Winter, David A. 1983a. "Energy Generation and Absorption at the Ankle and Knee during Fast, Natural, and Slow Cadences." *Clinical Orthopaedics and Related Research*, no. 175 (May): 147–54.
———. 1983b. "Energy Generation and Absorption at the Ankle and Knee during Fast, Natural, and Slow Cadences." *Clinical Orthopaedics & Related Research* 175 (May): 147–54.
———. 1984. "Kinematic and Kinetic Patterns in Human Gait: Variability and Compensating Effects." *Human Movement Science* 3 (1–2): 51–76. https://doi.org/10.1016/0167-9457(84)90005-8.
———. 1991. *The Biomechanics and Motor Control of Human Gait: Normal, Elderly and Pathological*. University of waterloo press Waterloo.
———. 2009. *Biomechanics and Motor Control of Human Movement*. John Wiley & Sons.
Winter, David A., Aftab E. Patla, James S. Frank, and Sharon E. Walt. 1990. "Biomechanical Walking Pattern Changes in the Fit and Healthy Elderly." *Physical Therapy* 70 (6): 340–47.
Winter, David A., and D. G. E. Robertson. 1978. "Joint Torque and Energy Patterns in Normal Gait." *Biological Cybernetics* 29 (3): 137–42. https://doi.org/10.1007/BF00337349.
Winter, David A., and H.J. Yack. 1987. "EMG Profiles during Normal Human Walking: Stride-to-Stride and Inter-Subject Variability." *Electroencephalography and Clinical Neurophysiology* 67 (5): 402–11. https://doi.org/10.1016/0013-4694(87)90003-4.
Wu, Ge, Sorin Siegler, Paul Allard, Chris Kirtley, Alberto Leardini, Dieter Rosenbaum, Mike Whittle, et al. 2002. "ISB Recommendation on Definitions of Joint

Coordinate System of Various Joints for the Reporting of Human Joint Motion—Part I: Ankle, Hip, and Spine." *Journal of Biomechanics* 35 (4): 543–48. https://doi.org/10.1016/S0021-9290(01)00222-6.

Yamane, K., and L. Trutoiu. 2009. "Effect of Foot Shape on Locomotion of Active Biped Robots." In *2009 9th IEEE-RAS International Conference on Humanoid Robots*, 230–36. https://doi.org/10.1109/ICHR.2009.5379576.

Yandell, Matthew B., Brendan T. Quinlivan, Dmitry Popov, Conor Walsh, and Karl E. Zelik. 2017. "Physical Interface Dynamics Alter How Robotic Exosuits Augment Human Movement: Implications for Optimizing Wearable Assistive Devices." *Journal of NeuroEngineering and Rehabilitation* 14 (May): 40. https://doi.org/10.1186/s12984-017-0247-9.

Yoon, Jungwon, Abdullah Özer, Gabsoon Kim, and Nandha Handharu. 2011. *A Bio-Robotic Toe & Foot & Heel Models of a Biped Robot for More Natural Walking: Foot Mechanism & Gait Pattern*. INTECH Open Access Publisher.

Zajac, Felix E., Richard R. Neptune, and Steven A. Kautz. 2002. "Biomechanics and Muscle Coordination of Human Walking: Part I: Introduction to Concepts, Power Transfer, Dynamics and Simulations." *Gait & Posture* 16 (3): 215–32. https://doi.org/10.1016/S0966-6362(02)00068-1.

Zelik, Karl E. 2017. "Motion Analysis | Zelik Lab for Biomechanics & Assistive Technology | Vanderbilt University." April 11, 2017. https://my.vanderbilt.edu/batlab/resources/motion-analysis/.

Zelik, Karl E., and Peter G. Adamczyk. 2016. "A Unified Perspective on Ankle Push-off in Human Walking." *J Experimental Biology*.

Zelik, Karl E., S. H Collins, Peter G. Adamczyk, A. D Segal, G. K Klute, D. C Morgenroth, M. E Hahn, M. S Orendurff, J. M Czerniecki, and A. D Kuo. 2011a. "Systematic Variation of Prosthetic Foot Spring Affects Center-of-Mass Mechanics and Metabolic Cost During Walking." *IEEE Transactions on Neural Systems and Rehabilitation Engineering* 19 (4): 411–19. https://doi.org/10.1109/TNSRE.2011.2159018.

Zelik, Karl E., Steven H. Collins, Peter G. Adamczyk, A. D. Segal, G. K. Klute, D. C. Morgenroth, M. E. Hahn, M. S. Orendurff, J. M. Czerniecki, and A. D. Kuo. 2011b. "Systematic Variation of Prosthetic Foot Spring Affects Center-of-Mass Mechanics and Metabolic Cost During Walking." *IEEE Transactions on Neural Systems and Rehabilitation Engineering* 19 (4): 411–19. https://doi.org/10.1109/TNSRE.2011.2159018.

Zelik, Karl E., and Jason R. Franz. 2017. "It's Positive to Be Negative: Achilles Tendon Work Loops during Human Locomotion." *PLOS ONE* 12 (7): e0179976. https://doi.org/10.1371/journal.pone.0179976.

Zelik, Karl E., and Eric C. Honert. 2018. "Ankle and Foot Power in Gait Analysis: Implications for Science, Technology and Clinical Assessment." *Journal of Biomechanics* 0 (0). https://doi.org/10.1016/j.jbiomech.2018.04.017.

Zelik, Karl E., Tzu-Wei P. Huang, Peter G. Adamczyk, and Arthur D. Kuo. 2014. "The Role of Series Ankle Elasticity in Bipedal Walking." *Journal of Theoretical Biology* 346 (April): 75–85. https://doi.org/10.1016/j.jtbi.2013.12.014.

Zelik, Karl E., and Arthur D. Kuo. 2010. "Human Walking Isn't All Hard Work: Evidence of Soft Tissue Contributions to Energy Dissipation and Return." *The Journal of Experimental Biology* 213 (24): 4257–64. https://doi.org/10.1242/jeb.044297.

———. 2012. “Mechanical Work as an Indirect Measure of Subjective Costs Influencing Human Movement.” *PLOS ONE* 7 (2): e31143. https://doi.org/10.1371/journal.pone.0031143.

Zelik, Karl E., Valentina La Scaleia, Yuri P. Ivanenko, and Francesco Lacquaniti. 2014a. “Can Modular Strategies Simplify Neural Control of Multidirectional Human Locomotion?” *Journal of Neurophysiology* 111 (8): 1686–1702. https://doi.org/10.1152/jn.00776.2013.

———. 2014b. “Coordination of Intrinsic and Extrinsic Foot Muscles during Walking.” *European Journal of Applied Physiology*, November, 1–11. https://doi.org/10.1007/s00421-014-3056-x.

Zelik, Karl E., Kota Z. Takahashi, and Gregory S. Sawicki. 2015. “Six Degree-of-Freedom Analysis of Hip, Knee, Ankle and Foot Provides Updated Understanding of Biomechanical Work during Human Walking.” *The Journal of Experimental Biology* 218 (6): 876–86. https://doi.org/10.1242/jeb.115451.

Zhang, W., F. Chen, M. Li, and Q. Huang. 2010. “Simulation of Humanoid Motion Based on the Foot with One Active Joint.” In *2010 IEEE International Conference on Robotics and Biomimetics*, 167–72. https://doi.org/10.1109/ROBIO.2010.5723321.

Zhou, Ping, Nina L. Suresh, and William Z. Rymer. 2007. “Model Based Sensitivity Analysis of EMG–Force Relation with Respect to Motor Unit Properties: Applications to Muscle Paresis in Stroke.” *Annals of Biomedical Engineering* 35 (9): 1521–31. https://doi.org/10.1007/s10439-007-9329-3.

Zhu, Jinying, Qining Wang, and Long Wang. 2014a. “On the Design of a Powered Transtibial Prosthesis With Stiffness Adaptable Ankle and Toe Joints.” *IEEE Transactions on Industrial Electronics* 61 (9): 4797–4807. https://doi.org/10.1109/TIE.2013.2293691.

———. 2014b. “Effects of Toe Stiffness on Ankle Kinetics in a Robotic Transtibial Prosthesis during Level-Ground Walking.” *Mechatronics* 24 (8): 1254–61. https://doi.org/10.1016/j.mechatronics.2014.06.005.